Petrography and Geochemistry of the Mesoproterozoic Gawler Range Volcanics, South Australia

by

Adam Bath

B.Sc. (University of Newcastle)

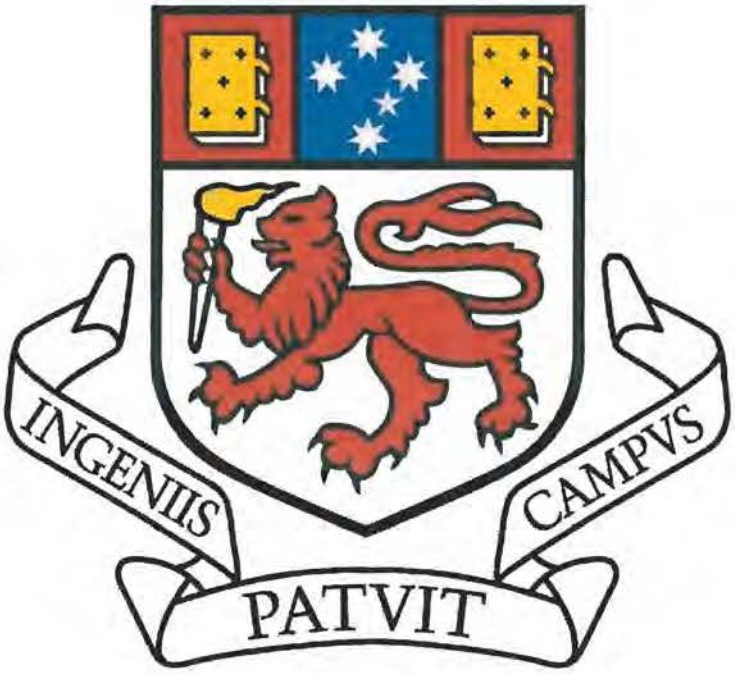

A research thesis submitted in partial fulfilment of the requirements of the Degree of Bachelor of Science with Honours

University of Tasmania

Australia

March, 31st 2005

Abstract

The Gawler Range Volcanics (GRV), located in the central region of South Australia, represents the eruption of enormous volumes of felsic lava (25,000km^3) at the beginning of the Mesoproterozoic (~1.59Ga) and is closely associated with the emplacement of the widespread Hiltaba Suite (HS) granites both spatially and temporally. Since the discovery of the Giant Olympic Dam Cu-U-Au-Ag deposit in 1975 (which is intimately related to the emplacement of the HS), both the HS and GRV have attracted vast amounts of attention from research, government and exploration groups. Efforts to understand the HS has been largely hampered by the thick regolith cover which blankets much of the central region of South Australia. The GRV in contrast, is well-exposed and detailed volcanology (Morrow, 1998; Garner and McPhie, 1999) and geochemical studies (Stewart, 1994) suggest that it represents lava flows, which were produced from the fractionation of a mafic source.

One problem associated with the GRV is the wide extent of its homogenous rhyolitic and dacitic lava flows. Creaser and White (1991) reported that the upper GRV, which represents a single emplaced unit >8000 km^2, is characterized by dry (<1wt% H_2O), high temperature magma (900-1010°C), which was derived from a single homogeneous source. Garner and McPhie (1999) advocated that the GRV are lava flows as opposed to ignimbrites (e.g. Stewart, 1994). The notion that these widespread homogenous volcanics are lava flows is at odds with the high viscosity associated with rhyolitic and dacitic lavas. Geochemical studies undertaken by myself however show that rhyolites from the GRV contain 1400-1800ppm of F and glass inclusions also from the GRV (which are thought to represent melt trapped at depth) contains up to 12,500ppm of F, which is remarkably high for degassed lava and trapped melt respectively. I propose that F, known as an effective depolymeriser, may have significantly reduced the viscosity of the lava and thus allowed it to flow over an extensive area.

Melt inclusions which are hosted within quartz phenocrysts from the upper units of the Eucarro Rhyolite (GRV) were collected from seven samples belonging to three different rock types, which included; 1) plagioclase rhyolite, 2) vesicular rhyolite, 3) quartz rhyolite *(also see* Morrow *et al.,* 2000). Each rock type contains excellent examples of large glass inclusions along with magmatic fluid inclusions which were found within the same trapping planes. Samples from the plagioclase rhyolite and the vesicular rhyolite also contain quartz with high-density CO_2 inclusions, glass inclusions and non-silicate melt inclusions. From the three rock types over fifty homogenized glass inclusions were analyzed for major elements (SX-100 Cameca microprobe) and over eighty for trace elements (laser ablation/IC-PMS). Comparisons were than made between the groundmass and melt inclusions. Each sample showed remarkable similarities in REE (except Eu, which is enriched within the groundmass). In contrast though, elements such as F, Mo (x1-6), W (x10-20), U (x1-2.5) and Pb (x3-9) were significantly enriched within melt inclusions. A similar REE concentration, between the groundmass and melt inclusions, suggests that both were derived from the same source, whereas enrichments of F (x6-7), Mo (x1-6), W (x10-20), U (x1-2.5) and Pb (x3-9) within melt inclusions may reflect the concentration of these elements within the melt at depth and therefore concentrations prior to eruption and subsequent degassing. The presence of high-density CO_2 inclusions, magmatic fluid inclusions and non-silicate melt inclusions suggests that a significant amount of degassing of the magma may have occurred at depth. This suggests that a significant amount of F, Mo, W, U and Pb may have been lost as volatiles from the melt and therefore have likely either ended up as mineral deposits within the country rock, or were released into the atmosphere during eruption. If the former was significant, than the location the volcanic vent(s) which link the GRV and HS may be of enormous economic value.

Table of Contents

Page

Chapter 3. Quartz-hosted magmatic inclusion from the Eucarro Rhyolite

Chapter 4. Geochemistry of the Hiltaba Granite, Eucarro Rhyolite, Yardea Dacite and melt inclusions from the Eucarro Rhyolite

Chapter 1
Introduction

1.1. Assessment of the problem and the purpose of this study

The role of volatiles within magmas plays an important part in controlling the manner in which magma is erupted. One of the most common volatiles is H_2O, which can be exsolved from the melt at shallow crustal depths, resulting in explosive eruptions, widespread ash-fall and pyroclastic flows. Sediments derived from hydroexplosive eruptions are identified based textural features, such as the presence of pumice, lapilli, graded bedding and fractured phenocrysts. In contrast the eruption of dry (<2 wt% H_2O), hot (900-1100°C), widespread (up to >12,000 km^2 e.g. Garner and McPhie, 1999) felsic volcanics (rhyolitic to dacitic), which are commonly found within LIP (Large Igneous Provinces), present special problems for interpretation, such as differentiating between densely welded ignimbrites and lava flows (Henry and Wolff, 1992). Examples of such provinces include the Neoproterozoic North Shore Volcanic Group, Minnesota (Green and Fitz, 1993), 11 to 8 Ma Snake River Plain volcanic province, Idaho (Bonnichen and Kauffman, 1987; Manley, 1992), Cretaceous Etendeka Formation, Nambia (Milner *et al.*, 1992; Renne *et al.*, 1996), Tertiary Trans-Pecos volcanic field, Texas (Henry *et al.*, 1988) and the early Mesoproterozoic Gawler Range Volcanics, South Australia (Fig 1-1) (Creaser and White, 1991; Garner and McPhie, 1999),

According to Manley (1992) a common misconception about rhyolitic lava flows is that they cannot advance far from their vents and are constrained to be small due to their high viscosities; however, thick viscous lava can flow quite slowly and may advance over large distances (e.g. 9 km from vent have been reported (Manley, 1995)) if the lava can retain enough heat and magma supply. Examples include several rhyolites from the Owyhee Plateau, Idaho, which were originally interpreted as densely welded ignimbrites (Ekren *et al.*, 1984), but were later suggested to be lava flows (Bonnichsen and Kauffman, 1987; Manley, 1995; Manley, 1996). Units from the upper Gawler Range Volcanics were also earlier classed as welded ignimbrites (e.g. Blissett, 1975, Giles, 1988 and Stewart, 1994), but have recently been concluded to be lava flows based on textural features and

the existence of matrix supported megablocks within the volcanics (Garner and McPhie, 1999). The widespread nature of the upper Gawler Range Volcanics (>12,000 km^2), suggests that they may represent the largest, most voluminous and widespread felsic lava flows on earth, and thus may have required a significantly large supply of high temperature lava, which was able to flow for a sustained period and a carapace which inhibited heat loss during the eruption (i.e.vesicular carapace).

The purpose of this study is to investigate the composition of melt from the upper Gawler Range Volcanics (GRV) and to determine if effective silicate depolymerizers were present within the melt, which would have aided in maintaining a low melt viscosity during the eruption. Tools used for the study include melt inclusions hosted in quartz, which represent melt which was trapped at depth and therefore are an effective tool for determining the volatile content of the melt prior to eruption.

Also investigated in this study is the distribution of trace elements (e.g. REE, U, Sn, W) between the host rock and melt inclusions, which has important implication for understanding the role of trace elements during magmatic degassing and mechanism of transportation of metals in A-Type magmatic systems.

The Thesis is divided into five chapters. Chapter 2 provides petrographic description of rocks from the Eucarro Rhyolite (upper GRV), Chapter 3 gives petrographic descriptions of quartz-hosted melt inclusions from the Eucarro Rhyolite and Chapter 4 presents and compares major and trace element data for whole rock, groundmass and melt inclusions. Chapter 5 discusses the role of fluorine in the melt and its effect on melt viscosity, as well as implications for the style of eruption. Chapter 5 also compares the Eucarro Rhyolite with felsic rocks from other LIP and addresses conclusions for the study.

1.2. Background

1.2.1. The Gawler Range Volcanics

The Mesoproterozoic Gawler Range Volcanics (GRV) covers an area of 25,000 km^2 of the central Gawler Craton (Fig 1-1) and represents the eruption of enormous

volumes of dominantly felsic magma between 1592±3 Ma and 1591±3Ma (U-Pb: Fanning *et al.*, 1988). The volcanics are undeformed and extensively oxidized, brick red in colour and overlie Archean and Palaeoproterozoic granitoid suites, metamorphic complexes and sedimentary formations of the Gawler Craton (GC), which has been tectonically stable since 1450 Ma, with the exception of some minor epeirogenic movement (Parker, 1993). The cause of the eruption is largely unknown; however Flint (1993) suggested they formed due to mantle upwelling and extensive anorogenic partial melting of the lower crust.

Stewart (1994) divided the GRV into lower and upper GRV, based on stratigraphical, spatial, volume, chemical and isotopic characteristics. The lower GRV is oldest, comprises of three discrete centers exposed along the western margin of the GRV province (Tarcoola, Kokatha and Glyde Hill Volcanic Complex), and a fourth area, termed the Southern Gawler Range Area (SGRA), which forms a discontinuous band of outcrops along the south-western and southern edge of the province (including Menninnie Dam; *see* Roache *et al.*, 2000). These successions amount to ~1000 m in thickness and are generally moderately dipping (Garner and McPhie, 1999). The lower GRV ranges in composition from basalt to rhyolite and is comprised of ignimbrites, minor sedimentary units and lavas, which are dominated by rhyolites to dacites, with basalts and andesites being subordinate.

The upper GRV consists of thick (200-300m), widespread crystal-rich rhyolitic to dacitic units, which are characteristic of lava flows (Garner and McPhie, 1999; Allen *et al.*, 2003). The units are flat lying or very gently dipping and are well exposed in the SGRA. Unit names were previously assigned by Blissett (1975); however a recent review by Allen *et al.* (2003) has reassigned the boundaries of some units and excluded others. Unit names and their distribution will be discussed further below.

1.2.1.1. Lower GRV

An extensive geochemical study on the lower GRV was carried out by Stewart (1994), which investigated basalts and rhyolites and found that the most mafic basalts (those which have the highest MgO content) were characterized by an enrichment of

LREE (light rare earth elements) and high LILE/HFSE (large-ion lithopile elements/high field-strength elements) ratios. Stewart (1994) advocated that the LREE enrichment and high LILE/HFSE ratio in basalts were unlikely a product of crustal assimilation or fractionation (due to the high MgO content), and were most likely a product of interaction between the continental mantle lithosphere (non-convecting) and asphenosphere (convecting), which according to Stewart (1994) were heterogeneous. Various authors (e.g. Ellam and Hawkesworth, 1988; Hildreth and Moorbath, 1988; Kempton et al., 1991) have suggested that large LILE/HFSE (incompatible/compatible) ratios can form within the mantle in areas of subduction, which led Stewart (1994) to hypothesize that the continental mantle lithosphere may have resembled arc chemistry from the disappearance of an earlier subduction zone. LREE enrichments on the other hand may be explained by the enrichment of LREE within pyroxene (Stewart, 1994). Another point made by Stewart (1994) was that MgO and εNd values correlate well, whereas εSr values and εNd values fail to correlate, which may represent two endmember mixing.

Although, some basalts show little evidence of crustal contamination and/or fractionation others appear to have been substantially contaminated and contain quartz, potassium feldspar xenocrysts and increased SiO_2 concentrations together with high compatible element values (e.g. Ni, Cr) and very high concentrations of incompatible elements such as Zr, Rb and REE (Stewart, 1994).

The origin of felsic rocks within the lower GRV also presents difficulties. One of the aims of Stewart's (1994) study was to determine if the felsic components were derived from: 1) partial melting of the Archean basement, 2) fractionation from a basaltic melt, 3) assimilation, fractionation, crystallization (AFC) or 4) magma mixing. Stewart (1994) used εNd values to tackle this problem. A plot of 143Nd/144Nd against 1/Nd showed that a group of samples from each volcanic centre plotted as a curve, which according to Stewart (1994) is best explained by an AFC process.

In summary, Stewart's (1994) work illustrates that the lower GRV basalts were likely derived from a conditioned mantle where at least two mantle end members were in co-existence (one from the asphenosphere and one from the lithosphere). Mixing of the end members produced basalts, which were enriched in incompatible elements relative to known OIB or MORB, but similar to arc basalts. As magma rose through the crust it

assimilated country rock and crystallized to produce fractionated volcanics which ranged from basalts to rhyolites. Some of the magma that was erupted was not significantly affected by crustal assimilation (i.e. Mg-rich basalt) (Stewart, 1994).

1.2.1.2. Upper GRV

The upper GRV were originally divided into five units, which includes the Nonning Rhyodacite, Eucarro Dacite (including a basal black section), Yannabie Rhyodacite, Paney Rhyolite and the Yardea Dacite (including a basal black section) (*see* Fig 2-1B) (Blissett, 1975). A recent review of the stratigraphy by Allen *et al.* (2003) however, suggests that the Nonning Rhyodacite, Eucarro Dacite and Yannabie Rhyodacite units are all rhyolites (at least in the SGRA), which are texturally and chemically similar, apart from granitoid clasts within the Nonning Rhyodacite and an increase in abundance of amygdaloidal quartz within the Yannabie Rhyodacite. Allen *et al.* (2003) also advocated that a mingled contact between Yannabie Rhyodacite and the Paney Rhyolite (Morrow and McPhie, 2000), which is compositionally more evolved and texturally distinct (described as partially intrusive), implies that they were both derived from a single emplaced unit. Hence, a review of the stratigraphy indicates that all four units can be referred to as a single mappable emplacement unit named the Eucarro Rhyolite (Allen *et al.*, 2003). For the remainder of this thesis the new reviewed name will be used.

The distribution of rocks belonging to the Yardea Dacite mostly remain unchanged from the Allen *et al.* (2003) review, except for two main areas within the western region of the Gawler Province which were previously mapped as the Eucarro Dacite and are now included as Yardea Dacite (*see* Allen *et al.*, 2003).

1.2.1.2.a. Eucarro Rhyolite

The Eucarro Rhyolite outcrops along the southern region of the Gawler province beneath the Yardea Dacite, as a thin band (4.5 to 14 km) which extends more than 225 km from west to east and discontinuously outcrops as far north as south of Mt Ive (Allen

et al., 2003). The unit is approximately 300m thick and according to Allen *et al.* (2003) is comprised of texturally uniform plagioclase rhyolite, with 15-21% crystals comprising of euhedral feldspar (7% plagioclase and 11% K-feldspar), ferromagnesian phases (2%; olivine, pyroxene or amphibole and Fe-Ti oxides), variable abundances of round and embayed quartz (trace to 1.5%) and accessory apatite and zircon (also see Chapter 2).

In contrast, the upper Eucarro Rhyolite (also known as the Quartz Rhyolite) is heterogeneous relative to the rest of the Eucarro Rhyolite. It contains less plagioclase (5% on average) and ferromagnesian phases (0.5%) and significantly more quartz (up to 5%) relative to the rest of the Eucarro Rhyolite (Allen *et al.*, 2003).

1.2.1.2.b. Yardea Dacite

The Yardea Dacite is the youngest unit of the GRV and dominates the central and southern region of the Gawler province (~12,000 km^2) and consists of two mappable facies; one being the black basal dacite layer (up to 20-30m thick) and the other being the upper volumetrically dominant facies (at least 200m thick), which is brick red in colour (Garner and McPhie, 1999). The true thickness of the Yardea Dacite is unknown, due to the fact that it is flat lying and that its roof has been eroided. The geochemistry of the Yardea Dacite is homogeneous throughout and contains, feldspar crystals, crystals of clinopyroxene (augite and pigeonite; Creaser and White, 1991), ilmenite, magnetite, apatite and zircon. Geothermometry was carried out on pyroxene and feldspar phenocrysts by Creaser and White (1991) and results yielded temperatures of between 900 and 1010°C.

1.2.2. Petrogenesis of the upper GRV

Previous work by Creaser *et al.* (1991) suggests that the origin of the Yardea Dacite can be explained by the partial melting of tonalite or granodiorite basement. Stewart (1994) however suggested that the parental magma for the upper GRV is consistent with that of the lower GRV (i.e. basaltic magma enriched in incompatible elements), which also underwent AFC processes to produce large amounts of felsic

magma. Stewart (1994) argued that partial melting of a tonalitic-granodiorite basement source would release water during the breakdown of amphibole, which is contrary to the dry nature of the upper GRV. Stewart (1994) also argued against a dehydrated intermediate source, suggesting that it would yield small volumes of melt per volume of source, and thus fails to explain to the enormous amounts of magma that was required to produce the widespread Hiltaba Suite and upper GRV volcanics. Furthermore εNd isotopic studies by Stewart (1994) revealed that mature phase volcanics have a homogeneous signature (e.g. -3.8 to -4.5), suggesting that they were all derived from a single magma chamber.

Chapter 2

Petrographic description of the Eucarro Rhyolite

2.1. Introduction

The aim of this chapter is to present a comprehensive petrographic overview of eight quartz-phyric samples from the upper Gawler Range Volcanics (GRV). All samples were chosen from Nicole Morrow's (1998) collection, and belong to mingled sequences from the Eucarro Rhyolite. Samples were collected from exposed outcrops along the southern region of the GRV (Fig 2-1) and exact AMG co-ordinates can be found in the Appendix 1.

Morrow (1998) provided detailed petrographic descriptions for the studied volcanics and some of her work is revisited in this chapter. In addition to Morrow's work, I have paid close attention to textural features, with particular reference to quartz. In the samples listed below up to five types of quartz are reported, some of which contains magmatic inclusions. An understanding of these features, and a view of the types of magmatic inclusions that each type of quartz contains, is particularly important in understanding magmatic processes that occurred during the eruption on the Eucarro Rhyolite.

2.2. Mineralogy and petrology

2.2.1 Samples from the Eucarro Rhyolite

Of the eight samples chosen from the Eucarro Rhyolite, one sample is from the Plagioclase Rhyolite member (formally known as the Eucarro Dacite) (GC17), three belong to the Vesicular Rhyolite member (formally known as the Yannabie Rhyodacite) (GC4, GC14 and GC15) and four belong to the Quartz Rhyolite member (formally known as the Paney Rhyolite member) (GC5, GC8, GC11 and GC16) (Fig 2-1). These

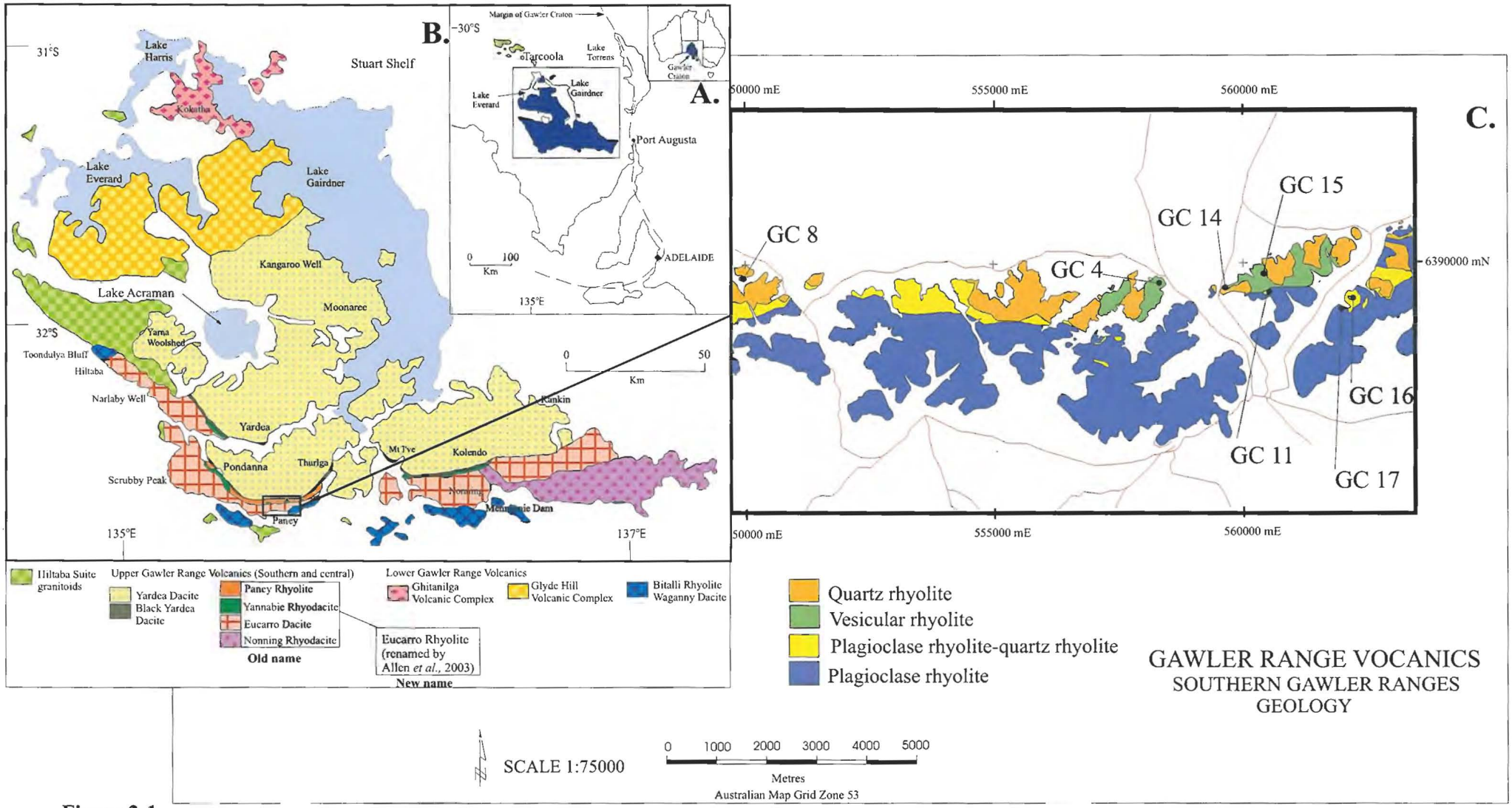

Figure 2-1

A. Location map of the Gawler Range Volcanics in the Gawler Craton, South Australia (after Allen *et al.*, 2003). **B.** Geological map o f the Gawler Range Volcanics, based on maps published by Blissett (1985 and 1986) and Blissett *et al.* (1988) (modified from Allen *et al.*, 2003).**C.** Geological map of the Eucarro Ryolite, which shows distribution of the studied rhyolite members and sample location sites. Note that sample GC 5 belonging to the Quartz Rhyolite member is not shown here, as it is located off the map sheet and further to the east. The exact UTM co-ordinates for this sample can be found in Appendix X (modified from Morrow *et al.*, 2000).

samples were chosen because they each contain quartz phenocrysts that host melt inclusions.

Although samples were selected from different members within the Eucarro Rhyolite (Fig 2-1), they have similar colour, phenocryst content and alteration, but differ in quartz content and modal composition. To avoid redundancy I have presented an overview of their similarities in section 2.1.2. Sections 2.1.4, 5 and 6 focus on unique characteristics of each member.

2.2.2. Petrographic overview of all samples from the Eucarro Rhyolite

All samples from the Eucarro Rhyolite are brick red (except sample GC15, which is brown *see* below), altered to sericite, chlorite, hematite and carbonate and contain quartz and feldspar phenocrysts (Figs 2-2 to 2-5). Quartz phenocrysts are colourless, unaltered, anhedral to euhedral (hexagonal), undeformed with sharp extinction angles, range in size from 0.25 to 8mm and make up between 2 and 9 modal% of the rock composition (*see* Tables 2-1 and 2-2). Feldspar phenocrysts are extensively altered to sericite and carbonate, 0.5-12mm in size, anhedral to euhedral, range in colour from cream to brick red, and make up between 12 and 27 modal% of the rock composition (see Table 2-1 and 2-2). The K-feldspar – plagioclase ratio is difficult to determine due to extensive alteration, although relic twinning in some crystals suggests that both were common phases. Other phenocrysts phases include mafics now completely altered to chlorite, but show relic cubic crystal form and may represent altered pyroxene (Fig 2-7). The groundmass of all samples is cryptocrystalline, micropoikilitic, altered to hematite, chlorite and sericite and makes up between 80 and 90% of the volcanics.

Accessory phases include apatite, fluorite, opaques and zircon (*see* Tables 2-1 and 2-2). Apatite is euhedral (acicular), ranges in size from ~1mm to 0.5mm and occurs within the groundmass and also as inclusions within quartz phenocrysts and zircon. Fluorite is anhedral, <0.1 to 0.3mm in size, colourless to purple and occurs within amygdaloidal quartz (*see* below) (Fig 2-8), as globular phases in the groundmass or as residual pockets of the groundmass with other accessory phases such as zircon, apatite, opaques and also chlorite (Fig 2-9). Zircons is euhedral (prismatic), 0.1-0.5mm in size

Figure 2-2 Polished section of sample GC17 (Plagioclase Rhyolite). Note that the arrow is pointing to a quartz phenocryst, which is classified as Type 2 quartz. Also note the abundance of feldspar phenocrysts in the groundmass.

Figure 2-3 Polished section of GC4 (Vesicular Rhyolite). Note the abundance of feldspar phenocrysts in the groundmass and the existence of dark globular chlorite.

Figure 2-4 Polished section of sample GC14 (Vesicular Rhyolite). Note that the arrow is pointing to a mafic xenolith, which is also common in other samples from the Plagioclase Rhyolite and the Vesicular Rhyolite.

Figure 2-5 Polished section of sample GC5 (Quartz Rhyolite). Note the flow banding and the abundant small quartz phenocrysts, but the lack of feldspar phenocrysts.

Figure 2-6 Thin section of sample GC15 (Vesicular Rhyolite) showing an altered feldspar grain which contains a cavity that is filled with late-magmatic quartz and chlorite. The cavity may represent a dissolution channel within the phenocryst (?).

Figure 2-7 Thin section of sample GC15 (Vesicular Rhyolite), which shows a relic crystal that has been completely altered to chlorite. Note the cubic shape of this crystal, which suggests that it may be an altered orthopyroxene crystal.

Figure 2-8 Thin section of amygdaloidal quartz from sample GC14 (Vesicular Rhyolite). Note the intergrowths of fluorite, which show that both silica and fluorine were important components that precipitated from late magmatic fluids.

Figure 2-9 Zircon crystals within the groundmass of the sample GC14 (Vesicular Rhyolite). Note that the arrow is pointing to fluorite within the groundmass, which is almost always intimately associated with zircons and apatite within the groundmass, and is believed to represent residual pockets in which incompatible elements were concentrated.

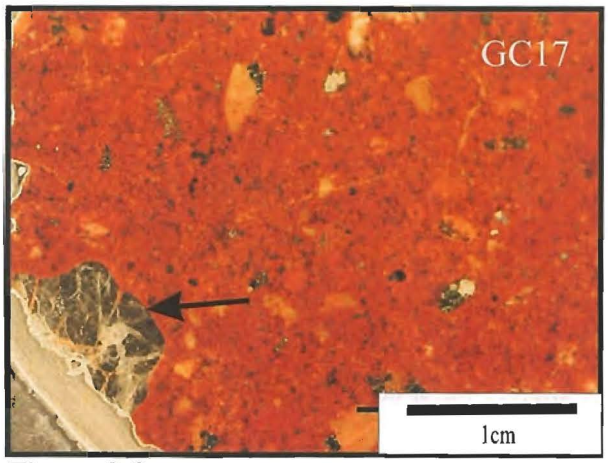

Figure 2-2

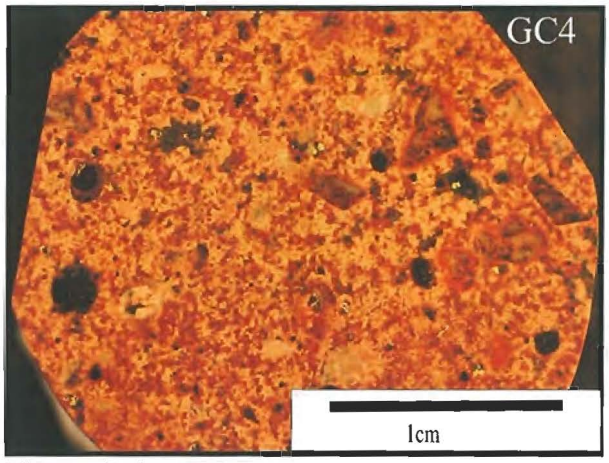

Figure 2-3

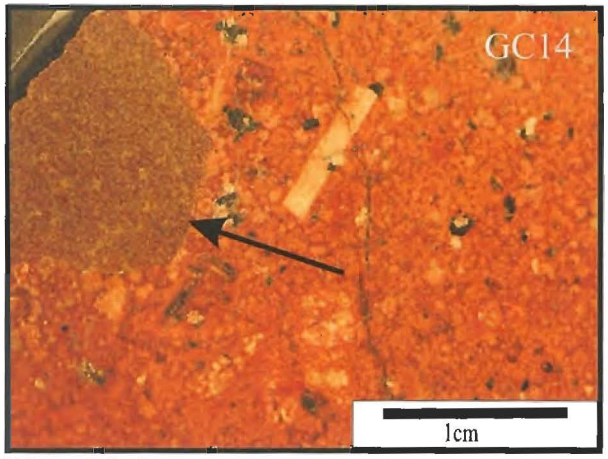

Figure 2-4

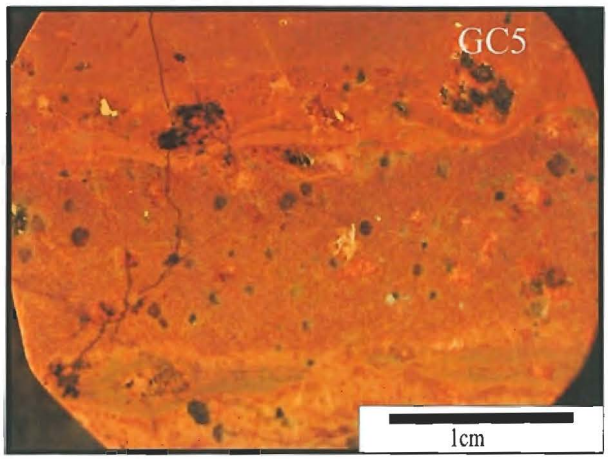

Figure 2-5

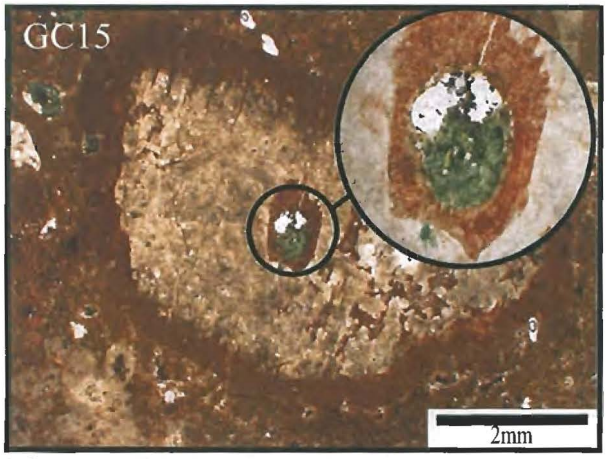

Figure 2-6

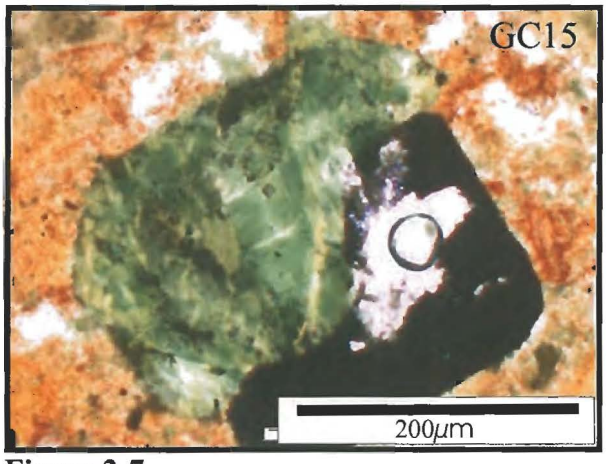

Figure 2-7

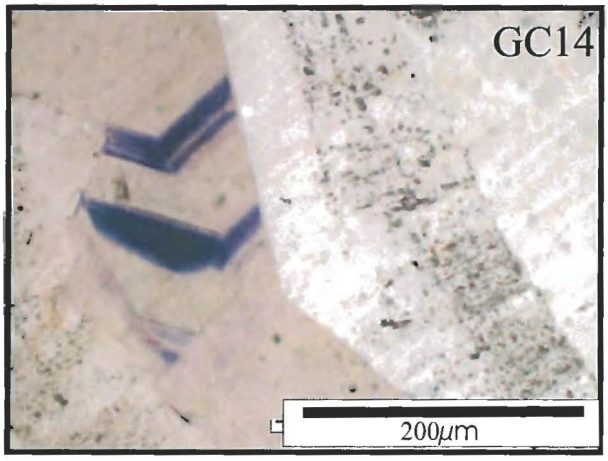

Figure 2-8

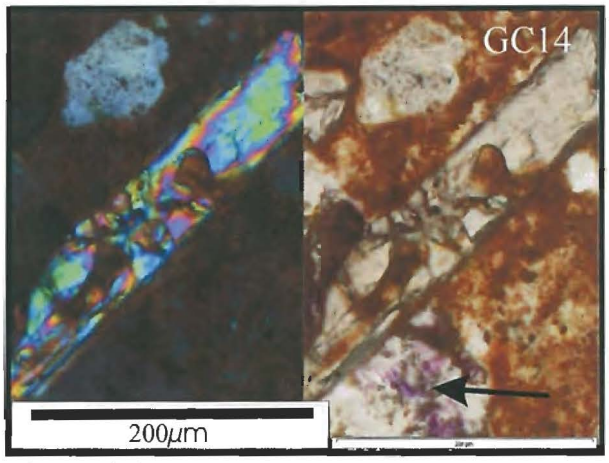

Figure 2-9

Table 2-1

A simplified table of the mineral assemblages of each rock sample from Plagioclase Rhyolite, Quartz Rhyolite and Vesicular Rhyolite. Abbreviations used for crystal form include: Euh=euhedral, Sub=subhedral and Anh=anhedral. Abbreviations used for alteration include: Chl=chlorite, Ser=sericite, Hem=hematite and Carb=carbonate. Abbreviations used for quartz include; AmQ=amygdaloidal quartz,and CaQ=cavity quartz. Also note that other accessory phases such as sphene, magnetite and rutile were also identified use EDS (sample GC14 0nly), however their distribution from sample to sample is unknown.

Sample	Ground-mass	Feldspar	Magmatic Type 1 Quartz	Magmatic Type 2 Quartz	Magmatic Vermicular Quartz	Late-magmatic Chlorite (amyg-daloidal)	Late-magmatic AmQ Quartz	Late-magmatic CaQ Quartz	Apatite	Zircon	Fluorite	Opaques	Mafic Xenoliths
GC 17 (Plagioclase Rhyolite)	Size Crypto-crystalline Texture Micro-poikilitic Modal % 80% Alteration Chl, Ser, Hem, Carb	Size 1-12mm Crystal form Euh-Anh Modal % 15% Alteration Ser, Hem, Carb, Chl	Size 0.3-1mm Crystal form Sub-Anh Modal % 1% Alteration	Size 5-8mm Crystal form Sub-Anh Modal % <1% Alteration		Size 0.1-0.5mm Crystal form Anh Modal % <1% Alteration	Size <0.5mm Crystal form Euh-Anh Modal % 2% Alteration		Size <0.1-0.2mm Crystal form Euh Modal % <1% Alteration	Size 0.1-0.2mm Crystal form Euh-Sub Modal % <<1% Alteration	Size <0.1-0.3mm Crystal form Anh Modal % <1% Alteration	Size <0.1mm Crystal form Sub-Anh Modal % 1% Alteration Hem	Size 2cm Shape Elliptical Modal % <1% Alteration Chl, Ser, Hem
GC 4 (Vesicular Rhyolite)	Size Crypto-crystalline Texture Micro-poikilitic Modal % 90% Alteration Chl, Ser, Hem, Carb	Size 0.5-3mm Crystal form Sub-Anh Modal % 5% Alteration Ser, Hem, Carb, Chl	Size 0.1-0.5mm Crystal form Sub-Anh Modal % 1% Alteration	Size 0.1-0.5mm Crystal form Sub-Anh Modal % <1% Alteration			Size <0.5mm Crystal form Sub-Anh Modal % <1% Alteration		Size <0.1-0.2mm Crystal form Euh Modal % <<1% Alteration	Size 0.1-0.5mm Crystal form Euh-Sub Modal % <<1% Alteration	Size <0.1-0.3mm Crystal form Anh Modal % <<1% Alteration	Size <0.1mm Crystal form Sub-Anh Modal % <<1% Alteration Hem	Size <0.1-2mm Crystal form Anh Modal % 2% Alteration
GC 14 (Vesicular Rhyolite)	Size Crypto-crystalline Texture Micro-poikilitic Modal % 87% Alteration Chl, Ser, Hem, Carb	Size 1-7mm Crystal form Euh-Anh Modal % 7% Alteration Ser, Hem, Carb, Chl	Size 0.1-0.5mm Crystal form Sub-Anh Modal % 1% Alteration	Size 0.1-0.5mm Crystal form Sub-Anh Modal % <1% Alteration	Size 0.5-2mm Texture Embayed Modal % <1% Alteration	Size <0.1mm Crystal form Anh Modal % <<1% Alteration	Size 0.5-2mm Crystal form Euh-Sub Modal % 1% Alteration		Size <0.1-0.2mm Crystal form Euh Modal % <1% Alteration	Size 0.1-0.5mm Crystal form Euh-Sub Modal % <<1% Alteration	Size <0.1-0.3mm Crystal form Anh Modal % <1% Alteration	Size <0.1mm Crystal form Anh Modal % <<1% Alteration Hem	Size 3-4cm Shape Elliptical Modal % 3% Alteration Chl, Ser, Hem
GC 15 (Vesicular Rhyolite)	Size Crypto-crystalline Texture Micro-poikilitic Modal % 80% Alteration Chl, Ser, Hem, Carb	Size 1-12mm Crystal form Euh-Anh Modal % 10% Alteration Ser, Hem, Carb	Size 0.1-0.5mm Crystal form Anh Modal % 1% Alteration			Size 0.1-1mm Crystal form Anh Modal % 2% Alteration	Size 0.1-5mm Crystal form Euh-Anh Modal % 2% Alteration		Size <0.1-0.2mm Crystal form Euh Modal % <1% Alteration	Size 0.1-0.5mm Crystal form Euh-Sub Modal % <<1% Alteration	Size <0.1-0.3mm Crystal form Anh Modal % <1% Alteration	Size <0.1mm Crystal form Anh-Sub Modal % <<1% Alteration Hem	Size 3-4cm Shape Elliptical Modal % 3% Alteration Chl, Ser, Hem

Table 2-2

A simplified table of the mineral assemblages of each rock sample from the Quartz Rhyolite. Abbreviations used for crystal form include: Euh=euhedral, Sub=subhedral and Anh=anhedral. Abbreviations used for alteration include: Chl=chlorite, Ser=sericite, Hem=hematite and Carb=carbonate. Abbreviations used for quartz include; AmQ=amygdaloidal quartz,and CaQ= cavity quartz. Note that other accessory phases such as sphene, magnetite and rutile were also identified using EDS (from sample GC14), however their distribution from sample to sample is unknown.

Sample	Ground-mass	Feldspar	Magmatic Type 1 Quartz	Magmatic Type 2 Quartz	Magmatic Vermicular Quartz	Late-magmatic Chlorite (amyg-daloidal)	Late-magmatic AmQ Quartz	Late-magmatic CaQ Quartz	Apatite	Zircon	Fluorite	Opaques	Mafic Xenoliths
GC 5 (Quartz Rhyolite)	Size: Crypto-crystalline Texture: Micro-poikilitic Modal %: 89% Alteration: Chl, Ser, Hem, Carb	Size: 0.5-3mm Crystal form: Euh-Anh Modal %: 5% Alteration: Ser, Hem, Carb, Chl	Size: 0.5-1mm Crystal form: Sub-Euh Modal %: 4% Alteration:						Size: <0.1-1mm Crystal form: Euh Modal %: <1% Alteration:	Size: 0.1-0.5mm Crystal form: Euh-Sub Modal %: Trace Alteration:	Size: <0.1-0.3mm Crystal form: Anh Modal %: <1% Alteration:	Size: <0.1mm Crystal form: Sub-Anh Modal %: 1% Alteration: Hem	
GC 8 Quartz Rhyolite)	Size: Crypto-crystalline Texture: Micro-poikilitic Modal %: 85% Alteration: Chl, Ser, Hem, Carb	Size: 1-5mm Crystal form: Euh-Anh Modal %: 6% Alteration: Ser, Hem, Carb, Chl	Size: 0.5-1mm Crystal form: Sub-Anh Modal %: 5% Alteration:					Size: 0.1-1mm Crystal form: Anh Modal %: 2% Alteration:	Size: <0.1-0.2mm Crystal form: Euh Modal %: <1% Alteration:	Size: 0.1-0.5mm Crystal form: Euh-Sub Modal %: Trace Alteration:	Size: <0.1mm Crystal form: Anh Modal %: Trace Alteration:	Size: <0.1mm Crystal form: Sub-Anh Modal %: <<1% Alteration: Hem	
GC 11 (Quartz Rhyolite)	Size: Crypto-crystalline Texture: Micro-poikilitic Modal %: 85% Alteration: Chl, Ser, Hem, Carb	Size: 1-4mm Crystal form: Euh-Anh Modal %: 5% Alteration: Ser, Hem, Carb, Chl	Size: 0.5-2mm Crystal form: Euh-Anh Modal %: 5% Alteration:					Size: 0.1-1mm Crystal form: Anh Modal %: 2% Alteration:	Size: <0.1-0.2mm Crystal form: Euh Modal %: <1% Alteration:	Size: 0.1-0.2mm Crystal form: Euh-Sub Modal %: Trace Alteration:	Size: <0.1-0.3mm Crystal form: Anh Modal %: Trace Alteration:	Size: <0.1mm Crystal form: Anh Modal %: <<1% Alteration: Hem	
GC 16 (Quartz Rhyolite)	Size: Crypto-crystalline Texture: Micro-poikilitic Modal %: 85% Alteration: Chl, Ser, Hem, Carb	Size: 0.5-7mm Crystal form: Euh-Anh Modal %: 8% Alteration: Ser, Hem, Carb, Chl	Size: 0.5-2mm Crystal form: Anh-Sub Modal %: 6% Alteration:	Size: >1mm Crystal form: ? Modal %: <1% Alteration:					Size: <0.1-0.2mm Crystal form: Euh Modal %: <1% Alteration:	Size: 0.1-0.5mm Crystal form: Euh-Sub Modal %: <1% Alteration:	Size: <0.1-0.3mm Crystal form: Anh Modal %: <1% Alteration:	Size: <0.1mm Crystal form: Euh Modal %: Trace Alteration: Hem	

and contains crystals and melt inclusions and is mostly found as clusters with other accessory phases as well as chlorite. Opaques phases are subhedral (sub-cubic) to anhedral and <0.1mm in size. Two opaque phases were identified from sample GC14, one being magnetite, which was separated using a magnet during heavy mineral separation, and the other rutile, which was identified using EDS (microprobe). Sphene was also identified in sample GC14 and it is likely that it also occurs as small crystals in other samples too.

2.2.3. Quartz from the Eucarro Rhyolite

From the eight samples analysed, five types of quartz were identified, which includes three types of magmatic quartz and two types of late-magmatic quartz (Fig 2-10). Magmatic varieties include Type 1 quartz, Type 2 quartz, and vermicular quartz. Type 1 quartz is anhedral to euhedral, ranges from 0.1 to 2mm in size and modal composition from 1% up to 7%, with Quartz Rhyolites typically containing more than 3% and other members 1%. Type 1 quartz is the only type of quartz that was identified in all samples (see Tables 2-1 and 2-2) and is characterised by melt inclusions and late-magmatic fluid inclusions (see Chapter 3).

Type 2 quartz ranges in size from 0.5 to 10mm, is subhedral to anhedral and was identified in samples from the Plagioclase Rhyolite, Vesicular Rhyolite and one sample from the Quartz Rhyolite (GC16), which all have a modal composition of <1%. Type 2 quartz is distinguished from other types of quartz by its 'dirty' appearance due to the presence of black vapour-rich CO_2 inclusions and extensive brittle fractures, which are associated with post-magmatic fluid inclusions (Fig 2-10). Other inclusions characteristically present in Type 2 quartz include various types of melt inclusions, crystal inclusions, composite inclusions, CO_2 inclusions, aqueous fluid inclusions and non-silicate inclusions.

Vermicular quartz is rare and was only identified in one sample from the Vesicular Rhyolite (GC4). Vermicular quartz forms an intergrowth with plagioclase and is a product of undercooling. The intergrowth cluster is about 2mm in size (Fig 2-10) and contains melt inclusions, which are similar to those in Type 1 quartz.

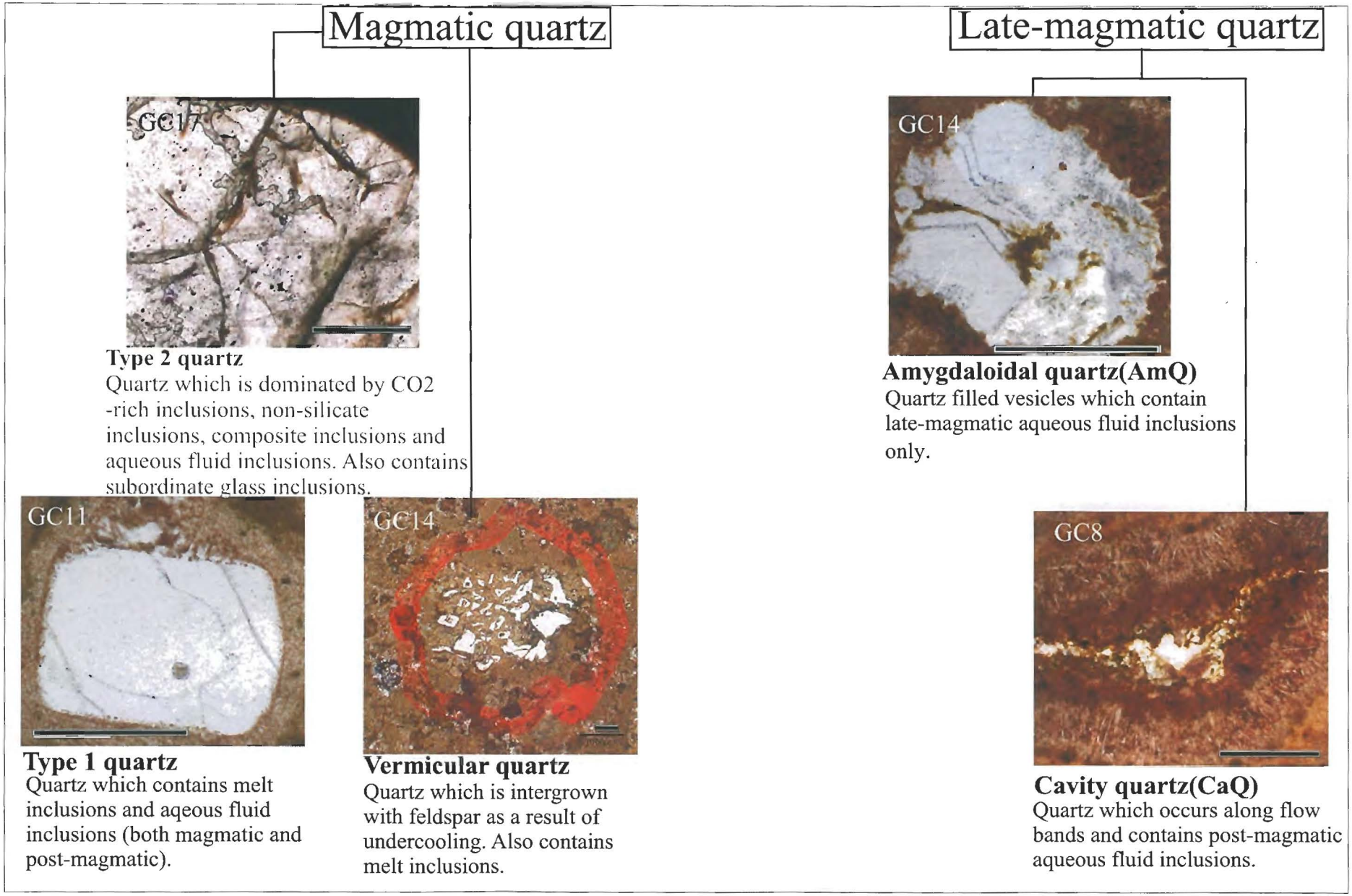

Figure 2-10
Flow chart showing the different types of magmatic and late-magmatic quartz found within the Plagioclase Rhyolite, Vesicular Rhyolite and Quartz Rhyolite from the Eucarro Rhyolite. Note that the scale bar represents 1mm in each photomicrograph.

Two types of late-magmatic quartz were identified, amygdaloidal quartz (AmQ) and cavity quartz (CaQ) (Fig 2-10). AmQ ranges in size from 0.1-5mm and consists of euhedral to anhedral quartz crystals which have filled spherical to ellipitical vesicles and contain aqueous fluid inclusions only. AmQ commonly occurs with intergrowths of chlorite and/or fluorite and is present in samples belonging to the Plagioclase Rhyolite and Vesicular Rhyolite, but absent in samples from the Quartz Rhyolite. The contact between AmQ and the groundmass is uneven, which appears to suggest that the groundmass was soft at the time AmQ formed. In some samples from the Vesicular Rhyolite (e.g. GC15), AmQ and chlorite appear to have infilled cavities within plagioclase phenocrysts, which may represent dissolution channels (?) (Fig 2-6).

CaQ occurs in cavities that are surrounded by spherulites and are only found in samples GC8 and GC11 from the quartz rhyolite. CaQ is anhedral, 0.1 to 1mm in size and appears to only contain a minor amount of aqueous fluid inclusions.

2.2.4. Plagioclase Rhyolite

Sample GC17 from the Plagioclase Rhyolite is a sericite+hematite+chlorite+carbonate-altered feldspar+quartz-phyric massive rhyolite with mafic xenoliths. Mafic xenoliths, which are ellipitical and 1-2 cm in size, have been extensively altered to chlorite, carbonate, hematite and sericite (Table 2-1). Xenoliths are rich in opaque phases, show holocrystalline texture, defined by bladed chlorite crystals and acicular sericite-altered feldspar crystals which both range in size from 0.1 to 0.5mm (Fig 2-4). The sample is also characterised by vesicles, which are 0.5-2mm in size, spherical to sub-spherical and have been in-filled with quartz and/or chlorite. Residual melt globules of fluorite, apatite, zircon, opaques and chlorite, which are 0.2 –1mm in size are also common within the groundmass (Fig 2-13).

Three types of quartz exist within the sample, which include magmatic Type 1 and Type 2, and post-magmatic AmQ (*see* Fig 2-10 and Table 2-1). AmQ is the most common (2%), with other types making up 1% or less. Most quartz ranges from 0.1-1mm in size and is mostly globular; however Type 2 quartz is much larger with, subhedral phenocrysts being up to 10mm in size.

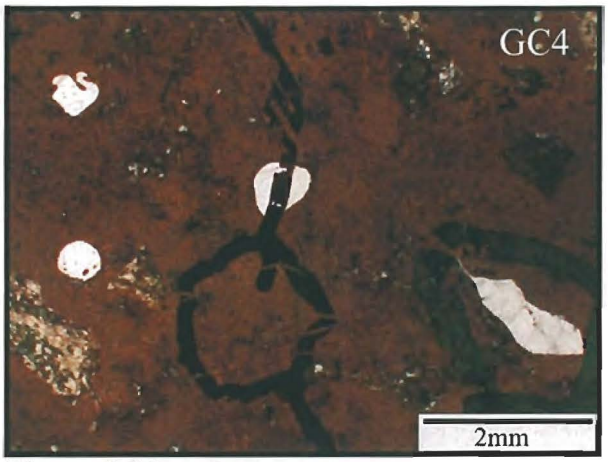

Figure 2-11

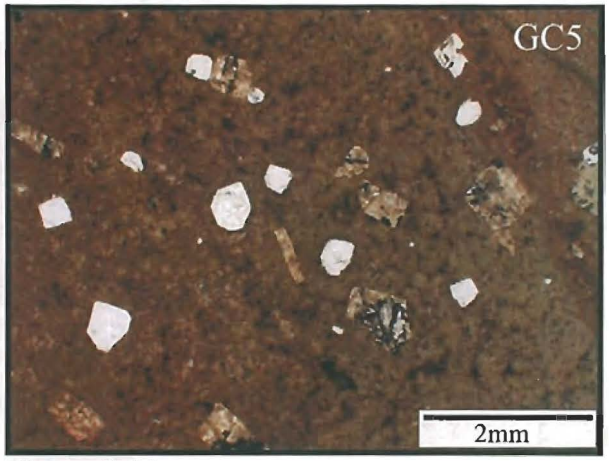

Figure 2-12

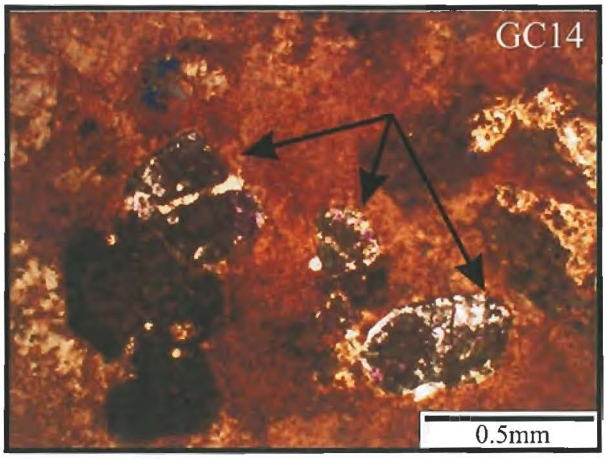

Figure 2-13

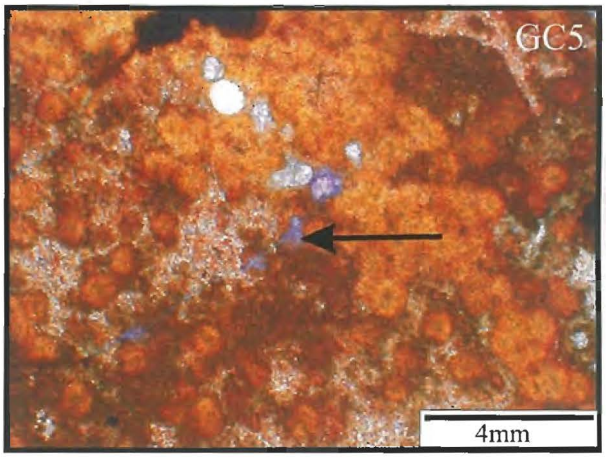

Figure 2-14

Figure 2-11 Thin section of sample GC4 (Vesicular Rhyolite) showing embayed and globular quartz, which is common in both the Vesicular Rhyolite and the Plagioclase Rhyolite.

Figure 2-12 Thin section of sample GC5 (Quartz Rhyolite) showing subhedral and euhedral quartz crystals.

Figure 2-13 Thin section of sample GC14 (Vesicular Rhyolite) showing residual globules of fluorite, chlorite, zircon and apatite, which are a common feature of the Vesicular Rhyolite and the Plagioclase Rhyolite.

Figure 2-14 Thin section of sample GC5 (Quartz Rhyolite) showing small veinlets and globules of fluorite in the groundmass (arrow).

2.2.5. Vesicular Rhyolite

Samples GC4, 14 and 15 from the Vesicular Rhyolite are sericite+hematite+chlorite+carbonate-altered feldspar+quartz-phyric massive rhyolites. Two samples (GC14 and 15) contain mafic xenoliths, which range in size from 1 to 4cm (Fig 2-4). All samples are brick red with the exception of GC15, which is brown due to a larger amount of chlorite in the groundmass. All samples contain vesicles, which are either quartz-filled (GC14 or 15) or void (GC4). Vesicles are spherical to elliptical and range in size from <1mm to 7mm. Samples also contain spherical dark chlorite-rich globules, which range in size from <1 to 4mm (Fig 2-6). Residual melt globules of fluorite, apatite, zircon, opaques and chlorite, which are 0.2 – 0.8mm in size, are also common within the groundmass (Fig 2-13).

Up to four types of quartz were identified in one sample (GC14), which includes magmatic varieties of Type 1, Type 2, Vermicular Quartz, and late-magmatic AmQ (*see* Fig 2-10 and Table 2-1). Four types of quartz were identified in sample GC4, which includes all of those in GC14 with the exception of Vermicular Quartz. Sample GC15 only contains two types of quartz, one being rare Type 1 and the other post-magmatic AmQ. Quartz in all samples ranged between 0.1 and 2mm, although AmQ, which was up 5mm, was identified in one sample (GC15). Type 1 quartz is mostly anhedral and ranges from globular to embayed (Fig 2-11). Mafic phase(s), which make up <1% of the modal composition, are euhedral (rectangular and cubic) to anhedral and have been altered to chlorite (Fig 2-7).

2.2.6. Quartz Rhyolite

Four samples from the Quartz Rhyolite were selected for analysis, GC5, GC8, GC11 and GC16 (Fig 2-1). All samples are sericite+hematite+chlorite+carbonate altered feldspar-quartz-phyric flow-banded rhyolites, with the exception of GC16, which is massive rather than flow-banded. Flow banding within the respective samples ranges in thickness from 1 to 10mm and is defined by a weak alignment of feldspar phenocrysts as well as darker

and lighter bands. Vesicles, which range in size from <1mm to 2mm, are common in sample GC11 and rare in other samples. Vesicles are spherical to elliptical and are void.

One to two types of quartz were identified in each sample. All samples contained Type 1 quartz, whereas rare Type 2 quartz was observed only in sample GC16. Post-magmatic cavity quartz was identified in two samples (GC8 and 11) (Table 2-2). Type 1 quartz mostly ranges from subhedral to euhedral (Fig 2-12).

Fluorite occurs as colourless and purple globules (typically ~0.1mm in size) within the groundmass of all samples (except GC8) and within some extensively altered feldspar phenocrysts. Sample GC5 contains the most amount of visible fluorite (<1%), and in addition to globular fluorite also contains thin fluorite veins (Fig 2-14). Fluorite in sample GC5 is most abundant within flow bands that show mottle-textured groundmass (Fig 2-14).

Some samples (GC8 and 11) contain spherical and axiolitic spherulites of feldspar crystals along the interface of flow bands (*see* Cavity Quartz Fig 2-10). Between flow bands micro-miarolitic cavities are present, which contain quartz (CaQ and MIQ), altered feldspar phenocrysts, chlorite, opaques and fluorite. Samples GC8 and GC11 also contain fragments of broken feldspar crystals which are only weakly altered and show multiple twinning.

2.3. Comparison of samples

Petrographic studies show that samples from the Plagioclase Rhyolite and Vesicular Rhyolite are similar in mineral composition, quartz content and texture. Both members contain mafic xenoliths, which are comparable in size, shape and mineralogy. In contrast, rocks from the Quartz Rhyolite differ significantly from the Plagioclase Rhyolite/Vesicular Rhyolite in the type of quartz they contain (compare Table 2-1 and 2-2), feldspar size and textural features (i.e. they all have flow banding except GC16), but are quite similar in their mineral assemblage and geochemical composition (*see* Chapter 6). Samples also differ in the crystal form of Type 1 quartz, with the Plagioclase Rhyolite and the Vesicular Rhyolite containing mostly embayed and globular quartz grains, whereas the Quartz Rhyolite is dominated by subhedral to euhedral quartz crystals.

Chapter 3

Quartz-hosted magmatic inclusions from the Eucarro Rhyolite

3.1. Introduction

The physical characteristics of melt inclusions can sometime reveal important information about their geochemistry. For example the presence of daughter phases (e.g. chalcopyrite) within melt inclusions can provide important information about the significance of certain elements (e.g. Cu) within the melt at the time of trapping. Furthermore, shrinkage bubbles within melt inclusions can be significantly enriched in certain metals (e.g. Kamenetsky *et al.*, 2004), and thus a shrinkage bubble:melt inclusion volume ratio can provide important information about the relative amounts of dissolved volatile within the melt at the time of trapping. Thus this chapter gives a detailed description of inclusion populations for the Eucarro Rhyolite. Daughter phases are identified where possible and bubble:melt inclusion volume ratios calculations are also presented.

Also covered in this chapter are heating experiments that were carried out on non-silicate melt inclusions, which was undertaken to determine the melting characteristics of non-silicate phases.

To date, no comprehensive and widely accepted terminology exists for the various types of magmatic inclusions; so for the purpose of this study I have created a chart, which outlines the various types of magmatic inclusions found within the Eucarro Rhyolite (Fig 3-1).

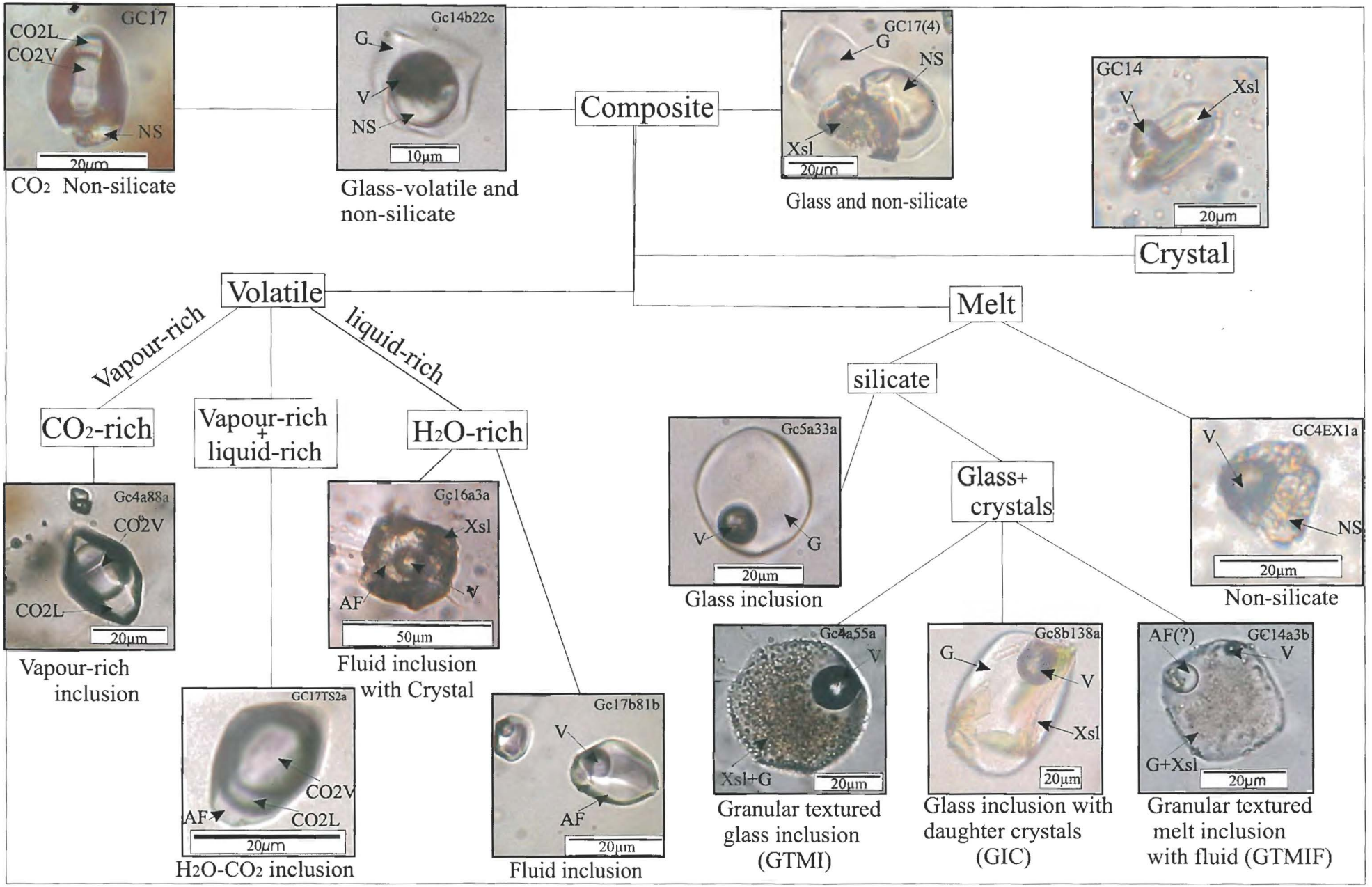

Figure 3-1
Flow chart of the different types of magmatic inclusions hosted by quartz within the Eucarro Rhyolite. Note that the inclusions can be divided into four main groups, which include; 1) Crystal inclusions, 2) Melt inclusions, 3) Volatile inclusions and 4) Composite inclusions. Abbreviations used include AF=aqueous fluid, CO2L=CO2 liquid, CO2V=CO2 vapour, Xsl=crystal, G=glass and NS=non-silicate

3.2. Inclusions selected for this study

Two broad categories of quartz were identified in every sample, which included late-magmatic quartz and magmatic quartz (except GC5, which only contains magmatic quartz) (*see* Fig 2-10). Late-magmatic quartz, which is comprised of amygdaloidal quartz (AmQ) and cavity quartz (CaQ), includes fluid inclusions that represent the trapping of late-magmatic fluids and do not contain magmatic inclusions. For the purpose of this study, the contents of late-magmatic fluids will not be covered, and therefore, AmQ and CaQ are ignored for the remainder of this chapter.

Magmatic quartz, which includes Type 1, Type 2 and vermicular quartz (*see* Chapter 2), contains numerous melt inclusions (1-15 inclusions within 0.3-0.5mm quartz fractions) and magmatic fluid inclusions that occur along crystal growth planes (Fig 3-6). All types of magmatic quartz contain fractures, which are filled with late-magmatic fluid inclusions (Fig 3-2). Magmatic inclusions which are intersected by late-magmatic inclusions are decrepitated (Fig 3-2), and are not included in this study. Only unaltered magmatic inclusions, which are thought to represent the trapping of melt during quartz growth, are included in this study. Also not covered in this study are crystal inclusions (Fig 3-1)

3.3. Types of magmatic inclusions

Twelve different types of magmatic inclusions were identified within quartz from the Eucarro Rhyolite (Fig 3-1). Each type can be pigeonholed into one of three categories, which include: 1) melt inclusions, 2) volatile-rich inclusions, and 3) composite inclusions (multiphase inclusions that may contain significant amounts of vapour-rich, glass, non-silicate and crystal phases).

3.3.1. Melt inclusions

Melt inclusions can be divided into silicate and non-silicate types, with silicate melt inclusions being the most abundant inclusion-type in all samples (44-100%) and

Figure 3-2 Polished quartz grain from sample GC16 (Quartz Rhyolite) that shows a fracture intersecting a decrepitated melt inclusion. Note that inclusions like this one, which are dark and appear to be altered, were excluded from this study.

Figure 3-3 Polished quartz grain from sample GC4 (Vesicular Rhyolite), which shows the co-existence of non-silicate melt inclusions (NS) and granular-textured melt inclusions (GTMI). Note that the co-existence of NS and GTMI demonstrates that silicate melt and non-silicate melt were trapped at the same time during the growth of quartz.

Figure 3-4 Glass inclusion with crystals (GIC) from sample GC11B1 (Quartz Rhyolite). Note that this inclusion was exposed for microprobe analysis. Two spots were analyzed in order to determine the major element composition of the glass (lower circle) and the approximate composition of the bladed crystal (upper circle). Note that the results from the analysis are presented on Table 3-3 (adjacent), which shows that the bladed crystal (note that some glass was probed together with the crystal) is significantly more enriched in Ca, Fe and F when compared to the glass. Table 3-3 also shows that the ratio between Ca:2F from the analysis quite similar to that of fluorite. Hence the bladed crystals are likely daughter crystals of fluorite, which crystallized from a fluorine-rich melt.

Table 3-3 A comparison of major group elements from microprobe analysis on glass and a bladed crystal within a GIC from sample GC11B1 (Quartz Rhyolite). See above (Figure 3-4).

Figure 3-5 GIC from sample GC14 (Vesicular Rhyolite). Microprobe analysis of the blue-green crystal (arrow) suggests that it most likely potassic-chlorohastingsite amphibole. (*see* Appendix 3).

Figure 3-6 Glass inclusions (GI) from sample GC5 (Quartz Rhyolite) that are aligned along a single crystal growth plane. Note that the darker inclusion at the bottom left hand side of the diagram is an aqueous fluid inclusion (arrow). This demonstrates that aqueous fluids and silicate melt co-existed at the time of quartz crystallization.

Figure 3-7 Polished quartz grain from sample GC14 (Vesicular Rhyolite), which shows GI and vapour + non-silicate melt inclusions aligned along a single crystal growth plane. This demonstrates that vapour-rich non-silicate melt and silicate melt co-existed as separate phases in the melt at the time of quartz crystallization.

Figure 3-8 Negative crystal shape vapour-rich inclusions (likely CO_2) from sample GC4 (Vesicular Rhyolite).

Figure 3-2

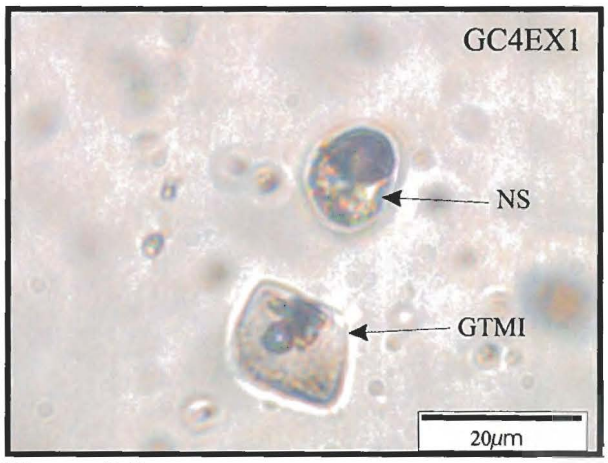

Figure 3-3

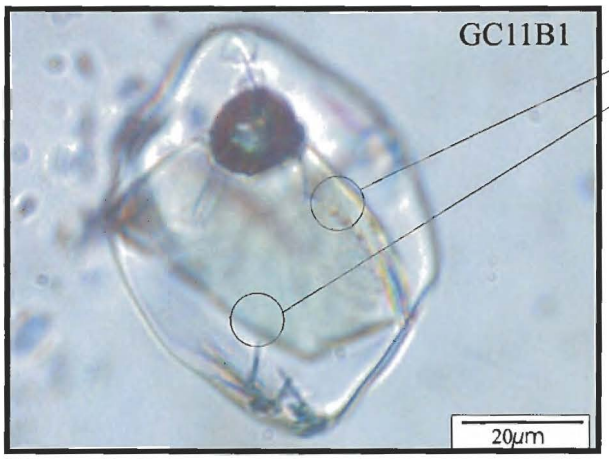

Figure 3-4

Sample	SiO2	Al2O3	Na2O	K2O	CaO
GC11B1_3	43.11	8.48	0.72	3.71	28.23
GC11B1_2	76.09	13.52	2.52	6.35	0.16

FeO	TiO2	MgO	Cl	F	Total
5.78	0.20	0.33	0.19	14.58	105.73
0.18	0.23	0.00	0.16	0.58	100.00

Fluorite = CaF2
Ca:2F
40:38
20:19

Sample GC11B1_3
Ca (wt%)=40/56*28.23
=20.2

Thus Ca:2F
20.2:14.58

Table 3-3

Figure 3-5

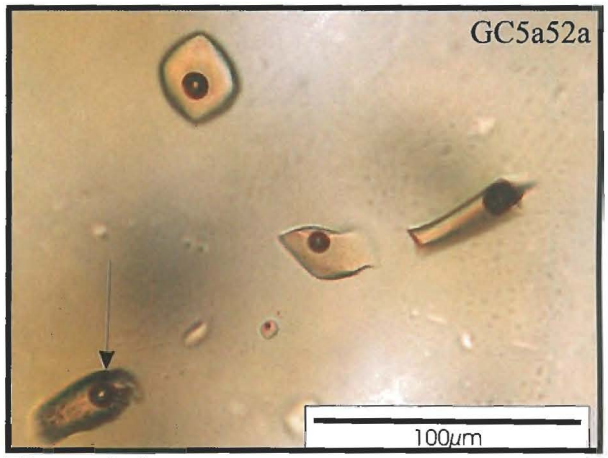

Figure 3-6

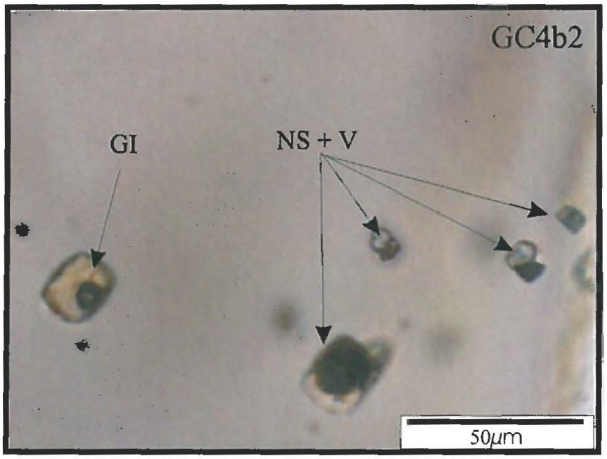

Figure 3-7

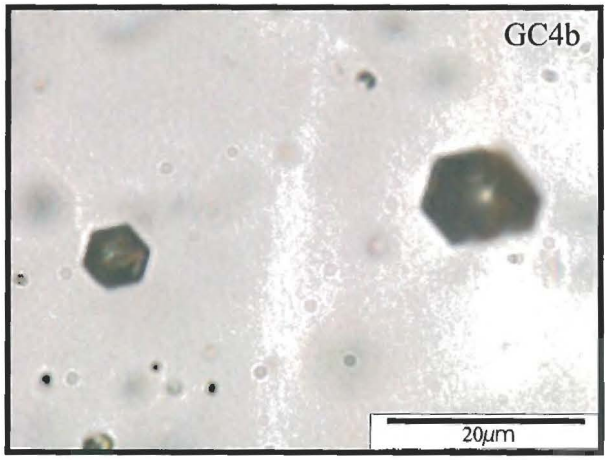

Figure 3-8

non-silicate inclusions being less common and only identified in two samples, including one from the Vesicular Rhyolite (GC4) and the other from the Plagioclase Rhyolite (GC17).

3.3.1.1. Non-silicate melt inclusions

Although less common, non-silicate melt inclusions can be distinguished from silicate melt inclusions by their low melting temperature (i.e. started to melt at 170°C and completely melted at 325°C) (*see* below), large vapour bubble (relative to inclusion size), their light transparent blue-green and pinkish colours and their granular texture (Fig 3-1). Non-silicate melt inclusions are found within Type-2 quartz and occur along the same crystal growth planes as silicate melt inclusions and magmatic volatile inclusions (Fig 3-3). At least seven different phases were identified within non-silicate melt inclusions, which include; 1) green prismatic silicate daughter phases, which failed to melt at 800°C (inferred to be co-trapped because they appear volumetrically too large to crystallize from the small amount melt within the inclusion), 2) colourless silicate globular phases, which also failed to homogenize with the melt at temperatures as high as 800°C (also inferred to be a co-trapped for the same reason as 1 *see* above), 3) CO_2 within the shrinkage bubble, which was identified during Laser Raman spectroscopy (*see* Appendix 2), 4) N_2 within the shrinkage bubble, also detected using Laser Raman spectroscopy (*see* Appendix 2), 5) transparent blue-green and pinkish non-silicate melt with high relief relative to quartz, 6) colourless non-silicate melt with similar relief to that of quartz, which was immiscible with the blue-green and pinkish non-silicate phase at temperatures below 330°C, and 7) an opaque phase at the shrinkage bubble-inclusion interface.

3.3.1.2. Silicate melt inclusions

Silicate melt inclusions can be divided into four groups, which include: 1) granular-textured glass inclusions (GTMI), 2) granular-textured glass inclusions with aqueous fluid bubbles (GTMIF), 3) glass inclusions (GI), 4) glass inclusions with daughter phase crystals (GIC).

GTMI are the most common type of inclusions within all samples (except GC5) (between 40 and 70%) and occur within all types of magmatic quartz (although far less common in Type-2 quartz (<<1%)). GTMI range in diameter from 5-100μm (average ~25μm), are rusty orange, have shrinkage bubble(s) (1 to 4) which make up between 1 and 10 vol% of the inclusion (average 4.6vol% with a standard deviation of 2.2vol%) and often contain small daughter phases of colourless acicular crystals (though to be apatite). Unknown rusty orange micro globular daughter crystals occur along the wall of GTMI, giving them their characteristic granular texture (Fig 3-1).

GTMIF are similar to GTMI except that they contain a colourless aqueous fluid bubble (may be an artefact (?)) and have only been identified in Type-1 quartz (Fig 3-1). GTMIF were found in three samples (GC17, GC4 and GC16), which included samples from the Plagioclase Rhyolite, Vesicular Rhyolite and Quartz Rhyolite (*see* Tables 3-1 and 3-2). Some examples of GTMIF contain unknown colourless bladed crystals within aqueous fluid bubbles and have small vapour bubble(s) along the outer region of the inclusion.

GI are common in sample GC5 (90%, Quartz Rhyolite), sparse in samples GC17 (6%, Plagioclase Rhyolite), GC4 (5%, Vesicular Rhyolite) and absent in all other samples (Fig 3-1). GI were identified within both Type-1 and Type-2 quartz, range in diameter from 10 to 60μm (average 25μm), are colourless to brown, range in shape from spherical to sub-spherical to elongate and have shrinkage bubble(s) (1 to 6) which make up between 1 and 6 vol% of the inclusion (average 3.2vol% and standard deviation of 1.3vol%).

GIC are indistinguishable from GI except that they contain daughter crystals, range in diameter from 10 to 110μm (average 30μm) and have shrinkage bubble(s) (1 to 2), which make up between 1-9.5 vol% of the inclusion (average 4.3 and standard deviation of 3.9). Daughter crystals include acicular phases (though to be apatite), bladed colourless crystals of fluorite (identified using microprobe) (Fig 3-4 and Table 3-3), cubic opaques (magnetite?) and unknown green prismatic crystals, which show chemical similarities to potassic-chlorohastingsite (Fig 3-5).

3.3.2. Volatile-rich inclusions

Volatile-rich inclusions can be divided into four groups, which include: 1) magmatic aqueous fluid inclusions, 2) magmatic aqueous fluid inclusions with crystals, 3) CO_2-rich inclusions and 4) H_2O-CO_2 fluid inclusions (Fig 3-1).

Magmatic aqueous fluid inclusions occur in both Type-1 and Type-2 quartz (*see* Tables 3-1 and 3-2 and Fig 3-9) from the Plagioclase Rhyolite, Vesicular Rhyolite and the Quartz Rhyolite. Inclusions range in size from <5 to 45μm, are sub-spherical to elongate, colourless, contain a vapour bubble and can be distinguished from glass inclusions by a dark outer rim, due to the large difference in the refractive index between the fluid and host quartz (Fig 3-1). Magmatic aqueous fluid inclusions are distinguished from late-magmatic fluid inclusions by their size (up to 35μm) (i.e. they are usually much larger), cubic to elongate shape, the presence of "sweat" halos and their existence along the same crystal growth planes as other magmatic inclusions (Fig 3-6).

Magmatic aqueous fluid inclusions with crystals are indistinguishable from magmatic aqueous fluid inclusions except that they contain daughter phases or co-trapped crystals which in Type-1 quartz are rusty orange and anhedral and may represent the crystallization of hematite (?) as well as some other unknown minerals (Fig 3-1). These inclusions also often contain a "sweat" halo.

CO_2 – rich inclusions are common within Type-2 quartz from all samples belonging to the Plagioclase Rhyolite and Vesicular Rhyolite, and rarely (<<1%) in localized areas from type-1 quartz within sample GC16 (Quartz Rhyolite). CO_2-rich inclusions make up between 5 and 27% of the magmatic inclusions within samples GC17, GC4, GC14 and GC16, and range in size from <5 to 30μm. They vary widely in shape (from diamond-shaped to elongate to sub-spherical to irregular to hexagonal), but are mostly diamond-shaped and often have their long axis aligned with other CO_2-rich inclusions as well as aqueous fluid inclusions. Some examples show CO_2 inclusions with negative-crystal shapes (Fig 3-8). Small CO_2 inclusions are mostly dark, whereas large CO_2 inclusions at room temperature contain a large vapour-rich bubble in a CO_2-rich liquid. When heated the vapour bubble within CO_2-rich inclusions showed variable behaviour. In some examples, on heating, the vapour bubble contracted and disappeared

Table 3-2
A simplified table for the magmatic inclusion population for each sample from the Plagioclase Rhyolite and the Vesicular Rhyolite. Abbreviations for crystal shape include S.sph=sub-spherical, Elo = Elongate, Diam=Diamond, Irre=Irregular, Cub=cubic, S.cub= Sub cubic. Abbreviations for crystals include Amp=amphibole, Apa=apatite and Hal=halite. Note that late magmatic inclusions are excluded from this table.

Sample	Types of melt inclusions					Types of volatile-rich inclusions			Composite
	Granular textured melt inclusions (GTMI)	Granular textured melt inclusions with fluid (GTMIF)	Glass inclusion (GI)	Glass inclusion with crystal(s) (GIC)	Non-silicate melt inclusion	Magmatic aqueous fluid inclusion ± crystals	3-phase volatile inclusion (CO2 liquid + vapour and aqueous)	CO2 rich inclusion	Glass, non silicate and volatiles ±crystals
GC 17 Plagioclase Rhyolite	Size: 10-40μm Shape: S.sph-S.cub Abundance: 31% Crystal types: Amp-Apa Shrinkage bubble volume %: 1.8-7.1% Range; 4.5% Mean; 1.5% Std	Size: ~60μm Shape: S.sph-Elo Abundance: <1% Crystal types: Amp-Apa (?)	Size: 15-40μm Shape: S.cub-Elo Abundance: 3% Shrinkage bubble volume %: 0.8-2.7% Range; 1.7% Mean; 0.8% Std	Size: 10-30μm Shape: Cub-S.cub-S.sph Abundance: 9% Crystal types: Amp, Apa Shrinkage bubble volume %: 1.7-2.7% Range; 1.8% Mean; 1.0% Std	Size: <5-20μm Shape: S.sph-Irre Abundance: 6% Crystal types: Hal, unknown blue-green phase	Size: <5-45μm Shape: S.sph-Elo Abundance: 20%		Size: <5-30μm Shape: Diam-Elo Abundance: 26%	Size: <5-10μm Shape: S.sph Abundance: 4% Crystal types:
GC 4 Vesicular Rhyolite	Size: 5-65μm Shape: S.cub-S.sph-Elo Abundance: 40% Crystal types: Amp, Apa Shrinkage bubble volume %: 1.4-3.3% Range; 1.7% Mean; 1% Std	Size: 19-35μm Shape: S.sph-Diam Abundance: 6% Crystal types: Amp, Apa, Opaq Shrinkage bubble volume %: 1.5-7.5% Range; 3.3% Mean; 2.3% Std	Size: 10-20μm Shape: S.sph-Elo Abundance: 20% Shrinkage bubble volume %: 1.5-6% Range; 3.2% Mean; 1.7% Std	Size: 10-25μm Shape: S.cub-S.sph Abundance: 1% Crystal types: Opaq, Unkn(green) Shrinkage bubble volume %: 8-16% Range; 12% Mean; 4% Std	Size: <5-15μm Shape: S.sph Abundance: 1% Crystal types: Unknown blue-green and colourless phases	Size: <5-40μm Shape: S.Sph-Elo Abundance: 3%		Size: <5-30μm Shape: S.sph-Diam-Irr Abundance: 25%	Size: <5-20μm Shape: S.Sph Abundance: 4%
GC 14 Vesicular Rhyolite	Size: 20-50μm Shape: Sph-S.sph Abundance: 60% Crystal types: Unknown Shrinkage bubble volume %: 1-5% Range; 2.5% Mean; 1.3% Std			Size: 15-50μm Shape: Elo-S.sph Abundance: 14% Crystal types: Opaq, Apa, Fps(?) Shrinkage bubble volume %: 1-18% Range; 7% Mean; 5.5% Std		Size: 5-20μm Shape: S.sph-Elo Abundance: 12%	Size: 10-15μm Shape: S.sph-S.cub Abundance: <1%	Size: <5-20μm Shape: S.sph-Diam-S.cub Abundance: 10%	Size: <5-20μm Shape: S.sph-S.cub Abundance: 3%

Table 3-3
A simplified table for the magmatic inclusion population for each sample from the Quartz Rhyolite. Abbreviations for crystal shape include S.sph=sub-spherical,Elo = Elongate, Diam=Diamond, Irre=Irregular, Cub=cubic, S.cub= Sub cubic. Abbreviations for crystals include Amp=amphibole, Apa=apatite and Hal=halite. Note that late magmatic inclusions are excluded from this table

Sample	Types of melt inclusions				Types of volatile-rich inclusions		
	Granular textured melt inclusions (GTMI)	Granular textured melt inclusions with fluid bubble (GTMIF)	Glass inclusion (GI)	Glass inclusion with crystal(s) (GIC)	Non-silicate melt inclusion	Aqueous fluid inclusions.	Aqueous fluid inclusions with crystal(s)	CO_2 rich inclusion
GC 5 (Quartz Rhyolite)			Size: 15-60μm Shape: Sph-S.cub-Elo Abundance: 90% Shrinkage bubble volume %: 1.5-6% (Range) / 3.5% (Mean) / 1.2% (Std)	Size: 30-110μm Shape: Sph-Elo Abundance: 5%; Crystal types: Apa Shrinkage bubble volume %: 1.5-2.5% (Range) / 2% (Mean) / 0.8% (Std)		Size: 10-20μm Shape: Irre Abundance: 4%	Size: 10-20μm Shape: Cub-S.sph Abundance: 1% Crystal types: Hal	
GC 8 (Quartz Rhyolite)	Size: 20-45μm Shape: S.cub-S.sph-Elo Abundance: 70%; Crystal types: Amp, Apat Hal, Fps(?) Shrinkage bubble volume %: 4-12% (Range) / 4.5% (Mean) / 2% (Std)			Size: 15-55μm Shape: S.cub-S.sph-Elo Abundance: 30%; Crystal types: Amp, Apa, Flu, Hal Shrinkage bubble volume %: 3-14% (Range) / 7% (Mean) / 3.3% (Std)				
GC 11 (Quartz Rhyolite)	Size: 20-100μm Shape: S.sph-S.cub Abundance: 45%; Crystal types: Apa, Amp Shrinkage bubble volume %: 0.2-6% (Range) / 3.3% (Mean) / 1.7% (Std)			Size: S.cub-S.sph Shape: 10-85μm Abundance: 45%; Crystal types: Apa, Amp, Flu Shrinkage bubble volume %: 1.5-8% (Range) / 3.9% (Mean) / 1.9% (Std)				
GC 16 (Quartz Rhyolite)	Size: 20-90μm Shape: S.sph-Elo Abundance: 64%; Crystal types: Amp, Apa, Hal Shrinkage bubble volume %: 1-12% (Range) / 7% (Mean) / 2.8% (Std)	Size: 20-40μm Shape: S.sph-Dia Abundance: 3% Crystal types: Amp, Apa		Size: 10-75μm Shape: Cub-Dia Abundance: 30%; Crystal types: Amp, Apa, Hal Shrinkage bubble volume %: 1-18% (Range) / 7% (Mean) / 5.5% (Std)			Size: <5-40μm Shape: S.cub Abundance: 2% Crystal types:	Size: <5-20μm Shape: Irre-S.sph Abundance: <1%

(homogenization into a liquid), whereas in others the vapour bubble expanded, (homogenization into a vapour). Some CO_2-rich inclusions also showed critical behaviour, where the vapour bubble disappeared by neither contracting nor expanding on heating, and rapidly returned when cooled, in a boiling-like manner (i.e. critical behaviour), which according to Roedder (1984) correlates to a density of about 0.4 gm/cm^3. Assuming a trapping temperature of 850°C (based on the homogenization temperature of glass inclusions pers. comm.. V.Kamenetsky, University of Tasmania), a trapping depth of ~1.4 kbars can be estimated (assuming that the inclusions are pure CO_2) (*see* Roedder 1984).

H_2O-CO_2 volatile inclusions were identified within Type-2 quartz (Fig 3-7) from the Plagioclase Rhyolite (GC17) and the Vesicular Rhyolite (GC4) (making up less than 1% of the inclusion type in each sample) (Table 3-1). Three-phase volatile inclusions are characterized by a CO_2-rich vapour bubble, a CO_2-rich fluid outer rim and an outer pocket of an aqueous liquid. They range in size from <5-20μm, are elongate to sub-spherical and are aligned with CO_2 inclusions. When heated to temperatures above room temperature, the CO_2 vapour bubble and CO_2 fluid rim showed variable behaviour, which was identical to that already described for CO_2-rich inclusions (see above paragraph).

3.3.3. Composite Inclusions

Composite inclusions are uncommon (0-<2% *see* Table 3-1 and 3-2) and each was identified from Type-2 quartz *senso stricto* (Fig 3-9) from the Plagioclase Rhyolite and the Vesicular Rhyolite. Composite inclusions can be divided into three groups (Fig 3-1), which include: 1) volatile-glass-non silicate inclusions, 2) glass-non silicate inclusions and 3) CO_2-non-silicate.

Volatile-glass-non silicate inclusions were identified within the Vesicular Rhyolite (GC4) and range from sub-cubic to irregular and from 5 to 20μm. Examples consist of an inner globular bubble which consists of volatile and non-silicate phases, whereas the outer region of the inclusion is silicate-glass (Fig 3-1).

Glass-non silicate inclusions were identified within the Plagioclase Rhyolite Quartz Rhyolite (GC17) and range in size from 10 to 40μm. They are elongate and are

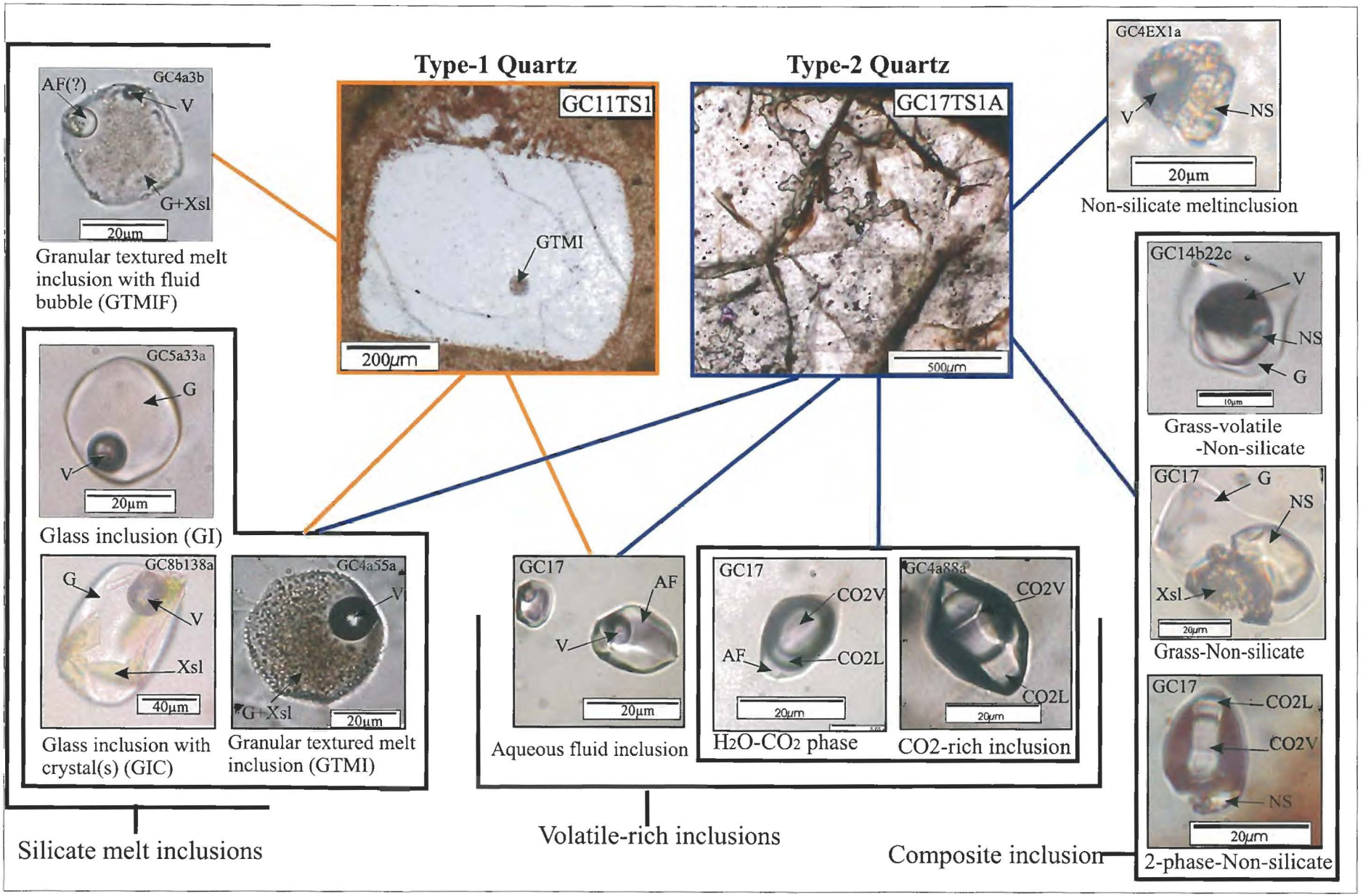

Figure 3-9
Flow chart of the different types of inclusions hosted by quartz from the Eucarro Rhyolite. Note that the blue lines link those inclusions which are found in Type 2 quartz, whereas orange lines link those that are found in Type 1 quartz. Abbreviations used include CO2L=CO2 liquid, CO2V=CO2 vapour NS=non-silicate melt, G=glass, V=vapour, Xsl=crystal and AF=aqueous fluid.

dominated by silicate glass with a sub-spherical, colourless bead of non-silicate melt within the central region of the inclusion, which makes up <20 vol% of the inclusion. These inclusions do not contain a shrinkage bubble. Some examples show patches of fine crystalline growths within the glass (Fig 3-1).

2-phase non-silicate inclusions are indistinguishable from CO_2 inclusions (*see* above) except that they contain a pocket(s) of colourless sub-spherical non-silicate melt along the inner walls of the inclusion. These inclusions were only identified in one sample from the Plagioclase Rhyolite.

3.4. Heating experiments on melt inclusions

3.4.1. Non-silicate melt inclusions

Heating experiments were performed on non-silicate melt inclusions to observe temperature of phase transformations (e.g. melting, homogenization and crystallization). A Linkam TS1500 heating stage with TMS 94 temperature control unit and an Olympus BX51 microscope with a DP11 digital camera were used. Heating and cooling rates throughout the experiment varied from 100 to 1°C/min.

Non-silicate inclusions from the Vesicular Rhyolite (GC4) were selected for the heating experiment (Fig 3-10A-H). Observations from the experiment include; 1) visible changes occurred at 170°C, with the rearrangement of solids and movement of the shrinkage bubble, 2) inclusions completely melted by about 330°C, 3) at above 330°C olive green acicular silicate crystals as well as colourless silicate globular phases were the only solid phases remaining within the inclusion, 4) between 400 and 500°C the boundary between the inclusion and host quartz became invisible, 5) movement of the bubble at 514°C and an opaque phase formed within the vapour bubble, 6) at 799°C the vapour bubble began to shrink, 7) during cooling at 330°C the non-silicate melt separated into two liquid phases. Several subsequent heating runs were carried on the inclusions and showed consistent results. During the final run the inclusion was cooled at a rate of 1°C/min and the immiscible phases were kept separate during crystallization (Fig 3-10H).

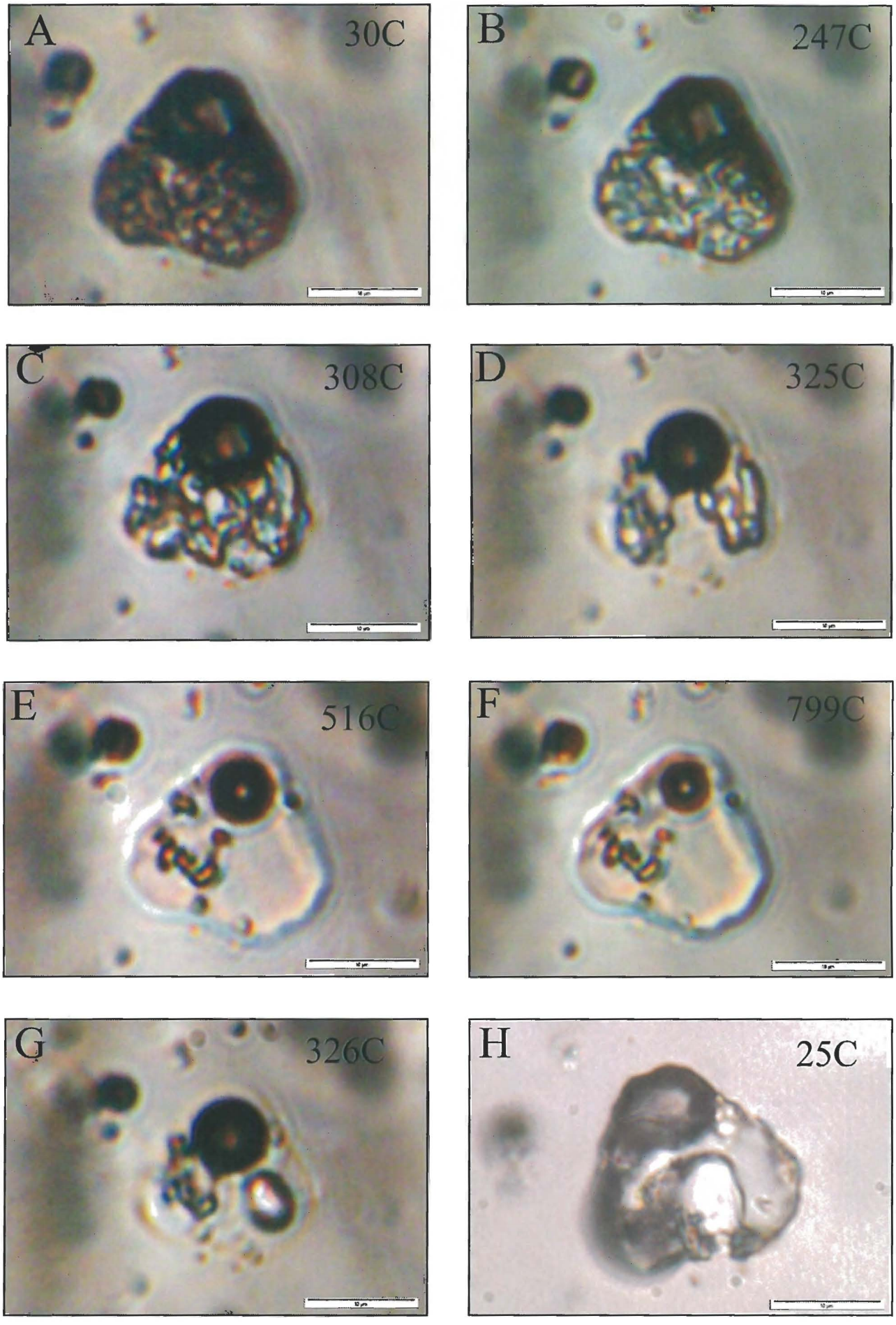

Figure 3-10
Phase transformations in non-silicate melt inclusions from Type 2 quartz (GC4) during heating stage experiments (*see* section 3.4.1. for details).

The characteristics of the above heating experiment are similar to those reported by Kamenestsky *et al.* (2004) for non-silicate phases from the Omsukchan granite, which were interpreted to be Cl-rich fluid (brine), although the final separation of the non-silicate into immisible phases was not reported by Kamenetsky *et al.* (2003). Moreover, Laser Raman spectroscopy also suggests that one of the immiscible phases may be Cl-rich.

3.5. Inclusions from the Plagioclase Rhyolite

Sample GC17 was selected from the Plagioclase Rhyolite for the magmatic inclusion study. This sample contains GTMI, GTMIF, GI, GIC, aqueous fluid inclusions, CO_2-rich inclusions, non-silicate melt inclusions and composite inclusions (Table 3-1), with GTMI (55%), GIC (20%) and CO_2-rich inclusions (15%) being the dominate inclusion type.

Figure 3-11 demonstrates that silicate melt inclusions are between 8 and 40μm in diameter (average 22μm) and have shrinkage bubbles which make up between 1 and 7vol% of the inclusion. Table 3-1 show that GTMI have larger shrinkage bubble-inclusion volume ratios (average 4.5 vol% (stdev =1.5 vol%)) when compared to GI and GIC (average 1.7 (stdev = 0.8 vol%) and 1.8 vol% (stdev = 1.0 vol%) respectively).

3.6. Inclusions from the Vesicular Rhyolite

Samples GC4 and GC14 were selected from the Vesicular Rhyolite for the magmatic inclusion study, whereas sample GC15 was excluded because it lacked magmatic quartz. Both studied samples contain GTMI, GI, GIC, non-silicate melt inclusions, aqueous fluid inclusions, CO_2-rich inclusions and composite inclusions, with GTMI (40-50%), GI (20-5%) and CO_2-rich inclusions (25-5%) being the dominant inclusion types for samples GC4 and GC14 respectively. GIC are also abundant within sample GC14 (25%), however they are sparse within sample GC4 (1%).

The diameter of silicate melt inclusions within the Vesicular Rhyolite ranges from 5 to 65μm (average 26μm) (Fig 3-10). Shrinkage bubbles within melt inclusions make up

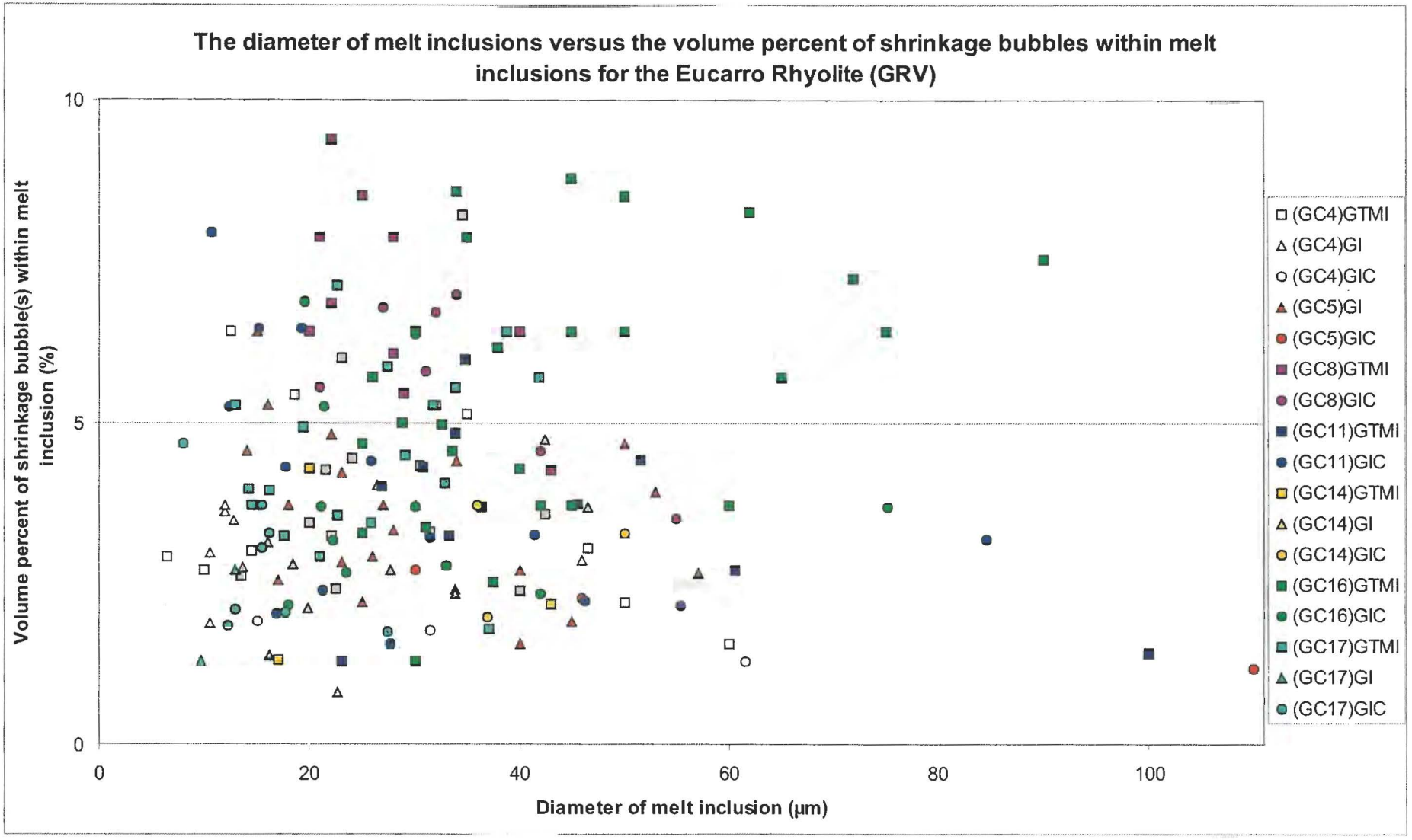

Figure 3-11

A distribution of the inclusion size versus the percent volume of their shrinkage bubble. Note that the diameter of melt inclusions was determined by carefully measuring the inclusions on large digital photos. Volumes were then calculated from the measured diameters for shrinkage bubbles and inclusions. Note that those inclusions that are not spherical had their volume calculated using the volume formula of other shapes that they resembled. From the diagram it can be determined that most melt inclusions are between 10 and 60 μm in diameter and most inclusions have shrinkage bubbles which make up between 1 and 8 vol% of the inclusion. Furthermore, inclusions from samples GC5, GC4 and GC14 mostly have shrinkage bubbles between 2 and 5vol%, whereas other samples show larger variations (particularly samples GC16 and GC8).

between 1 and 5 vol% of the inclusion and no significant difference exists between the average shrinkage bubble-inclusion volume ratio between inclusion types, which was between 3 to 3.6 vol% for all inclusion types (except a small number (1%) of GIC from sample GC4, which average 1.5 vol% and stdev 0.3 vol%), with a standard deviation between 1.3 vol% and 2.3 vol% (*see* Table 3-1).

3.7. Inclusions from the Quartz Rhyolite

Four samples (GC5, 8, 11 and 16) from the Quartz Rhyolite were selected for the magmatic inclusion study. All studied samples contain GIC, however only samples GC8, 11 and 16 contain GTMI, and only sample GC5 contain GI. GTMIF were only identified in sample GC16 (3%). Volatile-rich inclusions identified within the Quartz Rhyolite vary from sample to sample, with samples GC5 and GC11 containing aqueous fluid inclusions, and samples GC5 and GC16 containing aqueous fluid inclusions with crystals. CO_2-rich inclusions were identified in one sample (GC16). GTMI is the dominant inclusion type within all samples (45-70%), except sample GC5, which is dominated by GI (90%). GIC are abundant within all samples and make between 5 and 45% of the inclusion type (*see* Table 3-2).

Silicate melt inclusions within the Quartz Rhyolite range from 10 to 110μm across (average 36μm) (Fig 3-10), and have shrinkage bubble(s) which make up between 1 and 9 vol% of the inclusion. No significant difference in the shrinkage bubble(s)-inclusion volume ratio exists between GTMI, GIC (except GC5) and GI from all samples, with inclusions having average shrinkage bubble volumes between 3.5 and 6.6 volume percent and a standard deviation of between 1.2 and 2 vol% (*see* Table 3-2). One exception is GIC from sample GC5, which contain shrinkage bubbles which make up between 1.5 and 2.5 vol% of the inclusion (average 2 vol% and stdev 0.8 vol%). The lower ratio of shrinkage bubble-inclusion volume may, however, be attributed to an increase in volume due to the addition of large co-trapped apatite crystals which are common in sample GC5, but uncommon in other samples.

3.8. Comparison of samples

The population of inclusions within a particular sample is determined by the type of quartz present in the sample. Chapter 2 shows that Type-1 and Type-2 quartz is present in all samples from the Plagioclase Rhyolite and the Vesicular Rhyolite, whereas samples from the Quartz Rhyolite only contain Type-1 quartz. Thus, samples from the Plagioclase Rhyolite and the Vesicular Rhyolite both contain significantly more volatile-type inclusions, such as CO_2-rich inclusions, aqueous inclusions (±crystals), non-silicate inclusions and composite inclusions. In contrast, all samples from the Quartz Rhyolite have no composite inclusions, are free of CO_2-rich inclusions (one exception being GC16) and poor in volatile-rich inclusions. In contrast, silicate inclusions from all samples are quite similar in size, shape, and shrinkage bubble volume ratio.

Chapter 4

Geochemistry of the Hiltaba Granite, Eucarro Rhyolite, Yardea Dacite and melt inclusions from the Eucarro Rhyolite

4.1. Introduction

The purpose of this chapter is to determine if geochemical links exist between the Hiltaba Granite, Yardea Dacite, Eucarro Rhyolite and silicate melt inclusions from the Eucarro Rhyolite (both homogenized and non-homogenized) by comparing major and trace element data. This chapter also compares the composition of the groundmass of the Eucarro Rhyolite (degassed melt) with melt inclusions (melt trapped at depth) in order to determine which elements were lost during degassing.

One of the major problems with comparing the geochemistry of the Eucarro Rhyolite with melt inclusions, Hiltaba Granite (unaltered (Fig 4-1 and 4-2)) and Yardea Dacite (unaltered (Fig 4-3 and 4-4)) is the alteration of Eucarro Rhyolite (Chapter 2). This variable presents a significant problem, as there is no accurate way of determining which elements have been lost and to what degree they have been lost. Of serious concern are 'mobile' elements (e.g. alkalis, F and U) and of less concern are 'immobile' elements (e.g. Al, REE and Zr). In order to tackle this problem I have included, for the purpose of this chapter, major and trace element analysis from a fresh unaltered volcanic rock from the basal unit of the Yardea Dacite (1592±3Ma), which lies immediately above the Eucarro Rhyolite (1591±3Ma) and was erupted between 0-7 m.y. (best constraint) after the Eucarro Rhyolite (U-Pb zircon dating: Fanning *et al.*, 1988). This rock, the Hiltaba Granite and melt inclusions are used here to determine if the Eucarro Rhyolite, which has undergone hematite+chlorite+sericite and carbonate alteration, shows any significant geochemical deviations from simple fractionation. Furthermore, major and trace element data from other studies (Ferris, 2001; Allen *et al.*, 2003) are also used here

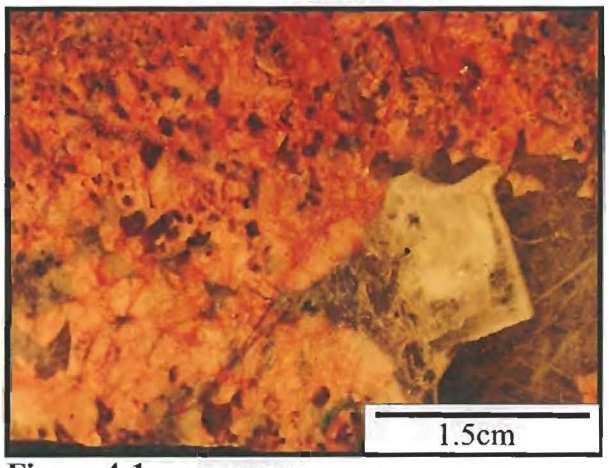

Figure 4-1

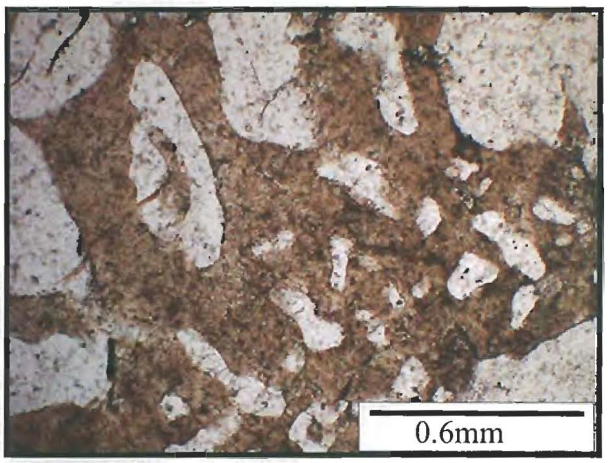

Figure 4-2

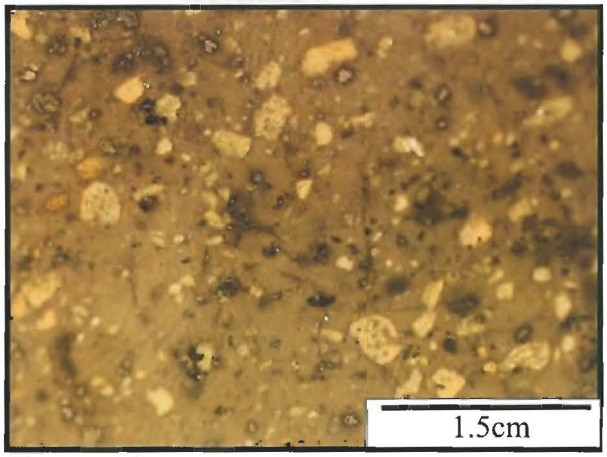

Figure 4-3

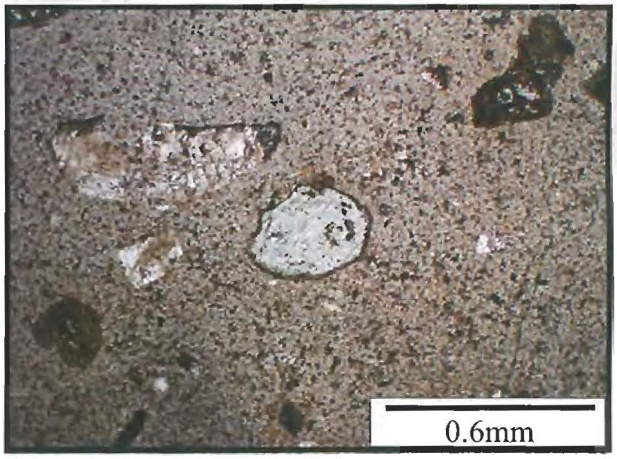

Figure 4-4

Figure 4-1 Polished thick section of the Hiltaba Granite collected from drill core and courtesy of Aquila Resourses (sample R650345: Weednanna OOWDD5, PIRSA drill core library) showing a miarolitic cavity on the right, which is filled with fluorite, calcite and quartz. Note that feldspar phenocrysts are fresh and unaltered.

Figure 4-2 Thin section of the Hiltaba Granite collected from drill core and courtesy of Aquila Resourses (sample R650345: Weednanna OOWDD5, PIRSA drill core library), which shows anhedral quartz grains intergrown with feldspar.

Figure 4-3 Polished block from the Yardea Dacite (sample YD 189: Sharon Allen's collection, UTas), which contains fresh feldspar and pyroxene phenocrysts.

Figure 4-4 Thin section of the Yardea Dacite (sample YD 189: Sharon Allen's collection UTas). Note the fresh pyroxene phenocryst in the center of the photo.

to determine if the samples used in this study are typical of the Hiltaba Granite, Eucarro Rhyolite and the Yardea Dacite.

4.2. Sample preparation and analytical methods

4.2.1. Whole rock

All samples analysed for this thesis were either collected from drill core (Hiltaba Granite) or outcrop, which were collected in the field by Nicole Morrow (Eucarro Rhyolite) and Dr Sharon Allen (Yardea Dacite). Not all of the whole rock data used in this chapter is my own; major element analysis from the Eucarro Rhyolite was previously undertaken by Nicole Morrow as part of her honours thesis (1998) (*see* Table 4-1), and some trace element data (x-ray fluorescence (XRF)), also obtained by Morrow (1998), is used in this chapter as a comparison with the new ICPMS (inductively coupled plasma emission mass spectrometer) data (*see* Table 4-3). Also, some rock powders previously prepared by Morrow (1998) were used in this study for trace element analysis of Eucarro Rhyolite.

Sample preparation techniques used by Morrow (1998) were followed on all new samples (*see* Appendix 4), except a tungsten carbide-faced ring mill was used on new samples, whereas a Cr and Fe-faced ring mill was used by Morrow (1998). Hence contamination within new samples is limited to W, C, Co and Ta; whereas Fe and Cr are contaminants in Morrow's samples (*see* Table 4-2). It is also important to note that all samples prepared by either Morrow (1998) or me were free of mafic xenoliths, lithic fragments, amygdaloidal quartz and weathered surfaces.

Major element data for whole rocks were obtained by XRF analysis (also a small range of trace element data) (Table 4-3), although fluorine was analyzed using an ion specific electrode (Table 4-2). Trace element data for whole rocks were obtained using an inductively coupled plasma emission mass spectrometer (ICPMS). A comparison of the XRF and ICPMS trace element data (Table 4-3) shows that XRF data for some elements (e.g. Ti, Y, Zr, Sr, Ce, Nd, Th and U) are within 10% of ICPMS values, whereas other elements are within 30% (e.g. Sc, V, Rb, Nb, La and Pb). In this study, the ICPMS data is

Table 4-1
A list of whole rock samples and their milling preparation prior to major and trace element analysis.

Sample	Description	Milling
GC17 (Eucarro Rhyolite)	Plagioclase Rhyolite	Cr-Fe faced mill
GC4 (Eucarro Rhyolite)	Vesicular Rhyolite	Cr-Fe faced mill
GC14 (Eucarro Rhyolite)	Vesicular Rhyolite	Cr-Fe faced mill
GC15 (Eucarro Rhyolite)	Vesicular Rhyolite	Cr-Fe faced mill
GC5 (Eucarro Rhyolite)	Quartz Rhyolite	Cr-Fe faced mill for major elements. Tungsten Carbide faced mill for trace elements and fluorine.
GC8 (Eucarro Rhyolite)	Quartz Rhyolite	Cr-Fe faced mill
GC11 (Eucarro Rhyolite)	Quartz Rhyolite	Cr-Fe faced mill
GC16 (Eucarro Rhyolite)	Quartz Rhyolite	Cr-Fe Faced mill
AB1 Hiltaba Granite	Coarse Grained Granite	Tungsten Carbide faced mill
AB3 Hiltaba Granite	Medium Grained Granite	Tungsten Carbide faced mill
AB4 Yardea Dacite	Pyroxene Phyric Dacite	Tungsten Carbide faced mill

the most accurate; however, Ba and Sr data from XRF analysis is used as opposed to ICPMS as these are found within the digestion solution (H_2SO_4), which was required for ICPMS preparation.

All analyses (including those from Allen *et al.*, 2003) were carried out at the University of Tasmania, except for fluorine analyses, XRF (by Morrow, 1998) and Hiltaba Granite analyses by Ferris (2001), which were carried out at SGS Welshpool Minerals, Western Australia, Mineral Resources, Tasmania and Ambel Laboratories, Adelaide respectively. In order to confirm that the results obtained for fluorine were satisfactory, a sample with a known fluorine concentration was included for the analysis, which subsequently proved to be within error (±0.0050 wt%) (Table 4-2).

Table 4-2
Fluorine analysis of whole rock from the Eucarro Rhyolite, Hiltaba Granite and Yardea Dacite. Analysis was carried out by SGS Welshpool Minerals, Western Australia using an Ion Specific Electrode with a detection limit of 50ppm. Note that a UTas internal standard was included in the analysis (Tas Granite), which is known to have a F concentration of between 700 and 740ppm. Abbreviations are PR=Plagioclase Rhyolite, VR=Vesicular Rhyolite, QR=Quartz Rhyolite, HG(C)=coarse grain Hiltaba Granite, HG(M)=medium grained Hiltaba Granite and YD=Yardea Dacite.

Sample	GC17	GC4	GC14	GC5	GC8	GC11	GC16	AB1	AB3	AB4	Tas Granite
Rock type	PR	VR	VR	QR	QR	QR	QR	HG(C)	HG(M)	YD	Internal standard
Fluorine concentration (ppm)	1450	1250	1450	1500	1650	1300	1700	450	1100	1100	680

*Detection limit 50ppm.

4.2.2. Groundmass of the Eucarro Rhyolite

A major element concentration of the groundmass was obtained from Kamenetsky *et al.* (2000) in which 120 spots were analyzed using a Cameca SX50 microprobe with a defocused beam (~25 X 25μm) at the University of Tasmania. Samples analyzed included GC17 (Plagioclase Rhyolite), GC4 and 14 (Vesicular Rhyolite) and GC8 and 11 (Quartz Rhyolite), and elements analyzed included Si, Ti, Al, Fe, Mg, Ca, Na, K and P (Table 4-4).

During this study trace element analysis of the groundmass was carried out using laser ablation-ICPMS (LA-ICPMS) at the University of Tasmania. Twenty four spots from six samples (GC17, 14, 5, 8, 11 and 16) were analyzed using a beam size of 110μm and a frequency of 10Hz. Elements analyzed included Al, Si, Ca, Ti, Cu, Zn, Rb, Sr, Y, Zr, Nb, Mo, Ag, Sn, Ba, La, Ce, Nd, Sm, Eu, Gd, Dy, Er, Yd, W, Au, Pb, Th and U (*see* Table 6-4) and concentrations were determined using SiO_2 from microprobe analysis as an internal standard. All thin sections analyzed by Kamenetsky *et al.* (2000) were

checked by using a microscope and are optically similar to those that were analyzed using LA-ICPMS.

SiO_2 was chosen as the internal standard because of the high concentration (~80 wt%) within the volcanics and the comparably low standard deviations (i.e. ±5 wt%). When lower SiO_2 values were used (e.g. 75 wt%) the calculated value for trace elements did not differ significantly.

4.2.3. Melt inclusions

For melt inclusion analysis, one set of 0.3-1mm quartz fractions (~150) for each sample from the Eucarro Rhyolite were placed into an oven and heated to 850°C for 70 hours and than air quenched to homogenize all inclusions and to expose decrepitated inclusions. A second set of 0.3-1mm quartz fractions was placed in an oven and heated to 850°C for 20 hours and than air quenched for the same purpose; while a third unheated set from one sample (GC11) was selected. Selected quartz sets were than glued into epoxy mounts and polished. Quartz fractions which hosted large non-decrepitated silicate melt inclusions (>40μm) were selected for analyses and were lifted from the epoxy mount using a soldering iron. Selected quartz grains were than glued again into a second epoxy mount and carefully polished until melt inclusions were exposed. Once melt inclusions were exposed, quartz grains were again lifted out of the epoxy mount and then glued into a final epoxy mount. The final mount was carefully polished and then cleaned in an ultrasonic cleaner for 40 minutes and finally wiped with methanol before being place in an oven (45°C) to dry for 30 minutes.

Exposed silicate melt inclusions and their daughter crystals were analyzed for Si, Al, Fe, Na, K, Ca, F, Cl, Mn, Ti, P, S, Ba and Mg by electron microprobe (Cameca SX 100). An accelerating voltage of 15 kV, a low beam current of 15 nA, a large beam diameter of 5-10 μm and a counting time of 3 sec were chosen to avoid volatilization of the alkalis from melt inclusions. Sodium, being the most prone element to volatize, was always analyzed first. One to three spots were analyzed on each inclusion, and to avoid overlap with the host quartz during analysis, measurements were made near the centre of the melt inclusion.

Those inclusions which were analyzed using microprobe were also used to analyze for trace elements with LA-ICPMS at the University of Tasmania. Elements analyzed included Be, B, Al, Ca, Ti, Cu, Zn, Rb, Sr, Y, Zr, Nb, Mo, Ag, Sn, Ba, La, Ce, Nd, Sm, Eu, Gd, Dy, Er, Yd, W, Au, Pb, Th and U (*see* Table 4-6) and concentrations were determined using Al_2O_3 from microprobe analysis as an internal standard. Some analyses were also carried out on unexposed inclusions, which were assumed to have the same average Al_2O_3 concentration as other exposed inclusion(s) that had previously been analyzed using microprobe and occurred within the same quartz grain. Laser conditions during analysis included a beam size of 55μm (although the beam was sometimes increased to 80μm for large inclusion (>100μm)) and a frequency of 5Hz. During some analyses, crystal phases were accidentally analyzed, which resulted in spikes (e.g. Fig 4-13 shows a Sn spike due to the accidental analyses of a crystal phase). In order to determine the composition of the glass within inclusions, spikes were removed.

4.3. Geochemistry of whole rocks

As mentioned above, one of the main objectives of this chapter is to compare rocks from the Eucarro Rhyolite with unaltered rocks from the Hiltaba Granite and Yardea Dacite. However, before any comparisons can be made it is first important to determine if all studied samples are representative of the province. To do this, I have included major element analyses from seventy seven samples from the Gawler Range Volcanics (from Allen *et al.*, 2003) and fifty one samples from the Hiltaba Granite (from Ferris, 2001) and plotted them collectively with samples chosen for this study on a series of Harker Diagrams (Fig 4-5) (all samples have been recalculated to 100% anhydrous compositions).

One of the difficulties with comparing volcanics and granites is that the latter are crystal-rich, whereas the former are groundmass (melt)- rich. This poses problems when comparing the concentration of incompatible elements (e.g. HREE and F), which are preferably partitioned into the melt (i.e. groundmass) rather than crystal phases during fractionation. As a result the coarse-grained granite is significantly depleted in HREE and

F when compared to the medium-grained granite and the volcanics (*see* Table 4-3 for comparison).

4.3.1. Major elements

Figure 4-5 demonstrates that all samples, apart from the Hiltaba Granite, are characterized by a tight range of SiO_2 values (e.g. Yardea Dacite (67-70 wt%), Quartz Rhyolite (73-75 wt%), Plagioclase Rhyolite and Vesicular Rhyolite (70-73 wt%)). The Hiltaba Granite in contrast is characterized by a large range of SiO_2 values (67-80 wt%), with the two samples chosen for this study having 75 and 78 wt%.

Major elements, such as Al, Fe, Ti and Mg, plot against SiO_2 as a linear array with a negative slope on the Harker Diagrams (Fig 4-5 A, B, and D and Fig 4-6F), which is consistent with crystallization (subtraction) dominated by pyroxene (Mg and Fe), FeTi oxides and plagioclase (Al). In contrast, Na, K and Ca plot as weak linear arrays which suggest limited element mobility (Fig 4-5C, E and F).

P_2O_5, from the volcanics shows an exponential decrease with increasing SiO_2 (Fig 4-5H), but a positive linear increase when plotted against Fe_2O_3+MgO (Fig 4-5I), suggesting that apatite fractionation is strongly associated with mafic minerals. P_2O_3 from the Hiltaba Granite is much more scattered than the volcanics when plotted against SiO_2 and Fe_2O_3+MgO, but overall shows similar trends to the volcanics.

Fluorine comparisons are not easily evaluated, as most geochemical studies previously carried out on the Gawler Range Volcanics and Hiltaba Granite have not included F. Studies from Olympic Dam (Creaser, 1991), however, showed that coeval felsic granites (~71 wt% SiO_2) yielded concentrations of 0.215 to 0.264 wt%, which are considerably higher than values of 0.045 and 0.11 wt% reported here. Creaser (1991) also reported a fluorine value of 0.18 wt% for the Yardea Dacite from the Stuart Shelf, which is also higher than the value of 0.11 wt% reported here. To my knowledge, no previous studies have reported F concentrations from the Eucarro Rhyolite and results reported here are 0.140 wt% (Plagioclase Rhyolite), 0.125-0.145 wt% (Vesicular Rhyolite) and 0.130-0.17 wt% (Quartz Rhyolite). The limited data presented in this study suggests that the volcanics show an increase in F with increasing SiO_2 (Fig 4-5G); however, this does

Table 4-3

Major group elements (XRF) and trace element (XRF and ICPMS) data of whole rocks from the Eucarro Rhyolite, Hiltaba Granite and Yardea Dacite. Note that all XRF data from the Eucarro Rhyolite (grey) was acquired from Nicole Morrow's honour thesis (1998). Abbreviations used for lithology include Plagioclase Rhyolite=PR, Vesicular Rhyolite=VR, Quartz Rhyolite=QR, CoarseHiltaba Granite=(C)HG, Meduim Hiltaba Granite=(M)HG and YD=Yardea Dacite. Also note that * corresponds to S% rather than S03%.

Sample	GC17	GC4	GC14	GC15	GC5	GC8	GC11	GC16	AB1	AB3	AB4
Lithology	PR	VR	VR	VR	QR	QR	QR	QR	(C)HG	(M)HG	YD 189
LOI%	1.56	1.34	1.53	1.17	1.04	0.73	0.86	1.01	1.79	1.98	1.08
SiO2%	69.60	69.97	70.32	69.81	73.78	73.76	74.51	73.98	77.39	74.97	68.61
TiO2%	0.41	0.45	0.41	0.43	0.26	0.25	0.26	0.26	0.13	0.17	0.72
Al2O3%	13.34	13.60	13.59	13.45	12.42	12.83	12.29	12.46	11.10	12.00	13.41
Fe2O3%	3.95	4.07	3.66	4.28	3.34	2.43	2.40	2.64	1.13	1.68	4.96
MnO%	0.10	0.11	0.06	0.12	0.09	0.07	0.06	0.06	0.03	0.03	0.10
MgO%	0.67	0.89	0.73	0.89	0.25	0.31	0.40	0.41	0.30	0.32	0.85
CaO%	1.07	0.44	0.41	0.57	0.33	0.59	0.40	0.46	0.57	0.58	1.92
Na2O%	2.77	2.96	3.27	2.97	2.20	2.94	2.22	2.60	2.64	2.73	3.02
SO3%	0.07	0.07	0.08	0.07	0.07	0.08	0.07	0.07	0.01	0.01	5.10
P2O5%	0.08	0.09	0.07	0.09	0.02	0.03	0.01	0.01	0.02	0.03	0.20
K2O%	5.64	5.43	5.26	5.50	5.78	5.48	6.13	5.49	4.87	5.38	1.08
SO3%	0.07	0.07	0.08	0.07	0.07	0.08	0.07	0.07	0.01*	0.01*	0.01*
Sum	99.26	99.42	99.39	99.35	99.58	99.50	99.61	99.45	99.96	99.87	99.98

7 Li	16.91	14.89	11.80	15.83	7.02	9.69	11.46	13.61	4.50	5.56	14.87
9 Be	5.22	3.44	3.93	4.91	6.87	5.60	3.57	5.25	6.36	7.01	4.29
45 Sc	8.54	8.95	8.79	9.14	6.13	5.10	5.27	5.51	1.85	3.74	11.26
Sc(XRF)	<9	9	<9	9	<9	<9	<9	<9	<2	3	9.27
47 Ti	2619	2784	2620	2817	1687	1499	1603	1662	721	1035	4565.65
Ti(XRF)	2500	2700	2500	2600	1558	1500	1600	1600	750	1032	4336.87
51 V	9.7	11.2	9.2	11.1	2.0	2.9	3.2	3.1	2.5	2.6	30.28
V(XRF)	11	18	11	15	7	<5	<5	<5	3	2	28.14
53 Cr	133.8	121.2	158.1	110.7	0.5	158.9	161.2	180.2	0.7	0.9	4.33
Cr(XRF)									1	2	5.15
55 Mn	729	819	483	912	749	552	481	452	223	264	814.88
59 Co	2.87	3.13	3.40	3.12	WC mill	1.30	1.37	1.28	WC mill	WC mill	WC mill
60 Ni	3.7	3.4	4.9	3.1	1.9	3.4	3.6	3.7	5.4	5.2	4.76
Ni(XRF)									7	6	7.53
63 Cu	3.0	19.7	4.8	4.4	2.0	4.9	3.7	8.0	1.6	2.8	8.23
Cu(XRF)									<1	<1	9.49
66 Zn	95	81	80	121	111.4	55	60	51	14	20	87.47
Zn(XRF)									13	18	83.70
71 Ga	21.4	21.1	22.5	21.1	21.3	19.7	20.9	20.7	17.6	19.8	20.94
85 Rb	331	261	255	304	283	319	366	338	284	340	240.61
Rb(XRF)	252	223	207	246	272	263	302	263	264	285	208.52
88 Sr	77.0	72.4	83.7	91.9	27.9	47.8	41.5	37.2	21.1	26.1	174.30
Sr(XRF)	58	79	89	95	36	51	47	41	24	28	176.80
89 Y	61.1	61.6	62.4	61.6	58.6	69.1	65.4	65.1	28.9	51.4	53.30
Y(XRF)	69	62	63	66	60	68	65	66	29	49	52.08
90 Zr	482	475	488	499	385	376	398	400	137	131	452.07
Zr(XRF)	467	444	460	440	365	351	366	367	138	130	459.85
93 Nb	25.9	25.4	25.8	26.5	25.8	27.1	28.4	29.4	11.1	15.5	17.80
Nb(XRF)	25	24	24	23	28	27	29	28	16	21	20.82
95 Mo	1.19	1.56	1.17	1.59	0.71	1.40	1.30	1.60	0.43	0.58	2.08
118 Sn	4.50	4.61	4.53	4.78	5.38	5.49	5.55	5.85	9.28	7.91	4.62
121 Sb	0.44	0.43	0.31	0.34	0.34	0.36	0.24	0.42	0.01	0.02	0.25
133 Cs	3.25	2.68	1.61	3.21	2.00	2.00	2.30	2.55	0.74	0.86	2.72
137 Ba	1060	1163	1026	1054	708	726	756	631	118	99	866.73
Ba(XRF)	1064	1167	1040	1138	609	653	687	585	112	94	1128.24
139 La	87.8	87.6	81.4	82.2	103	112.4	96.7	98.1	84.8	136.4	73.05
La(XRF)	111	110	104	98	109	142	123	125	85	129	72.61
140 Ce	171.8	166.7	161.5	165.3	202	197.6	188.3	190.4	164.9	263.4	148.58
Ce(XRF)	186	180	184	183	200	221	200	202	171	262	156.11
141 Pr	20.2	20.1	19.1	19.3	23.4	24.2	21.7	21.9	17.1	27.7	17.19
146 Nd	74.7	73.2	70.7	71.8	78.8	85.9	78.1	80.3	52.3	86.8	63.12
Nd(XRF)	79	69	65	69	28	83	76	82	56	94	67.04
147 Sm	13.94	13.83	13.26	13.53	14.1	15.46	14.37	14.41	7.78	14.09	11.95
153 Eu	2.29	2.34	2.28	2.27	1.23	1.39	1.23	1.13	0.38	0.55	1.90
157 Gd	11.99	11.85	11.92	11.71	11.4	13.49	12.26	12.05	5.37	9.99	10.19
159 Tb	1.89	1.88	1.88	1.88	1.84	2.06	1.99	1.92	0.85	1.58	1.61
163 Dy	11.12	10.96	11.02	11.04	10.4	11.89	11.68	11.44	4.89	9.12	9.47
165 Ho	2.22	2.22	2.21	2.22	2.05	2.38	2.32	2.30	1.03	1.78	1.89
166 Er	6.66	6.56	6.57	6.66	6.23	6.90	6.86	6.82	3.31	5.23	5.58
169 Tm	0.99	0.97	0.97	0.98	0.93	1.01	1.03	1.03	0.52	0.80	0.82
172 Yb	6.21	6.21	6.25	6.37	6.07	6.54	6.53	6.54	3.43	5.19	5.36
175 Lu	0.95	0.92	0.95	0.96	0.91	0.98	0.96	0.97	0.53	0.75	0.81
178 Hf	11.72	11.46	11.64	12.03	10.7	10.11	10.59	10.31	5.20	4.31	10.82
181 Ta	1.22	1.17	1.24	1.25	2.61	1.35	1.37	1.29	1.63	1.59	1.04
182 W	1.12	0.97	0.51	0.90	WC mill	0.36	0.26	0.76	WC mill	WC mill	WC mill
205 Tl	1.38	1.02	0.93	1.16	1.20	1.19	1.33	1.26	1.56	1.63	0.95
208 Pb	7.49	10.9	5.4	11.1	7.47	34.7	7.52	8.42	16.4	18.6	30.64
Pb(XRF)									15	18	31.55
209 Bi	0.11	0.30	0.03	0.20	0.17	0.13	0.14	0.08	0.06	0.07	0.11
232 Th	33.1	30.1	30.7	31.8	37.4	37.7	39.2	40.6	80.3	114.7	26.26
Th(XRF)									87	123	27.45
238 U	6.28	6.2	5.97	6.78	3.23	9.02	7.41	7.23	18.9	19.0	5.61
U(XRF)									20	21	6.06

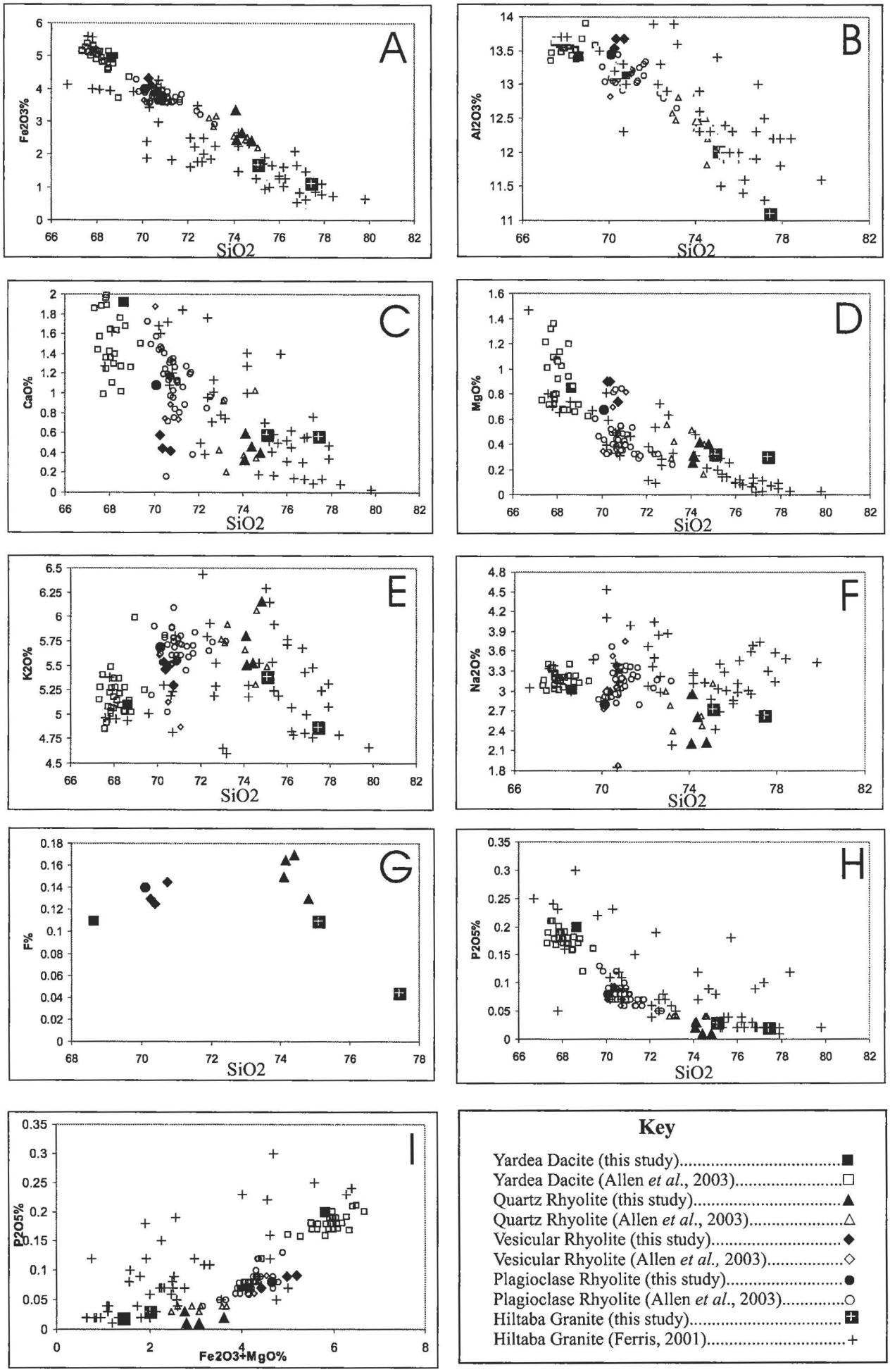

Figure 4-5. Major element geochemistry of whole rocks from the Hiltaba Granite, Yardea Dacite, and the Plagioclase Rhyolite, Vesicular Rhyolite, Quartz Rhyolite from the Eucarro Rhyolite. Note that data used in this study are filled, whereas comparison unfilled shapes represent and samples from other studies (*see* Key).

not determine if F has been lost from the Eucarro Rhyolite from alteration, and therefore it is difficult to ascertain if this is a true fractionation trend.

Samarium and fluorine are similar in their compatibility during fractionation and mantle melting (Sun and McDonough, 1989). Thus, Sm and F in magmatic systems both become enriched in the melt during fractionation (Fig 4-6A). Alternatively though, Sm, unlike F, is immobile during alteration processes and therefore acts as an effective indicator to determine if significant amounts of F have been lost during alteration, or gained during hydrothermal activity. To determine if significant amounts of F have been lost or gained from the volcanics, F/Sm is plotted against SiO_2 (Fig 4-6B) and demonstrates that the volcanics (both altered and unaltered) show a marginal increase in F relative to Sm with increasing SiO_2, which is possibly a result of late-magmatic activity, an idea consistent with the observed fluorite veinlets present within some Quartz Rhyolites (e.g. sample GC5 *see* Chapter 2). Limited data from Hiltaba Granites shows a general decrease in the F/Sm ratio with increasing SiO_2, which may be explained by a loss of F during hydrothermal activity.

4.3.2. Trace elements

Plots of Sc, Ti, Nb, Zn, U and Th versus SiO_2 for the volcanics and Hiltaba Granite show strong linear correlations (Fig 4-6). Sc and Ti both decrease in concentration with increasing SiO_2 (Fig 4-6C and D), which is inferred as a fractionation trend. The depletion of Sc and Ti with fractionation may be explained by the crystallization of pyroxene, which is a common phase within the least fractionated volcanics (e.g. Yardea Dacite) and ilmenite, sphene and rutile, which were all identified within the Eucarro Rhyolite and Hiltaba Granite.

U and Th versus SiO_2 (Fig 4-6E and F) both show strong positive correlations within the volcanics. Limited data from the granite, suggests that the granite is significantly more enriched in U and Th relative to the volcanics. Although the granite is more enriched in Th and U, granite Th/U values are (4.6 to 6.0) similar to the volcanics (4.1 to 5.6) and also to melt inclusions (average 4.4 and stdev 1), which can be attributed to the similar behaviour of U and Th during fractionation.

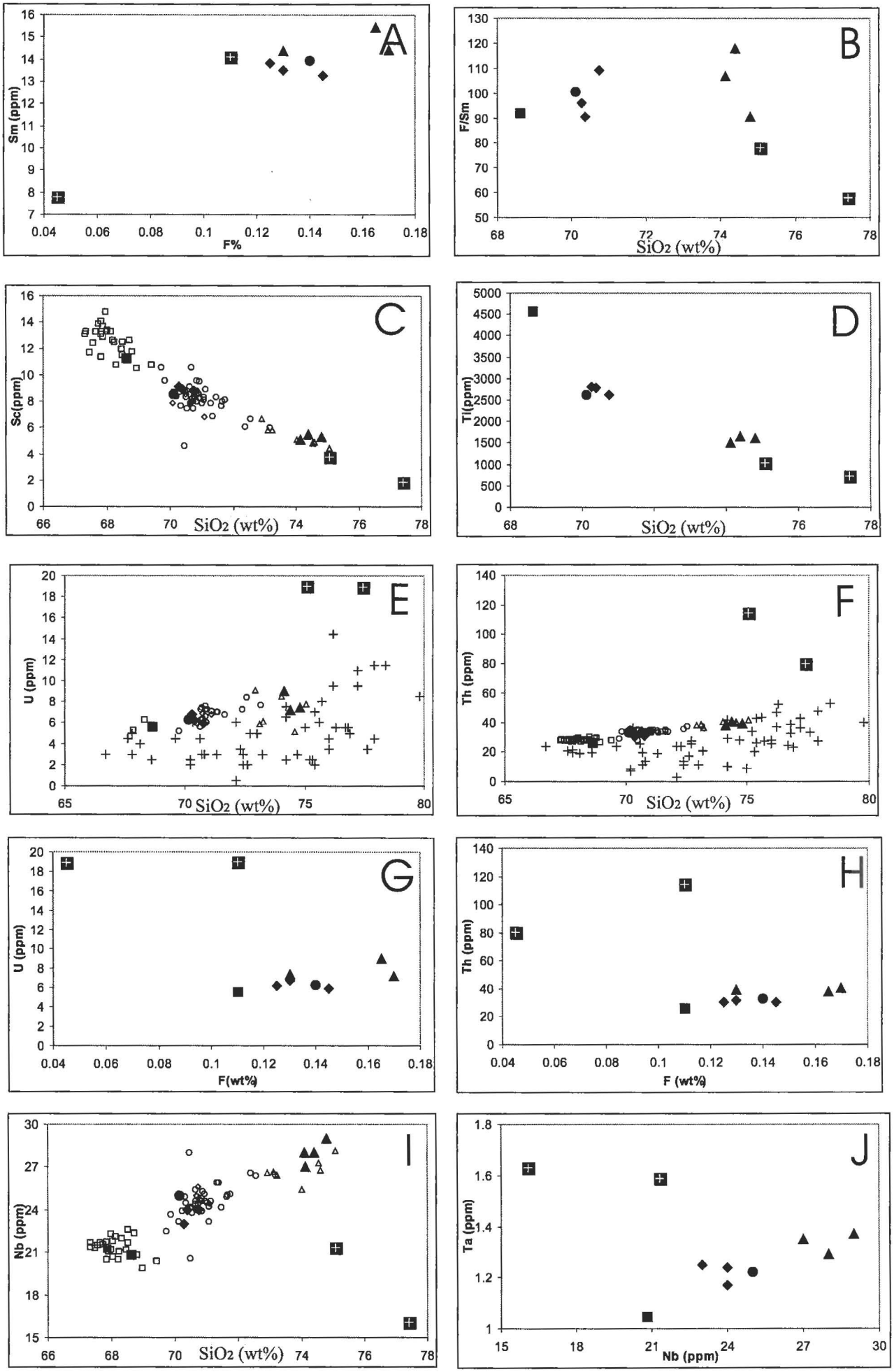

Figure 4-6. Trace and major elements of whole rocks for the Hiltaba Granite, Yardea Dacite, and the Plagioclase Rhyolite, Vesicular Rhyolite, Quartz Rhyolite from the Eucarro Rhyolite. Note that data used in this study are filled, whereas comparison unfilled shapes represent samples from other studies (*see* Figure 4-5 for Key).

A plot of Nb verses SiO_2 (Fig 4-6I) shows a strong positive correlation for the volcanics, whereas the granite is significantly depleted in Nb relative to the volcanics. Moreover a plot of Nb verses Ta (Fig 4-6J) shows that the volcanics plot as a positive linear array in which the most fractionated volcanics (Quartz Rhyolite) have the highest amounts of Nb and Ta. In contrast, the granite contains higher concentrations of Ta relative to the volcanics. It is unlikely that this feature is a result of milling contamination, as the Yardea Dacite, which was also prepared using a tungsten carbide mill shows no enrichment of Ta compared to the Eucarro Rhyolite. According to Wedepohl (1978) both Nb and Ta tend to increase with increasing SiO_2, however biotite tends to concentrate Nb relative to Ta, which can therefore change the ratio of Nb and Ta with fractionation. Thus the relative decrease of Nb in the granite may be explained by the earlier crystallization of biotite. In the case of the volcanics the fractionation of biotite was either insignificant or did not occur, which is supported by the presences of pyroxene and the dry nature of the volcanics (<1 wt% H_2O; Creaser and White, 1991).

Zr versus SiO_2 (Fig 4-7A) shows at first a linear increase in Zr (419 to 504ppm) with SiO_2 (from 67 to 71%), which is then followed by a sharp linear decrease in Zr (504 to 137ppm) with increasing SiO_2 (from 71 to 78%) (although some of the granites studied by Ferris (2001) do not follow this trend). The cause of this trend may be shown by petrographic studies, which show that those volcanics which optically contain the most zircon (Plagioclase Rhyolite and Vesicular Rhyolite) also contain the most of Zr. Furthermore, almost all of the observed zircon occurs within pockets surrounded by groundmass, and is intimately associated with fluorite and apatite. These pockets are inferred to be residual melt (*see* Chapter 2), which crystallized at roughly the same time as the groundmass due the irregular contact between the two. Thus, Zr was likely concentrated into these pockets during the crystallization of the groundmass, which subsequently led to the crystallization of zircon (Fig 2-9).

Trace elements such as Eu, Ba, Sr and Rb (Fig 4-7C, D, E and F) all show trends which are consistent with the fractionation of feldspar i.e. Ba, Eu and Sr decrease in concentration with increasing SiO_2 (plagioclase fractionation), whereas Rb increases in concentration with increasing SiO_2 (i.e. increase of K-feldspar within most fractionated samples).

4.3.2.1. Geochemical comparison of studied rocks normalized to primitive mantle

Trace element concentrations for the studied rocks have been normalized to a primitive mantle (PM) to demonstrate their relative enrichment or depletion from a mantle source as a result of fractionation and/or assimilation. PM normalized trace element concentrations are plotted on a spider diagram (Fig 4-8) to illustrate the elements that have been enriched or depleted between the various rock types (in order of least compatible to most compatible from left to right). Figure 4-8 illustrates that both the Plagioclase Rhyolite and the Vesicular Rhyolite are indistinguishable in their trace element geochemistry. It also illustrates that the Yardea Dacite is very similar compositionally to the Vesicular Rhyolite and the Plagioclase Rhyolite except for higher concentrations of Pb, Mo, Sr and Ti, and lower concentrations of K, La, Nb, U, Th, Ce, Eu, Sb and HREE, which are consistent with fractionation trends. The Quartz Rhyolite also follows a similar trend to all other volcanics, apart from having lower concentrations of Ti, P, Sr and Eu, and higher concentrations of U and Th, which is also consistent with fractionation trends. Tungsten on average is also less concentrated in the Quartz Rhyolite.

Trace element data from the Hiltaba Granite also illustrates that the granite is compositionally similar to the volcanics, apart from lower concentrations of Ba, Sr, Ti, Mo, Cs, Sb, Zr, Hf and Eu, and higher concentrations of U, Th and Sn. A significant variation in REE and F concentration exists between the two granite samples, with the coarse-grained granite having significantly lower REE and F concentrations. This dissimilarity can be explained by the coarse-grained granite being crystal-rich and therefore contains only minor amounts of "groundmass" in which REE and F are partitioned.

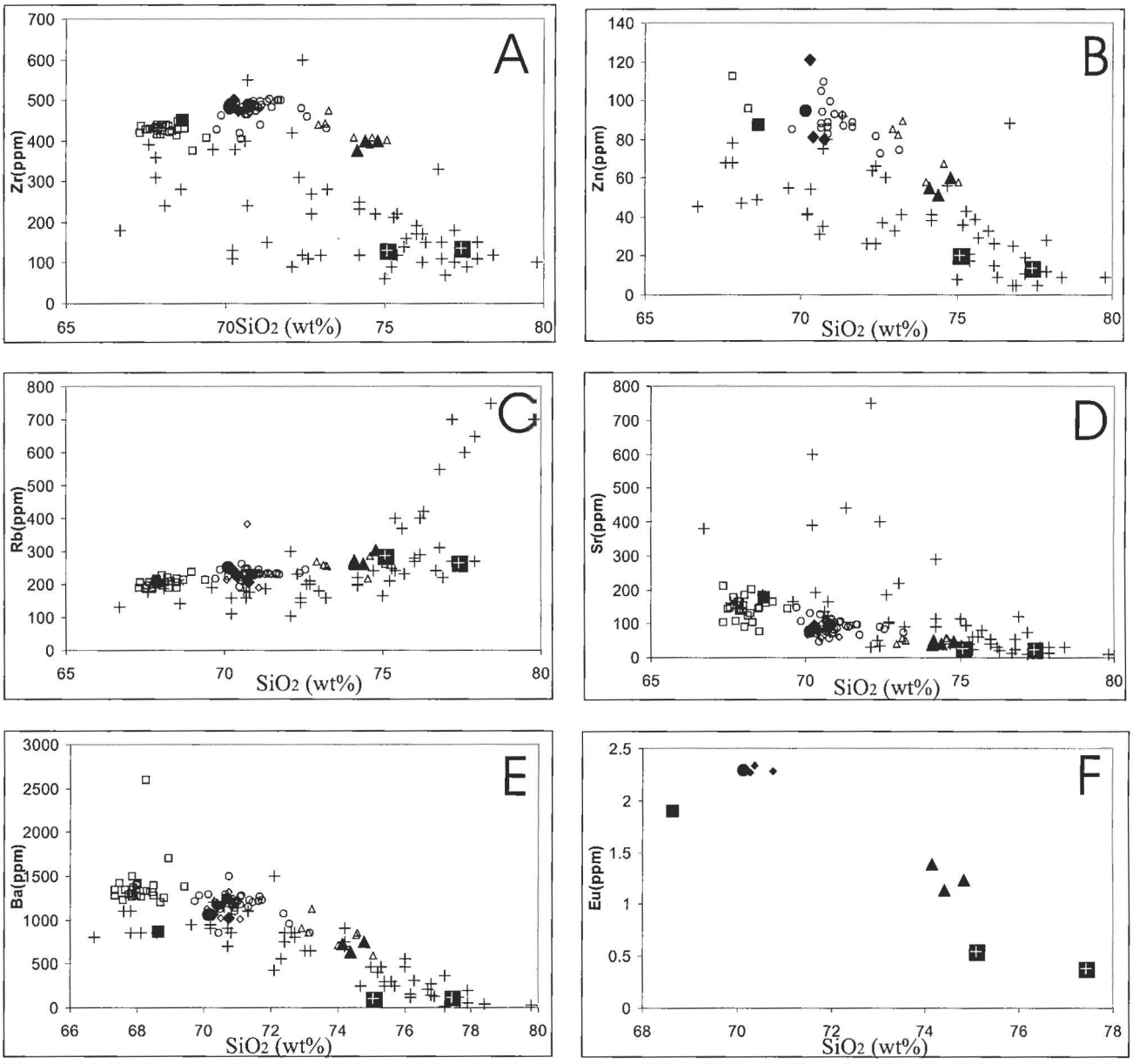

Figure 4-7. Trace and major elements from whole rocks of the Hiltaba Granite, Yardea Dacite, and the Plagioclase Rhyolite, Vesicular Rhyolite, Quartz Rhyolite from the Eucarro Rhyolite. Note that data used in this study are filled, whereas comparison unfilled shapes represent samples from other studies (*see* Figure 4-6 for Key).

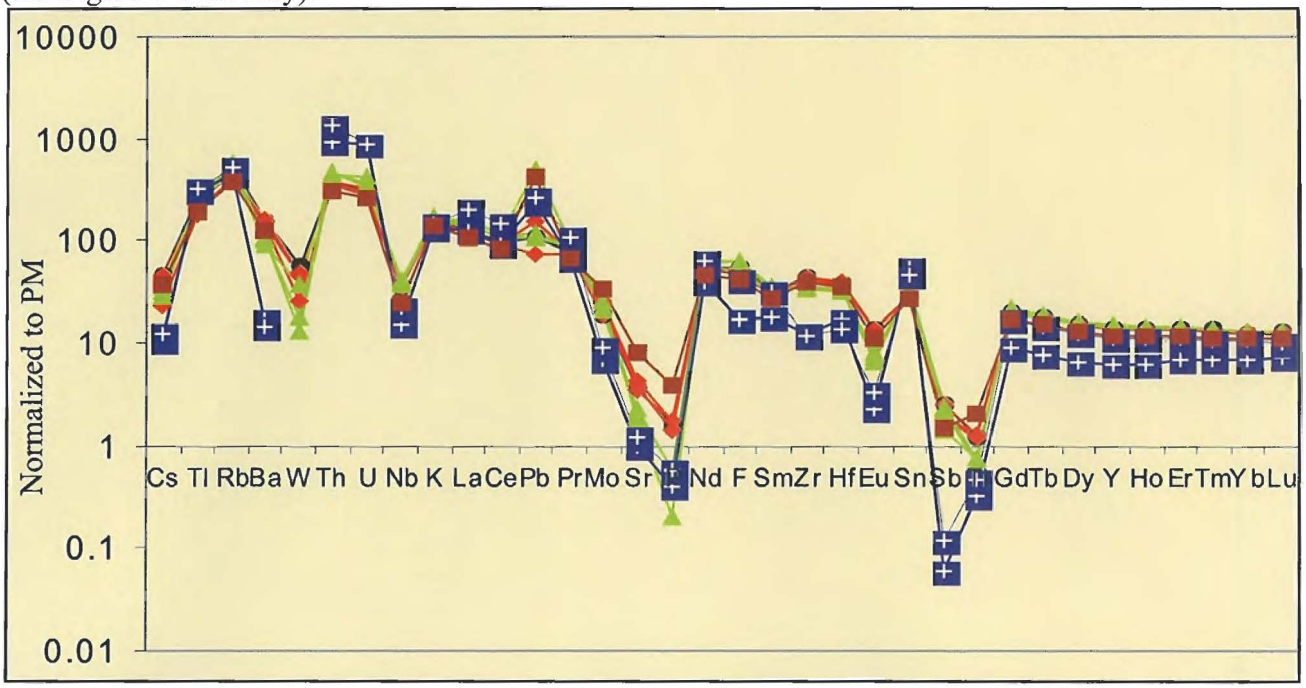

Figure 4-8. Spider diagram for whole rocks from the Plagioclase Rhyolite (black), Vesicular Rhyolite (red), Quartz Rhyolie (green), Hiltaba Granite (blue) and Yardea Dacite (brown), all normalized to a primitive mantle (PM) (Sun and McDonough, 1989).

4.4. Geochemistry of the Eucarro Rhyolite groundmass

Analysis of the groundmass was undertaken in order to determine the geochemistry of volcanic glass, which is thought to represent degassed melt. One significant problem with analyzing the groundmass is its microcrystalline texture (i.e. heterogeneous), which poses significant problems when analyzing small discrete spots (110μm) by microprobe and LA-ICPMS (e.g. note the variability in cps for each element from the LA-ICPMS graph Fig 4-8). To minimize the chance of error an average was taken from a number on analyses; however it should be noted that large standard deviations are associated with these average values and thus caution should be applied when interpreting the data set. One major concern is the residual pockets of fluorite, apatite and zircon which occur within the groundmass (*see* Chapter 2), but were excluded from analysis of the groundmass and may contain significant concentrations of trace elements such as LREE, which are associated with apatite (Deer *et al.*, 1992). Concentrations Zr, U, Pb and Th may also be significantly more enriched in the groundmass than the analysis shows as they are common components of zircon.

A comparison of the microprobe data with the LA-ICPMS data shows that there are discrepancies in the Al_2O_3 values (Table 4-4), with the LA-ICPMS data from one example (GC8) being much greater than microprobe (i.e. 13.21 verses 10.54 wt%) (excluding one clear outlier of 20% Al_2O_3). In contrast though, sample GC17 shows a lower Al_2O_3 LA-ICPMS value (i.e. 10.00 verses 11.78 wt%) than measured by microprobe. Hence there is no consistent higher or lower Al_2O_3 value by either method and discrepancies in the data are likely related to sample size. Thus more confidence should be placed in the microprobe data due to the larger number of points analyzed.

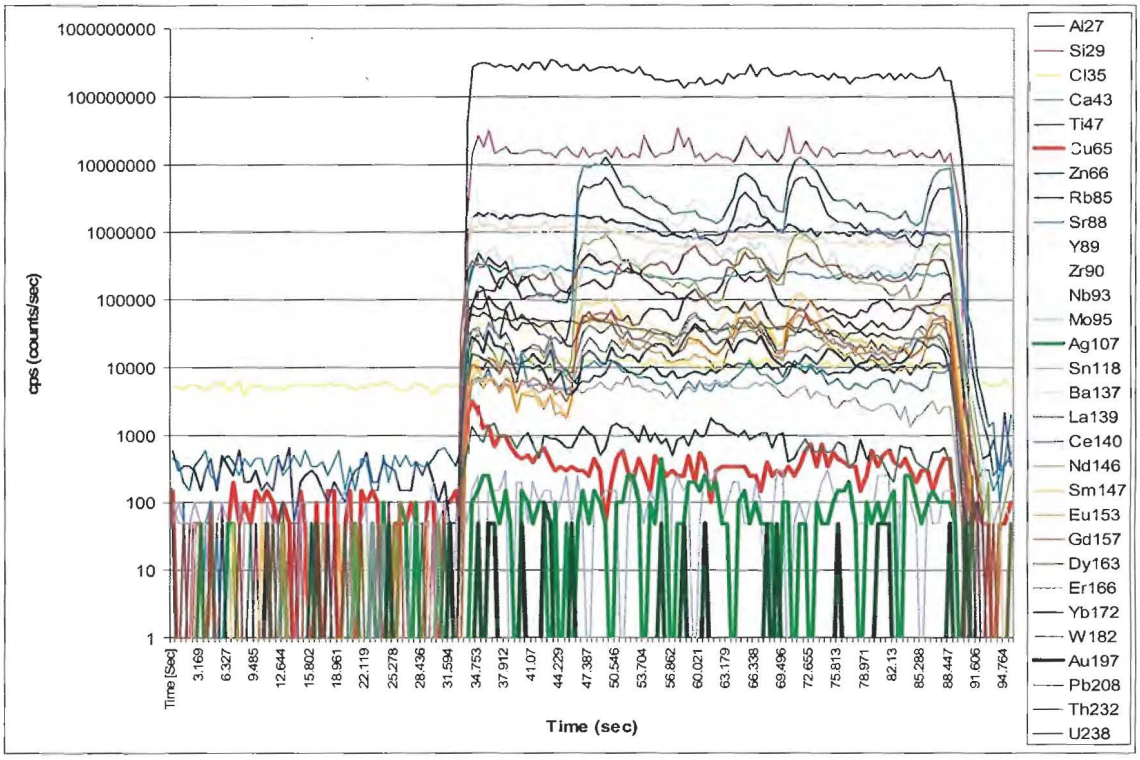

Figure 4-9 A counts per second versus time graph for the analysis of the groundmass of the Eucarro Rhyolite (sample GC11) using LA-ICPMS. Note that analysis of the groundmass was carried out between 33 and 88 seconds, whereas background measurements are between 0 and 32 seconds. Also note the large variability of cps for each element during the analysis, which illustrates the heterogenous nature of the groundmass.

4.4.1. Major elements

Major element analysis of the groundmass was previously carried out by Kamenetsky *et al.* (2000) and their data is presented in Table 4-4. In order to obtain a best estimate, Kamenetsky *et al.* (2000) averaged the groundmass for each sample (*see* Appendix) and concluded that the groundmasses are rhyolitic in having a very high SiO_2 content (77.8-80.5 wt%), exceeding the whole rock SiO_2 range by ~6-8 wt%. Kamenetsky *et al.* (2000) also demonstrated that average CaO (0.09-0.29 wt%) and Al_2O_3 (9.68-11.78 wt%) concentrations are depleted in the groundmass relative to the whole rock; however Na_2O (1.88-2.72 wt%) and K_2O (4.82-6.42 wt%) concentrations are similar. Furthermore Kamenetsky *et al.* (2000) concluded that the groundmass of the Quartz Rhyolite and Vesicular Rhyolite are indistinguishable in terms of all elements, but

Table 4-4

Calculated average concentrations for the groundmass of the Eucarro Rhyolite. Major elements (grey colour and top table) are from Kamenetsky *et al.* (2003) (microprobe analysis), whereas trace element data were obtained using LA-ICPMS (all analysis carried out at the University of Tasmania). Note that SiO2 was used as the internal reference (see text) for LA-ICPMS concentrations. All major elements are presented in weight percent, whereas trace element data is presented in ppm. Abbreviations used include Plagioclase Rhyolite=PR, Vesicular Rhyolite=VR and Quartz Rhyolite=QR.

Sample	GC17	GC4	GC14	GC5	GC8 D1	GC11	GC16
Rock type	PR	VR	VR	QR	QR	QR	QR
Si2O	76.48	78.43	80.05		79.52	80.67	
TiO2	0.04	0.04	0.11		0.04	0.02	
Al2O3	11.78	10.80	10.37		10.54	9.68	
Fe2O3	1.06	0.78	0.80		0.77	0.70	
MnO	0.02	0.02	0.02		0.04	0.02	
MgO	0.04	0.03	0.06		0.02	0.06	
CaO	0.16	0.10	0.09		0.29	0.18	
Na2O	2.60	1.88	2.58		2.72	2.01	
K2O	6.27	6.42	4.82		4.93	5.07	
Cr2O3	0.01	0.02	0.01		0.01	0.01	
total	98.47	98.52	98.91		98.88	98.43	

Al2O3(wt%)	10.00		10.94	11.13	14.99	12.42	10.71
Si2O(wt%)	76.48		80.05	80.35	79.52	80.67	80.35
Ca	589.23		1542.65	1628.19	2861.43	2673.38	1692.50
Ti	188.44		1300.65	1413.21	793.26	2182.16	1672.30
Cu	0.47		2.43	0.46	2.06	0.89	1.59
Zn	58.99		45.77	59.45	74.52	58.09	59.03
Rb	302.45		252.26	254.38	371.98	293.48	213.30
Sr	25.60		29.03	23.86	42.89	58.14	50.73
Y	56.88		46.68	49.61	52.01	63.57	50.71
Zr	270.79		242.77	294.28	140.91	394.93	311.90
Nb	4.52		17.28	19.37	15.18	19.21	14.43
Mo	0.23		0.34	0.65	0.63	0.20	0.15
Ag	0.05		0.04	0.06	0.09	0.06	0.04
Sn	2.77		3.58	4.68	2.96	4.44	2.79
Ba	501.07		486.19	591.19	744.19	1031.72	969.02
La	39.91		18.41	68.81	104.44	95.66	19.98
Ce	75.62		37.87	141.15	185.50	191.55	46.33
Nd	31.84		14.92	52.64	82.89	72.34	21.33
Sm	6.44		3.18	9.58	13.66	12.51	5.37
Eu	0.60		0.30	0.93	0.97	1.87	1.10
Gd	6.83		3.73	7.93	10.59	10.70	6.72
Dy	9.62		7.54	8.52	9.00	11.33	9.01
Er	6.20		5.38	5.08	4.96	6.77	5.39
Yb	6.53		5.80	5.22	4.73	7.04	5.54
W	0.23		0.72	1.04	0.79	1.08	0.64
Au	0.00		0.01	0.01	0.00	0.00	0.00
Pb	6.11		6.95	4.78	43.04	9.59	4.00
Th	34.79		35.56	30.12	24.80	35.55	25.87
U	5.67		5.40	6.09	5.31	5.73	3.69

appeared to be more Si-rich and Al-, Na- and K-poor than the groundmass in the Plagioclase Rhyolite. Major element plots for the groundmass are shown on Figures 4-10, which shows that the groundmass lies along the same fractionation trends as the whole rock for Ti, Al, Fe, Na and Ca, and in all cases are more fractionated than the whole rock. K_2O in some samples (GC4 and GC17), also weakly plots along a fractionation trend; however in all other samples K_2O is significantly lower than the fractionation trend (Fig 4-10D), which may be attributed to losses during alteration.

4.4.2. Trace element

Trace element plots of La, Sm, U, Sr, Rb and Y versus SiO_2 for the groundmass, whole rock and melt inclusions are shown on Figures 4-10H-I and 4-11A-D. A comparison of whole rocks and groundmass shows that La, Sm, U, Rb and Y are lower in concentration within the groundmass compared to fractionation trends for the whole rock. In contrast, Sr is higher in concentration for three of the four samples compared with whole rock fractionation trends.

Trace element plots of Yb, U, Zr, La and Mo versus Th show that the groundmass, melt inclusions and whole rock plot as strong linear trends (Figs 4-10E-I). However, these trends show that the groundmass is depleted in trace elements compared to whole rocks and melt inclusions, which suggests that the groundmass is less fractionated compared with whole rock and melt inclusions, and is thus the opposite to major element trends. One explanation for this anomaly is that residual fluorite, apatite and zircon pockets within the groundmass, which were not analyzed, contain significant concentrations of trace elements (*see* below).

Average trace element values for the groundmass and whole rocks were normalized to a primitive mantle and plotted on spider diagrams for comparison (Fig 4-14). Spider diagrams illustrate that the groundmass of the Plagioclase Rhyolite, Vesicular Rhyolite and Quartz Rhyolite all show similar distribution patterns and are consistently enriched or depleted in certain elements relative to the whole rock. Five notable similarities are observed for all samples, which include; 1) all LREE within the groundmass are depleted compared with whole rock (Fig 4-10), 2) LREE concentrations

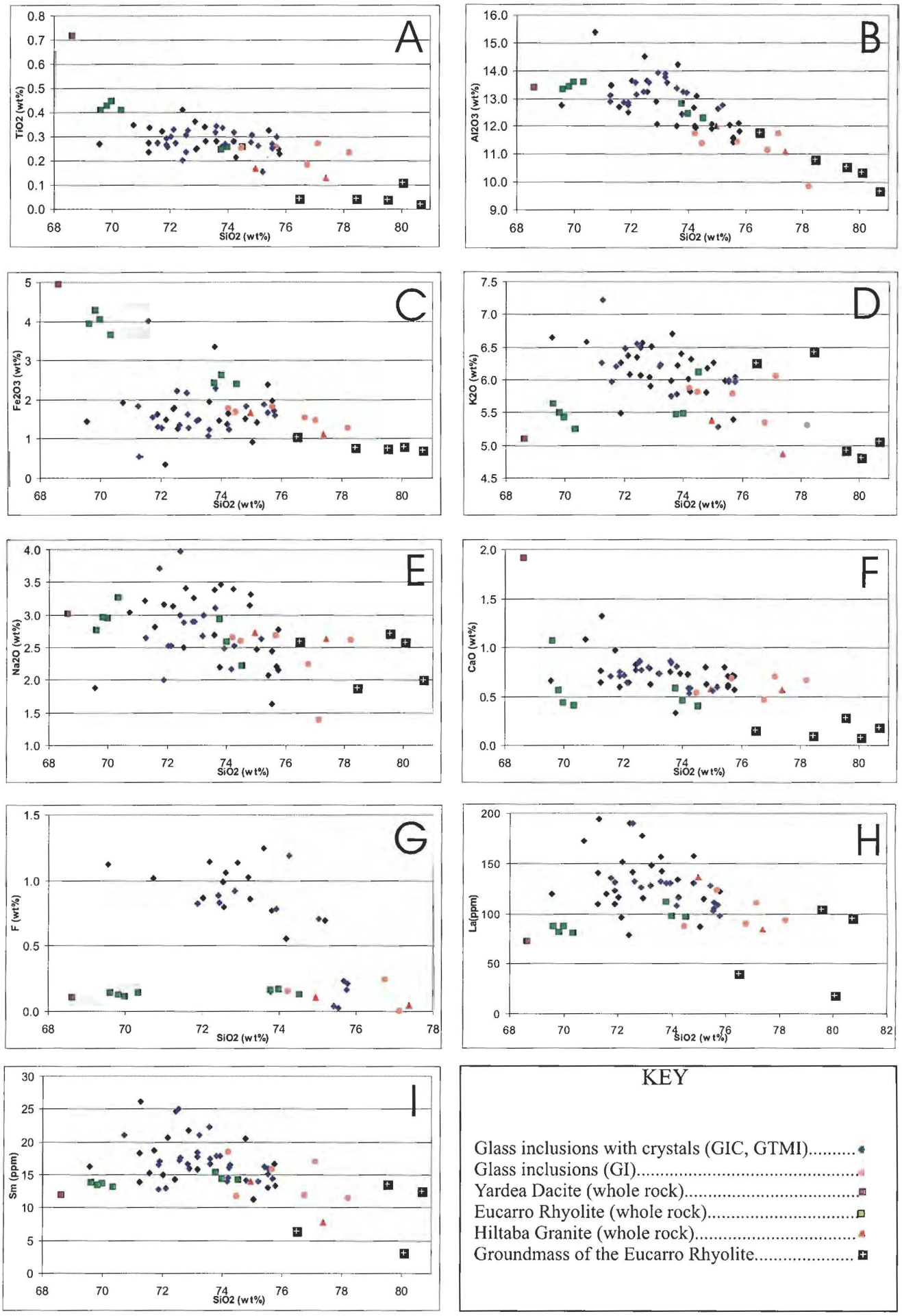

Figure 4-10. Major and trace element plots for melt inclusions (Eucarro Rhyolite), whole rock (Eucarro Rhyolite, Hiltaba Granite and Yardea Dacite) and groundmass (Eucarro Rhyolite).

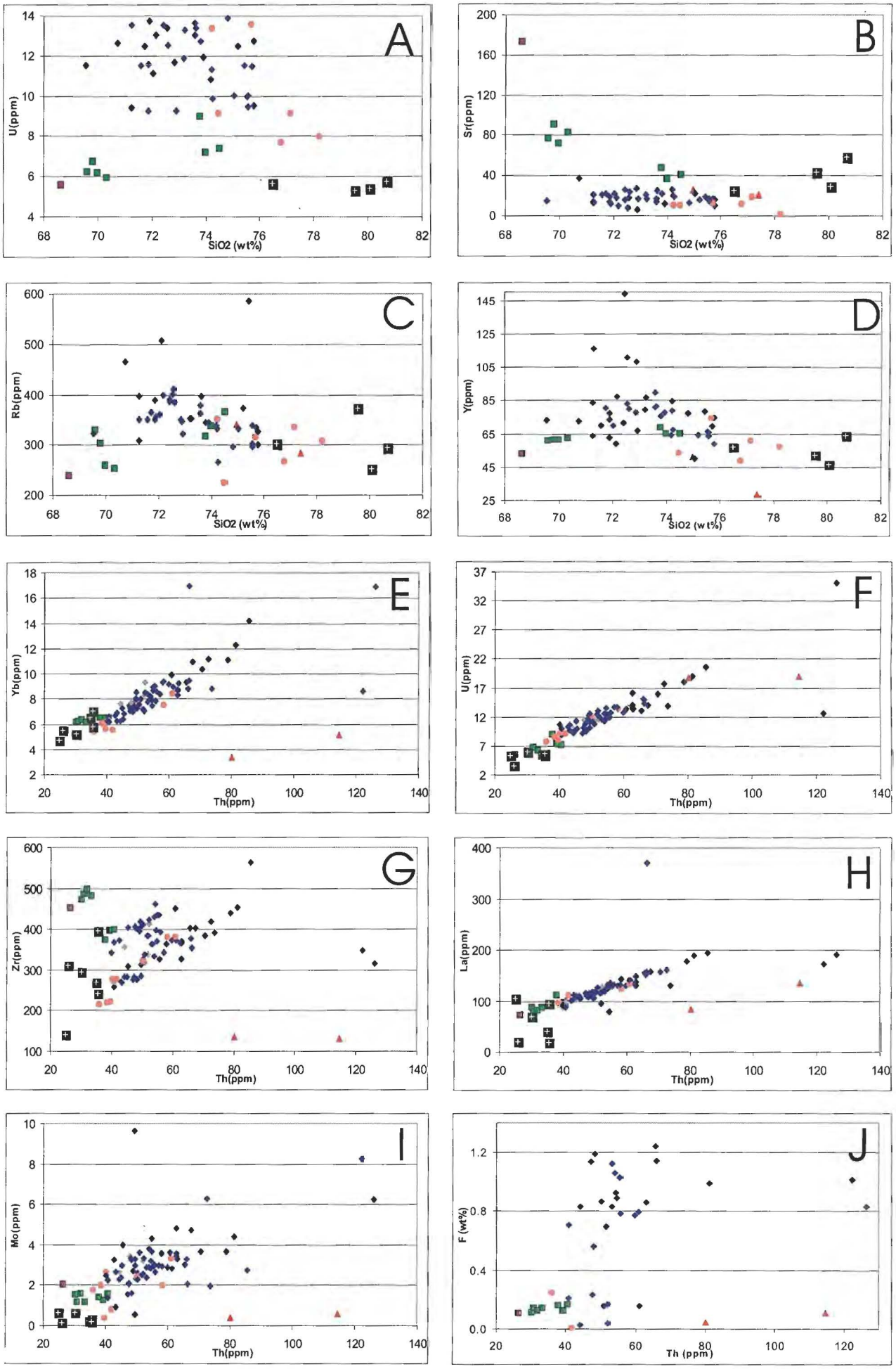

Figure 4-11. Major and trace element plots for melt inclusions (Eucarro Rhyolite), whole rock (Eucarro Rhyolite, Hiltaba Granite and Yardea Dacite) and groundmass (Eucarro Rhyolite). See Figure 4-10 for key. Note that the grey diamonds represent GIC and GTMI inclusions that have low fluorine concentrations.

have large standard deviations, which suggests that LREE concentrations are significantly heterogeneous throughout the groundmass of all samples, 3) HREE within the groundmass are depleted relative to the whole rock, but are less depleted than LREE and become closer to whole rock concentrations with increasing atomic weight (especially true for the Plagioclase Rhyolite and Vesicular Rhyolite), 4) Rb and Pb groundmass concentrations are indistinguishable from the whole rock, and 5) Nb, Mo, Zr and Sn concentrations for the groundmass are always on average lower than the whole rock.

In contrast elements Ba, W, U, Th, Sr and Ti show a dissimilar trend for groundmass and whole rock for each sample. Ba, Ti and Sr are both depleted in the groundmass of the Plagioclase Rhyolite and Vesicular Rhyolite, but for the Quartz Rhyolite Ba is enriched within the groundmass, whereas Sr and Ti are indistinguishable between the groundmass and whole rock. W is lower in concentration in the groundmass of the Plagioclase Rhyolite, similar in concentration in the Vesicular Rhyolite and higher in concentration within the Quartz Rhyolite. U and Th from the groundmass are both similar in concentration to the whole rock within the Plagioclase Rhyolite and Vesicular Rhyolite, but are lower in concentration for the Quartz Rhyolite.

It is difficult to explain the variations between those elements which show dissimilar trends between the whole rock and groundmass from sample to sample. One explanation is that small crystals may have been accidentally analyzed with the groundmass, thus resulting in enrichments or depletion of certain elements e.g. plagioclase may have caused enrichments of Sr and Ba. Although these inconsistencies exist it is important to point out the consistent depletion of LREE compared to HREE within the groundmass (Fig 4-12). This feature is most pronounced in the Plagioclase Rhyolite and Vesicular Rhyolite (Fig 4-9). According to Krauskopf and Bird (1995) LREE are more incompatible than heavy ones, but if apatite, monazite, allanite etc are crystallizing, than LREE are highly compatible. Thus LREE may have concentrated into either residual pockets in the groundmass or apatite crystals, which were not analyzed here. Although not tested in this study, residual pockets of fluorite, apatite and zircon, which are most abundant within the Plagioclase Rhyolite and Vesicular Rhyolite, may

account for the significant LREE discrepancy between the analyzed groundmass and wholerock.

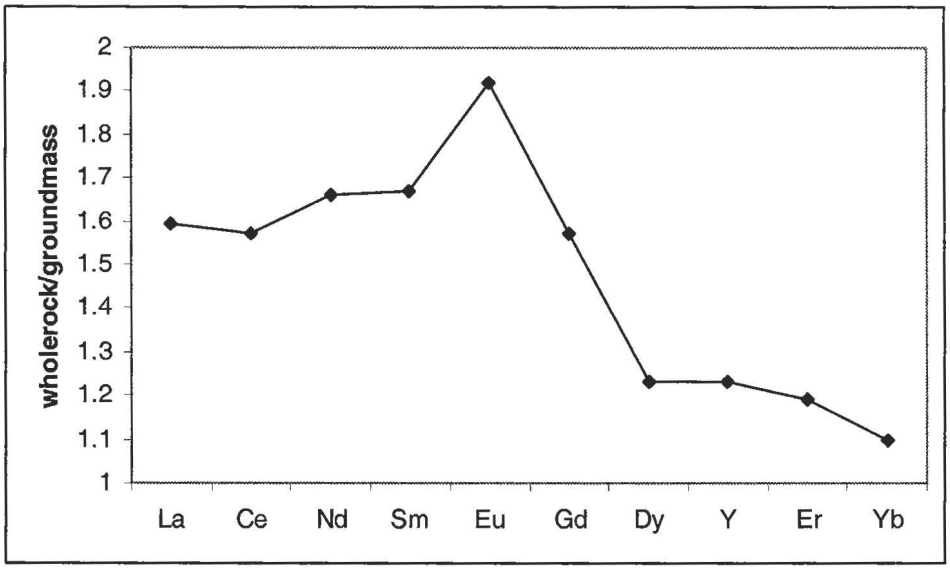

Figure 4-12 A comparison between the average REE concentration from the whole rock and groundmass of the Eucarro Rhyolite. Note the relative enrichment of LREE versus HREE within the whole rock compared to the analysed groundmass, which may be a result of LREE being hosted within residual apatite-zircon-fluorite pockets of the groundmass or crystalline in the whole rock. Also note the relative enrichment of Eu in the whole rock, which is consistent with Eu being strongly partitioned into feldspar relative to other REE.

4.5. Geochemistry of melt inclusions from the Eucarro Rhyolite

Fifty one inclusions belonging to the Plagioclase Rhyolite, Vesicular Rhyolite and Quartz Rhyolite were analyzed for major elements using microprobe, and eighty one samples for trace elements by LA-ICPMS. Inclusions analyzed include glass inclusions (GI), granular-textured melt inclusions (GTMI) and glass inclusions with crystals (GIC), which were homogenized at 850°C for 70 or 20 hours (Table 4-5). A set of inclusions from sample GC11, which were unheated, were also analyzed in order to compare heated

and unheated inclusions. With the exception of Cu, Ag and Au all major and trace elements showed no significant difference between heated and unheated samples. In heated samples Cu and Ag were significantly more enriched in almost all samples, whereas Au show significant enrichment in only some heated inclusions (*see* Table 4-6). Thus all significant enrichments of Cu, Ag and Au are thought to be artefacts.

4.5.1. Major elements

Harker diagram plots for major elements Al, Fe, Mg, Ti, Na, K, F and Ca versus SiO_2 (Figure 6-6 and 6-7) show that melt inclusions have SiO_2 concentrations between 68 and 79 wt%, with GI from samples GC5 (Quartz Rhyolite) and GC4 (Vesicular Rhyolite) having a higher concentrations of SiO_2 (74-79 wt%), and GIC from samples GC8 (Quartz Rhyolite) and GC11 (Quartz Rhyolite) having a lower concentration of SiO_2 (68-75 wt%). For elements Al, Ti and Ca there is a negative correlation with SiO_2 (Fig 4-10A, B and F), which is consistent with fractionation trends for the whole rock and groundmass. In contrast, Fe does not correlate with SiO_2 (Fig 4-10C), Na shows a weak correlation with both SiO_2 and whole rock fractionation trends (Fig 4-10E), and K shows a weak negative trend, which is the opposite to the fractionation trend of whole rocks and groundmass (Fig 4-10D). Fluorine versus SiO_2 shows a negative correlation for melt inclusions, and is on average significantly more enriched in inclusions compared to the whole rock, although all GI and some GIC have F concentrations which are similar to the whole rock (Fig 4-10G). Analysis of apatite and hornblende were carried out on samples from the Eucarro Rhyolite by Stewart (1994), and result yielded ~3 wt% and ~0.8 wt% F respectively. This supports the notion that F may have been lost during fractionation. Alternatively, some fluorine may have also been lost during degassing.

Table 4-5 Major element geochemistry of melt inclusions from the Eucarro Rhyolite. Note that those inclusions that are highlighted in grey were heated for 20 hours, whereas those that were heated for 70 hours are plain. Unheated inclusions are in bold and at the bottom of the table. Abbreviations used include PR=Plagioclase Rhyolite, VR=Vesicular Rhyolite and QR=Quartz Rhyolite. All analyses were carried out by microprobe at the University of Tasmania.

	Sample	Inclusion type	SiO2%	TiO2%	Al2O3%	Fe2O3%	MgO%	CaO%	Na2O%	K2O%	Cl%	F%	Total
PR	GC17m1	GIC	74.82	0.31	11.90	1.84	0.03	0.63	3.31	6.18	0.21	0.37	99.61
	GC17m3	GIC	73.56	0.13	13.06	1.93	0.01	0.30	3.47	6.25	0.21	0.46	99.12
VR	GC4m2	GI	70.93	0.62	14.63	1.71	0.04	1.84	5.62	2.99	0.21		97.34
	GC4m3	GIC	78.20	0.24	9.89	1.28	0.04	0.67	2.62	5.31	0.12		96.29
	GC4m4	GI	74.22	0.28	11.76	1.78	0.05	0.73	2.66	5.88	0.21	0.16	96.85
	GC4m6	GIC	75.78	0.23	11.83	1.61	0.04	0.57	2.16	6.05	0.15	0.21	97.91
	GC4m7a	GIC	75.77	0.25	12.12	1.72	0.06	0.70	2.77	5.97	0.21	0.17	99.24
	GC4m2_7a	GI	75.55	0.17	11.43	2.39	0.06	0.79	1.64	5.97	0.44	0.03	98.91
	GC14m1	GI	72.85	0.36	12.88	2.18	0.06	0.79	2.89	6.04	0.23	0.23	98.29
QR	GC5m3	GI	75.56	0.25	11.60	1.68	0.04	0.71	2.45	5.99	0.13		98.96
	GC5m5	GI	77.13	0.27	11.75	1.49	0.06	0.71	1.40	6.07	0.05	0.01	99.81
	GC5m6	GI	75.70	0.30	11.47	1.98	0.14	0.72	2.21	5.40	0.17	0.29	98.33
	GC5m7	GI	74.47	0.26	11.41	1.69	0.03	0.54	2.61	5.83	0.18		99.60
	GC5m8	GI	75.68	0.26	11.45	1.83	0.04	0.69	2.69	5.80	0.19		97.81
	GC5m2_2a	GI	76.76	0.18	11.16	1.55	0.05	0.47	2.26	5.35	0.10	0.25	97.11
	GC8m4	GI	73.59	0.28	12.01	1.96	0.05	0.75	3.39	5.75	0.20		97.90
	GC8m7a	GI	72.13	0.33	13.56	0.35	0.02	0.64	2.52	6.38	0.06		97.74
	GC8m8	GIC	72.61	0.33	13.58	1.36	0.05	0.77	3.41	6.56	0.19	1.06	100.59
	GC8m9	GIC	72.89	0.25	12.07	1.63	0.05	0.79	3.26	5.90	0.28		97.38
	GC8m11	GIC	73.24	0.28	13.56	1.49	0.03	0.73	2.99	6.24	0.20	0.86	98.74
	GC8m2_1a	GIC	75.05	0.26	12.63	0.91	0.02	0.56	2.47	6.27	0.14	0.71	97.46
	GC8m2_2b	GIC	73.93	0.27	13.21	1.48	0.03	0.73	2.49	6.40	0.18	0.79	99.52
	GC8m2_8b	GIC	74.19	0.28	12.67	1.37	0.03	0.73	2.17	6.01	0.15	0.56	98.26
	GC8m2_10a	GIC	72.03	0.30	13.63	1.28	0.05	0.71	2.52	6.49	0.23	0.87	97.09
	GC8m2_10b	GIC	72.56	0.31	13.63	1.27	0.03	0.87	2.50	6.49	0.19	0.80	97.76
	GC8m2_11a	GIC	75.20	0.16	12.75	1.43	0.03	0.60	2.64	5.29	0.21	0.70	98.50
	GC8m2_11b	GIC	69.56	0.27	12.75	1.46	0.05	0.66	1.89	6.65	0.21	1.12	99.11
	GC8m2_11c	GIC	71.88	0.27	12.75	1.64	0.06	0.71	2.01	5.50	0.26	0.83	99.40
	GC8m2_12a	GIC	70.73	0.35	15.40	1.93	0.06	1.08	3.03	6.58	0.35	1.02	100.49
	GC11m1	GIC	73.62	0.34	14.21	1.25	0.04	0.85	3.10	6.71	0.18		99.67
	GC11m3	GIC	71.58	0.28	12.71	4.02	0.09	0.71	2.82	5.98	0.17	0.80	99.00
	GC11m4a	GIC	74.23	0.32	11.94	1.64	0.05	0.54	3.40	5.82	0.22	0.88	99.93
	GC11m7	GIC	71.26	0.28	12.90	1.84	0.05	0.76	3.22	6.26	0.18	0.94	98.40
	GC11m8	GIC	72.18	0.28	13.15	1.50	0.05	0.64	3.13	6.09	0.30	1.14	99.90
	GC11m9a	GIC	71.90	0.26	12.87	1.32	0.08	0.75	3.17	6.27	0.20		97.10
	GC11m10	GIC	71.74	0.32	12.87	1.55	0.05	0.98	3.71	6.21	0.20		99.52
	GC11m11	GIC	71.26	0.24	13.12	1.84	0.05	0.65	3.22	6.26	0.18		95.93
	GC11m12	GIC	74.80	0.28	12.07	1.51	0.07	0.80	3.14	5.81	0.20		98.56
	GC11m2_5	GIC	73.20	0.34	13.76	1.47	0.06	0.73	2.68	6.21	0.21	1.03	94.40
	GC11m2_6	GIC	74.27	0.22	13.07	1.23	0.05	0.58	2.52	6.32	0.23	1.19	96.89
	GC11m2_10	GIC	72.92	0.25	13.94	1.27	0.07	0.62	2.90	6.51	0.15	1.14	95.43
	GC16m2	GIC	73.82	0.34	13.24	2.28	0.06	0.80	3.47	6.22	0.27		98.72
	GC16m3	GIC	72.54	0.24	13.24	2.22	0.06	0.85	2.89	6.07	0.25	0.99	97.64
	GC16m4	GIC	71.28	0.34	13.48	0.55	0.08	1.32	2.65	7.23	0.10	0.77	99.66
	GC16m7	GIC	72.42	0.41	13.24	1.76	0.05	0.77	3.98	6.55	0.18	0.89	99.26
	GC11 B1_2	GIC	**74.43**	**0.28**	**12.63**	**0.21**	**-0.01**	**0.17**	**2.63**	**6.32**	**0.15**	**0.58**	96.85
	GC11 B1_4	GIC	**72.79**	**0.24**	**13.36**	**0.72**	**-0.02**	**0.15**	**2.97**	**6.53**	**0.17**	**0.66**	97.00
	GC11 B1_5	GIC	**70.16**	**0.27**	**14.56**	**0.49**	**0.02**	**0.17**	**3.96**	**5.65**	**0.37**	**0.74**	95.81
	GC11 B1_6	GIC	**73.82**	**0.24**	**13.44**	**0.13**	**0.00**	**0.06**	**2.80**	**6.74**	**0.10**		97.47
	GC11 B1_7	GIC	**68.90**	**0.25**	**13.66**	**3.59**	**0.12**	**0.19**	**2.69**	**6.66**	**0.16**		96.31
	GC11 B1_8	GIC	**72.97**	**0.18**	**12.88**	**0.31**	**0.01**	**0.15**	**2.99**	**6.60**	**0.15**	**0.63**	96.31

4.5.2. Trace elements

Trace elements La, Sm, U, Sr, Rb and Y versus SiO_2 were plotted on Harker Diagrams to compare melt inclusions with the whole rock and groundmass. All plots, with the exception of Y, show that trace elements do not correlate with fractionation trends from whole rock analysis (Figs 4-10H-I and 4-11A-D). Furthermore, trace elements such as La, Sm, U, Rb are enriched in melt inclusions compared to the whole rock, whereas Sr is depleted in melt inclusions, which is likely attributed to its affinity with feldspar. Y shows a weak correlation with the whole rock and groundmass. Moreover a comparison of La, Sm and Y, shows that with increasing atomic weight there is a greater correlation between the whole rock, groundmass and inclusions.

Plots of U, La (LREE) and Yb (HREE) versus Th all show strong positive linear trends, Mo and Zr versus Th show moderate positive trends (Fig 4-11E) and F versus Th shows a very weak positive trend (Fig 4-11J). As these elements are all incompatible, the positive correlation between these elements demonstrates that some inclusions are more enriched in incompatible elements than others. An inspection of the cps graph from LA-ICPMS (Fig 4-13) shows that inclusions, which are enriched in trace elements, have high cps for the full time span of ablation, and therefore crystal phases or shrinkage bubbles, which show spikes when ablated (e.g. crystal Sn and Cu peaks on graph A Fig 4-13), are not responsible for increased concentrations within inclusions. Hence some inclusions have glass which is more enriched in the above trace elements than others. Furthermore, with the exception of Zr, inclusions are enriched in trace elements relative to the whole rock and groundmass, which also correlate with the linear trend of inclusions.

A number of other studies (e.g. Schmitt *et al.*, 2002; Chabiron *et al.*, 2001) have also reported enrichment within melt inclusions relative to the whole rock. Schmitt *et al.* (2002) reported that interactions with post-magmatic F-rich aqueous fluids can cause local remobilization of incompatible elements in the host rock, whereas Chabiron *et al.* (2001) suggested that REE may decrease in the melt with fractionation i.e. LREE-rich phases fractionate as the tonalite to trondhjemite transition in low-K intrusives show REE depleting as SiO_2 increases due to the amphibole-apatite fractionation. Whole rock major

Table 4-6 Trace element data from melt inclusions of the Eucarro Rhyolite. All analyses were carried out at the University of Tasmania using LA-ICPMS. Note that Al2O3 was used as the internal standard, which was analyzed using microprobe at the University of Tasmania. Abbreviations include PR=Plagioclase Rhyolite, VR=Vesicular Rhyolite and QR=Quartz Rhyolite. Note that areas coloured grey represent analysis from inclusions that were heated for 20 hours, whereas non-coloured regions represent inclusions that were heated for 70 hours. Unheated inclusions are in bold (see over pages)

	Sample	inclusion type	Al2O3	Be	B	Ti	Cu	Zn	Rb	Sr	Y	Zr	Nb	Mo	Ag	Sn	Ba	La
PR	GC17m1	GIC	11.90	3.30	32.68	1833.42	271.77	117.53	297.07	12.99	77.31	390.69	34.40	1.98	4.01	7.31	148.23	130.66
	GC17m3	GIC	13.06	3.21	2.17	775.74	149.93	111.01	122.10	4.77	27.59	161.59	11.71	0.78	1.82	6.64	55.27	45.67
VR	GC4m1	GIC	11.94	5.50	9.01	1685.11	612.23	80.52	332.60	20.23	71.46	317.11	29.69	2.54	2.64	6.32	253.45	117.77
	GC4m2	GI	11.94	5.11	251.21	3710.66	861.24	197.43	2067.59	9.06	179.12	2049.58	41.63	7.04	1.72	33.87	142.01	96.49
	GC4m3	GIC	9.89	5.38	18.45	1428.51	403.44	67.03	308.53	2.49	57.23	224.11	22.94	0.43	1.20	6.95	4.94	93.79
	GC4m4	GI	11.76	6.51	16.66	1686.67	595.89	95.27	352.09	10.74	84.65	381.47	36.73	3.33	1.36	7.69	93.11	134.28
	GC4m5	GI	11.94	5.76	12.05	1492.88	131.29	78.98	440.29	13.34	66.27	312.80	32.65	2.33	0.76	6.49	143.94	106.30
	GC4m6	GIC	11.83	4.83	18.11	1378.88	378.96	77.95	300.99	15.91	59.01	269.45	26.86	2.30	0.71	55.22	175.74	98.25
	GC4m7a	GIC	12.12	7.13	20.31	1479.24	554.49	119.04	327.08	9.97	74.75	338.53	32.14	3.22	3.25	9.30	100.82	122.03
	GC4m2_4a	GTMI	11.43	7.13	18.54	1947.13	91.88	113.76	585.30	18.91	78.21	413.46	36.38	4.81	0.80	8.36	237.08	128.30
	GC4m2_7a	GI	11.94	10.21	25.51	1045.26	88.60	145.90	403.86	1.82	135.96	336.36	52.75	5.37	0.24	89.50	10.98	149.11
	GC4m2_7b	GI	11.94	6.75	13.23	1409.05	114.58	77.00	323.93	4.74	79.23	369.90	33.00	3.67	0.55	6.85	27.79	128.07
	GC4m2_10	GI	11.94	5.28	11.37	1620.86	122.15	83.72	296.98	16.83	66.25	356.21	28.73	2.66	0.40	5.46	211.28	103.05
	GC14m1	GI	12.88	6.42	12.30	2182.82	1023.58	102.47	351.67	26.86	78.08	462.54	33.39	2.85	3.10	6.64	359.39	126.59
QR	GC5m2	GI	11.49	13.45	24.95	1222.91	362.17	110.72	387.93	26.32	148.69	314.91	57.35	6.23	27.62	8.82	331.76	190.24
	GC5m3	GI	11.60	5.46	17.58	1515.92	140.70	82.52	302.41	16.40	65.81	277.82	25.91	1.61	1.36	12.56	168.59	111.51
	GC5m5	GI	11.75	4.97	25.41	1640.98	244.31	106.09	336.48	19.13	61.13	279.01	26.87	0.82	0.35	7.31	194.95	111.59
	GC5m6	GI	11.47	5.70	16.91	1807.74	478.94	90.76	334.75	17.27	69.67	403.95	32.31	3.44	42.58	6.47	200.34	109.12
	GC5m7	GI	11.41	3.60	17.29	1530.02	179.54	80.14	225.43	11.01	54.02	279.31	23.76	2.66	1.75	4.19	110.11	87.48
	GC5m8	GI	11.49	6.10	21.19	1564.02	259.76	109.64	317.51	12.98	74.89	382.17	32.88	2.04	5.12	13.90	78.33	123.98
	GC5m9	GI	11.49	5.63	15.41	1524.40	203.45	82.68	338.21	14.96	63.83	308.49	29.62	3.99	17.36	11.30	199.87	105.40
	GC5m2_1b	GI	11.49	5.10	15.51	1504.60	23.59	79.77	558.55	9.52	69.76	322.12	31.91	2.43	1.37	6.81	89.53	118.12
	GC5m2_2a	GI	11.49	4.40	13.61	1107.89	78.17	73.55	268.47	12.07	49.16	217.59	22.03	1.80	0.78	10.82	123.81	90.06
	GC5m2_2b	GI	11.49	4.81	11.17	1189.62	88.45	70.17	277.85	11.90	53.90	222.30	23.19	2.01	1.24	5.43	126.15	96.52
	GC5m2_3	GI	11.49	4.67	10.67	1777.82	30.78	83.41	341.54	22.40	61.33	372.33	28.01	3.26	0.45	452.21	316.79	100.77
	GC5m2_5	GI	11.49	3.60	19.48	1497.72	138.23	76.40	299.74	15.26	56.56	272.79	28.14	0.92	3.02	5.85	144.81	101.98
	GC5m2_8	GI	11.49	6.26	11.30	5480.50	27.61	50.79	190.15	47.52	56.50	460.78	63.70	1.92	0.01	87.05	20.89	153.52
	GC8m2	GI	13.16	4.73	14.85	1750.80	127.87	80.06	349.79	18.89	62.65	283.81	27.89	2.29	0.94	6.16	217.60	109.26
	GC8m4	GI	12.01	5.41	12.73	1692.32	323.87	86.31	362.02	13.93	80.76	363.58	35.58	3.56	2.75	9.15	142.69	132.48
	GC8m7a	GI	13.56	5.52	18.24	1970.03	251.46	78.51	506.82	18.24	58.96	383.89	32.81	2.55	1.02	7.88	220.92	95.89
	GC8m8	GIC	13.58	5.95	16.04	1963.73	515.08	110.93	384.51	23.73	79.74	430.74	35.79	3.81	12.13	11.25	298.77	132.34
	GC8m9	GIC	12.07	7.95	17.59	1486.05	182.19	113.16	347.35	5.91	108.32	440.12	43.63	3.67	3.29	9.82	19.89	177.47
	GC8m11	GIC	13.56	6.44	15.46	1680.21	359.96	111.63	353.76	17.55	86.83	365.89	34.81	3.32	3.86	13.49	160.86	148.34
	GC8m2_1a	GIC	12.63	4.65	13.84	1576.27	101.90	59.83	332.01	22.53	50.08	367.54	25.58	2.24	0.45	4.75	305.43	87.35
	GC8m2_1b	GIC	13.21	5.33	13.52	1585.42	58.58	18.29	486.19	12.19	55.73	342.23	27.67	2.48	0.18	4.78	63.54	91.88
	GC8m2_2a	GIC	13.16	6.71	16.15	1712.50	385.13	89.00	350.41	16.32	238.64	354.62	34.79	2.06	0.35	10.22	122.30	369.94
	GC8m2_2b	GIC	13.21	6.29	17.81	1616.18	318.40	85.45	344.53	12.28	77.96	327.57	30.32	3.02	-0.19	7.83	111.79	130.48
	GC8m2_3	GIC	13.16	5.51	12.07	1783.01	212.59	77.33	378.40	20.28	66.00	394.82	32.17	2.71	18.49	7.21	237.73	110.51
	GC8m2_5a	GIC	13.16	4.76	11.98	2189.82	206.25	46.94	937.86	20.98	59.24	404.89	29.98	2.98	1.78	7.18	97.64	106.66
	GC8m2_8a	GIC	13.16	5.99	12.02	1627.30	242.30	61.17	316.30	25.61	62.82	406.43	28.37	2.12	0.48	5.70	324.73	111.09
	GC8m2_8b	GIC	12.67	5.33	9.48	1692.59	218.71	89.51	338.86	25.85	64.11	402.02	28.69	3.35	0.20	5.36	370.75	108.31
	GC8 m2_10a	GIC	13.63	6.96	10.32	1798.84	113.21	79.85	361.58	21.70	70.16	412.58	29.78	2.30	0.44	5.54	255.95	116.60
	GC8 m2_10b	GIC	13.63	6.65	15.17	1834.21	107.96	90.81	411.11	18.52	83.28	449.77	35.86	3.60	0.47	11.57	183.85	141.05
	GC8 m2_11a	GIC	12.75	6.07	14.22	939.54	36.87	93.94	372.08	15.94	64.24	384.50	17.67	2.54	0.46	5.74	146.37	114.82
	GC8 m2_11b	GIC	12.75	5.23	15.76	1614.87	100.22	86.59	321.70	15.07	73.19	363.89	31.12	2.90	0.46	6.64	163.18	119.92
	GC8 m2_11c	GIC	12.75	6.47	12.30	1589.39	91.74	95.66	388.02	13.75	73.67	362.87	30.66	2.37	0.28	7.31	127.58	122.61
	GC8m2_12a	GIC	15.40	5.53	7.46	2079.43	227.01	123.77	466.23	36.77	72.85	347.72	29.31	8.25	0.78	7.65	283.20	171.99

Table 4-6 continued

	Sample	Inclusion type	Ce	Nd	Sm	Eu	Gd	Dy	Er	Yb	W	Au	Pb	Th	U
PR	GC17m1	GIC	286.17	96.59	14.23	0.59	16.57	15.01	7.66	8.82	4.45	0.04	59.05	73.88	13.91
	GC17m3	GIC	92.82	37.09	5.36	0.24	4.56	4.99	2.52	3.12	1.11	0.01	24.80	20.54	3.93
VR	GC4m1	GIC	237.05	87.29	14.65	0.56	12.95	12.81	7.42	7.35	3.43	-0.03	52.44	51.02	11.34
	GC4m2	GI	228.39	97.41	13.42	0.44	17.12	26.18	23.52	26.24	5.93	1.39	55.54	258.38	63.69
	GC4m3	GIC	190.66	67.78	11.51	0.06	8.11	10.96	6.98	5.70	2.50	0.63	45.83	39.73	8.03
	GC4m4	GI	276.15	103.72	18.52	0.43	15.34	15.49	8.44	8.46	3.97	0.21	57.34	61.09	13.42
	GC4m5	GI	208.54	80.51	14.31	0.38	11.67	11.83	6.75	7.31	5.22	28.89	48.80	49.81	11.25
	GC4m6	GIC	204.72	76.87	13.38	0.47	10.43	10.59	6.27	6.33	2.66	-0.03	45.20	40.90	9.52
	GC4m7a	GIC	251.18	93.24	16.65	0.46	12.90	12.96	7.42	8.28	4.17	0.11	54.86	52.13	12.74
	GC4m2_4a	GTMI	256.50	98.65	16.28	0.31	13.22	16.49	8.47	9.32	3.39	2.68	54.71	52.29	11.55
	GC4m2_7a	GI	302.70	109.50	20.32	0.13	22.04	25.47	14.66	16.22	8.63	1.50	94.85	96.56	24.48
	GC4m2_7b	GI	259.39	97.69	17.22	0.31	14.74	14.32	8.58	8.70	3.74	0.12	48.91	54.96	12.06
	GC4m2_10	GI	212.24	81.13	15.99	0.73	12.59	11.80	6.94	7.66	2.83	0.01	45.26	44.40	10.00
	GC14m1	GI	249.42	95.35	16.68	0.93	14.92	14.72	8.23	7.94	3.96	0.11	55.59	54.51	11.67
QR	GC5m2	GI	379.48	136.67	24.61	0.86	22.18	24.18	14.75	16.92	11.45	0.85	76.35	126.33	35.00
	GC5m3	GI	223.35	84.70	15.08	0.43	11.40	12.16	6.78	7.00	3.09	0.04	48.98	48.35	9.50
	GC5m5	GI	240.79	83.20	17.02	0.64	9.03	9.05	7.28	5.61	2.92	0.00	45.52	41.90	9.15
	GC5m6	GI	222.47	80.16	14.41	0.71	11.84	12.48	7.09	7.75	3.74	0.01	49.33	47.97	11.48
	GC5m7	GI	192.94	68.61	11.87	0.36	10.21	10.38	7.10	6.24	3.32	0.80	40.17	40.38	9.16
	GC5m8	GI	257.44	96.04	15.96	0.50	12.42	11.08	8.54	7.60	3.69	0.09	55.19	58.37	13.59
	GC5m9	GI	215.69	78.01	13.04	0.58	12.23	11.77	6.79	6.83	3.02	0.33	51.67	45.57	10.02
	GC5m2_1b	GI	247.63	92.25	15.59	0.26	12.51	12.90	7.63	7.71	3.30	-0.03	47.22	50.23	11.96
	GC5m2_2a	GI	186.15	68.24	11.97	0.41	8.97	9.32	5.23	5.42	2.56	0.07	41.65	36.01	7.73
	GC5m2_2b	GI	198.62	73.07	12.79	0.52	10.03	9.92	5.74	6.09	2.78	0.07	42.74	38.67	8.59
	GC5m2_3	GI	213.48	84.15	14.09	0.73	11.26	11.87	6.69	6.71	2.94	-0.01	48.28	42.69	10.32
	GC5m2_5	GI	203.63	75.74	13.10	0.42	10.83	12.34	5.54	6.24	2.94	0.31	45.24	43.28	9.78
	GC5m2_8	GI	412.71	147.74	22.25	0.28	15.14	10.87	5.11	4.67	8.24	-0.02	35.74	137.56	42.93
	GC8m2	GI	224.19	82.14	12.84	0.49	10.78	11.17	6.35	6.28	2.48	-0.02	52.38	44.39	9.26
	GC8m4	GI	271.08	99.08	17.46	0.55	13.86	14.20	8.69	9.32	4.63	0.07	59.03	58.05	13.67
	GC8m7a	GI	200.17	70.20	12.94	0.57	10.45	10.40	6.40	7.04	3.58	0.18	49.42	52.12	13.04
	GC8m8	GIC	268.77	98.44	17.61	0.79	13.94	14.50	7.87	8.22	3.72	0.23	58.59	54.02	12.56
	GC8m9	GIC	365.39	134.16	21.81	0.31	19.19	20.09	10.79	11.11	5.36	0.03	70.07	78.97	17.98
	GC8m11	GIC	299.35	116.02	21.11	0.59	14.27	15.99	9.13	9.25	3.77	0.14	62.06	63.07	13.32
	GC8m2_1a	GIC	181.19	63.37	11.32	0.78	8.81	9.14	5.69	6.16	2.78	0.06	46.36	40.93	10.04
	GC8m2_1b	GIC	188.32	67.71	11.21	0.32	10.19	9.94	5.61	6.28	3.35	0.32	30.61	40.14	10.63
	GC8m2_2a	GIC	861.57	414.03	73.44	1.38	63.94	50.56	22.83	17.00	4.25	-0.02	57.98	66.50	15.02
	GC8m2_2b	GIC	269.15	103.26	17.89	0.62	12.23	13.53	8.33	7.87	3.85	0.06	52.54	55.87	11.96
	GC8m2_3	GIC	218.07	77.82	14.26	0.82	11.25	12.00	7.21	7.38	3.45	0.09	50.77	49.12	11.69
	GC8m2_5a	GIC	217.06	81.29	13.33	0.64	11.28	10.21	6.42	6.43	3.82	0.51	268.26	45.36	11.31
	GC8m2_8a	GIC	218.33	81.81	13.54	0.95	12.01	10.36	7.03	7.31	3.14	-0.03	48.29	47.64	10.25
	GC8m2_8b	GIC	221.41	80.09	14.02	1.00	11.42	11.95	8.01	7.15	3.15	0.25	50.83	48.10	10.81
	GC8 m2_10a	GIC	231.30	87.65	15.00	0.92	12.33	12.57	7.83	7.61	3.95	0.07	53.60	50.34	11.13
	GC8 m2_10b	GIC	280.87	102.67	17.13	0.70	15.27	15.16	9.25	9.92	4.69	-0.07	62.15	60.85	13.40
	GC8 m2_11a	GIC	213.55	71.97	14.09	0.44	13.64	12.60	8.28	7.23	4.02	-0.11	59.82	51.69	12.48
	GC8 m2_11b	GIC	242.41	90.88	16.18	0.55	13.28	13.07	7.94	8.37	3.97	0.08	51.49	53.29	11.56
	GC8 m	GIC	253.55	93.49	16.55	0.62	14.04	13.54	8.07	7.79	3.80	-0.05	56.13	53.38	11.59
	G	GIC	353.28	125.41	21.08	0.64	14.39	11.80	6.67	8.62	2.31	-0.21	91.31	122.33	12.63

Table 4-6 continued

Sample	Inclusion type	Al2O3	Be	B	Ti	Cu	Zn	Rb	Sr	Y	Zr	Nb	Mo	Ag	Sn	Ba	La
GC11m1	GIC	14.21	6.90	15.80	2056.00	178.60	124.02	396.64	25.08	81.60	382.01	36.14	2.95	0.92	24.56	322.68	142.55
GC11m2	GIC	13.01	5.53	12.94	1592.30	103.40	88.30	334.58	21.30	73.88	334.37	32.06	2.88	22.46	6.71	239.18	125.07
GC11m3	GIC	12.71	5.88	14.25	1653.45	108.48	83.60	350.17	20.76	70.09	326.98	31.79	2.61	23.18	6.49	227.20	120.06
GC11m4a	GIC	11.94	5.58	21.28	1902.62	488.25	113.68	350.26	10.83	78.96	365.41	36.91	4.82	40.65	9.04	73.84	134.30
GC11m5	GIC	10.65	8.65	21.07	979.92	142.92	111.58	320.00	3.96	115.35	285.09	43.76	2.93	36.41	18.34	14.57	124.13
GC11m7	GIC	12.90	6.39	15.67	1648.77	122.41	94.87	350.70	12.94	83.61	371.89	36.40	2.83	9.41	7.93	116.44	140.89
GC11m8	GIC	13.15	6.75	20.73	1653.31	183.47	107.41	398.67	9.55	87.05	377.65	40.22	3.33	122.31	8.51	46.12	151.84
GC11m9a	GIC	12.87	6.13	17.10	1549.25	170.19	84.54	357.53	12.55	77.50	343.26	35.98	2.98	23.54	9.44	115.83	131.06
GC11m10	GIC	12.87	5.55	16.33	1920.91	398.69	101.47	364.10	21.71	80.53	435.41	35.08	4.33	57.15	7.36	273.37	135.63
GC11m11	GIC	13.12	4.81	13.32	1418.30	124.67	79.72	309.34	20.65	63.91	282.46	28.10	2.05	28.87	6.18	257.24	110.02
GC11m12	GIC	12.07	8.05	15.19	1668.50	527.55	113.77	390.94	16.34	102.30	424.09	43.56	3.96	35.06	8.48	151.76	157.39
GC11 m2_2	GIC	13.94	8.28	10.79	1506.76	385.11	98.36	354.71	10.39	99.48	402.61	39.56	4.73	3.87	9.30	76.91	158.44
GC11 m2_4	GIC	13.01	6.14	19.42	1794.67	44.98	84.03	639.50	19.88	70.57	396.07	34.27	9.64	2.27	6.74	218.98	116.56
GC11 m2_5	GIC	13.76	7.57	14.65	2034.96	15.22	68.56	351.95	20.87	79.39	435.61	29.53	2.95	4.57	7.13	277.67	127.64
GC11 m2_6	GIC	13.07	4.47	10.02	1295.21	55.19	71.21	266.77	19.21	67.45	277.08	27.21	3.25	0.79	6.76	243.69	116.50
GC11 m2_7	GIC	13.01	7.90	19.49	1908.69	32.24	121.97	378.51	17.46	89.87	403.50	39.82	3.02	0.42	9.87	153.22	156.61
GC11 m2_8	GIC	13.01	8.74	14.63	1409.44	269.14	84.33	796.19	7.57	101.46	383.26	40.27	3.67	0.61	9.60	37.64	158.69
GC11 m2_9	GIC	13.01	4.52	4.04	1247.86	50.08	25.64	331.78	18.04	65.63	284.64	28.35	0.87	1.75	4.92	225.39	113.15
GC11 m2_10	GIC	13.94	5.40	12.29	1508.64	30.98	104.86	322.72	17.34	66.92	276.55	26.00	1.54	3.23	104.08	208.26	115.77
GC11 m2_11	GIC	13.94	5.48	14.69	1487.88	16.38	70.97	566.44	15.25	58.89	257.94	26.43	1.39	0.65	6.21	154.38	100.28
GC16m1	GIC	13.30	6.25	17.07	1796.46	198.87	91.02	362.10	14.16	80.42	370.38	34.85	3.46	18.63	18.11	145.64	137.95
GC16m2	GIC	13.24	7.16	20.38	2026.36	111.78	115.51	345.53	21.81	75.83	372.91	32.83	2.87	6.68	157.37	268.76	130.83
GC16m3	GIC	13.24	8.16	16.98	1417.99	149.70	122.08	400.36	8.51	110.75	453.67	42.55	4.39	29.44	9.83	20.92	189.78
GC16m4	GIC	13.48	7.14	19.94	2019.16	385.25	126.98	397.11	14.40	116.12	563.94	47.01	2.77	100.65	11.60	50.96	194.36
GC16m7	GIC	13.24	6.91	21.10	2456.85	102.28	125.52	391.11	15.87	71.72	398.20	36.98	3.21	1.89	9.63	143.40	78.72
GC11 UH2	GTMI	13.14				**3.81**	**71.31**	**378.15**	**20.64**	**72.90**	**418.28**	**34.21**	**2.99**	**0.13**	**6.45**	**239.87**	**116.76**
GC11 UH3	GTMI	13.14				**0.55**	**91.93**	**423.01**	**15.53**	**81.17**	**326.58**	**39.08**	**3.57**	**0.00**	**8.15**	**121.77**	**129.55**
GC11 UH4	GTMI	13.14				**5.54**	**76.81**	**367.13**	**11.71**	**80.31**	**393.62**	**35.10**	**2.66**	**-0.01**	**6.49**	**95.41**	**132.78**
GC11 UH6	GIC	13.14				**1.47**	**88.61**	**372.56**	**22.16**	**75.87**	**339.42**	**33.20**	**3.63**	**-0.11**	**6.58**	**283.49**	**127.19**
GC11 UH9	GIC	13.14				**0.21**	**60.54**	**370.73**	**20.12**	**67.86**	**405.19**	**30.56**	**3.31**	**0.14**	**5.63**	**244.43**	**105.72**
GC11 UH11	GIC	13.14				**4.98**	**87.09**	**358.74**	**22.49**	**76.45**	**423.23**	**33.16**	**3.36**	**0.11**	**6.04**	**292.94**	**117.16**
GC11 UH12a	GTMI	13.14				**5.33**	**74.05**	**335.64**	**15.39**	**61.27**	**283.64**	**28.43**	**2.37**	**0.05**	**5.72**	**140.56**	**110.03**
GC11 UH12b	GIC	13.14				**3.13**	**88.69**	**358.90**	**25.42**	**61.21**	**270.47**	**30.77**	**2.66**	**0.13**	**5.94**	**181.79**	**112.25**

QR

Figure 4-6 continued

Sample	Inclusion type	Ce	Nd	Sm	Eu	Gd	Dy	Er	Yb	W	Au	Pb	Th	U
GC11m1	GIC	291.64	105.91	16.66	0.66	15.05	15.23	8.89	9.43	3.91	-0.12	66.08	58.41	13.39
GC11m2	GIC	252.53	94.47	15.95	0.68	14.01	13.56	7.69	8.04	3.52	0.12	57.65	54.07	11.27
GC11m3	GIC	244.82	89.35	15.21	0.68	13.25	12.29	7.40	7.63	3.53	0.10	54.32	50.44	11.56
GC11m4a	GIC	278.66	102.41	16.04	0.51	16.21	13.21	7.44	8.78	5.46	0.37	60.49	62.75	14.08
GC11m5	GIC	253.09	94.09	18.56	0.16	18.81	20.87	12.23	13.39	6.09	0.04	78.84	82.25	22.03
GC11m7	GIC	286.35	105.11	18.36	0.48	15.35	14.86	8.83	8.98	4.46	0.06	60.32	61.34	13.57
GC11m8	GIC	305.87	112.15	20.66	0.45	14.67	15.29	8.77	8.81	5.17	0.21	68.11	66.07	15.23
GC11m9a	GIC	280.87	99.89	17.01	0.47	14.04	14.66	8.18	8.35	4.54	0.18	57.13	57.26	13.73
GC11m10	GIC	276.12	104.11	18.75	0.82	13.82	15.58	8.63	8.95	3.95	0.08	58.19	54.86	12.51
GC11m11	GIC	229.12	87.13	13.84	0.61	12.34	12.33	6.58	7.08	3.12	0.25	48.63	47.58	9.43
GC11m12	GIC	328.37	119.87	20.51	0.52	17.81	18.47	9.54	9.49	4.10	0.30	63.07	66.44	14.44
GC11 m2_2	GIC	317.61	120.43	23.69	0.47	17.87	17.54	10.07	10.96	4.20	-0.35	59.49	67.51	13.99
GC11 m2_4	GIC	237.88	88.19	15.81	0.70	11.94	14.32	7.16	8.04	134.53	3.32	68.54	49.31	12.34
GC11 m2_5	GIC	256.11	94.72	18.49	0.93	15.06	13.92	8.16	9.04	3.94	0.45	52.13	55.40	11.90
GC11 m2_6	GIC	237.74	85.17	16.55	0.66	13.03	12.62	6.59	7.62	3.90	0.10	43.37	48.35	9.89
GC11 m2_7	GIC	310.23	111.84	22.25	0.50	18.39	17.38	10.40	9.37	2.83	0.15	57.41	65.76	13.07
GC11 m2_8	GIC	324.09	124.76	19.44	0.32	19.92	17.74	12.08	10.40	5.45	2.55	34.01	70.73	15.97
GC11 m2_9	GIC	224.79	87.32	12.62	0.59	11.69	12.03	7.79	8.56	3.56	0.42	48.06	49.71	10.20
GC11 m2_10	GIC	236.90	86.92	15.95	0.65	13.03	11.88	6.43	7.52	2.37	-0.14	52.42	47.29	9.27
GC11 m2_11	GIC	206.73	74.99	12.68	0.58	10.24	10.30	6.35	6.59	3.11	0.89	28.17	40.88	8.87
GC16m1	GIC	281.70	103.87	16.47	0.61	14.68	13.91	8.74	8.29	4.64	0.23	65.47	62.90	13.36
GC16m2	GIC	258.56	106.54	17.91	0.76	15.29	14.65	8.35	9.21	3.33	0.59	80.19	59.91	12.73
GC16m3	GIC	384.45	142.76	25.01	0.35	19.01	20.05	11.59	12.25	5.67	0.14	75.44	81.28	19.01
GC16m4	GIC	404.35	152.00	26.19	0.43	24.26	21.33	12.25	14.18	6.05	0.37	79.75	85.59	20.70
GC16m7	GIC	157.93	66.78	14.26	0.73	12.13	12.83	7.87	7.53	4.45	0.02	68.00	54.77	13.57
GC11 UH2	GTMI	**244.99**	**91.86**	**16.03**	**0.74**	**13.52**	**13.58**	**7.88**	**8.02**	**3.75**	**0.02**	**48.86**	**12.60**	
GC11 UH3	GTMI	**278.47**	**96.71**	**17.24**	**0.48**	**14.36**	**14.74**	**8.53**	**8.68**	**5.37**	**0.00**	**60.10**	**16.07**	
GC11 UH4	GTMI	**269.15**	**99.74**	**16.73**	**0.45**	**14.20**	**14.76**	**8.39**	**8.57**	**4.85**	**0.01**	**53.30**	**12.79**	
GC11 UH6	GIC	**261.45**	**97.60**	**18.58**	**0.66**	**12.65**	**12.26**	**8.16**	**7.98**	**3.81**	**0.01**	**49.35**	**10.86**	
GC11 UH9	GIC	**217.59**	**80.72**	**14.55**	**0.61**	**12.08**	**12.09**	**7.13**	**7.29**	**3.39**	**0.01**	**47.46**	**11.09**	
GC11 UH11	GIC	**240.58**	**93.45**	**16.58**	**0.88**	**13.90**	**13.95**	**8.25**	**8.54**	**3.66**	**-0.03**	**51.81**	**12.07**	
GC11 UH12a	GTMI	**227.92**	**82.28**	**14.01**	**0.51**	**11.24**	**11.60**	**7.05**	**7.27**	**2.54**	**0.03**	**48.46**	**9.70**	
GC11 UH12b	GIC	**254.88**	**85.74**	**15.01**	**0.58**	**11.44**	**11.67**	**6.73**	**6.95**	**3.32**	**0.01**	**56.44**	**10.74**	

QR

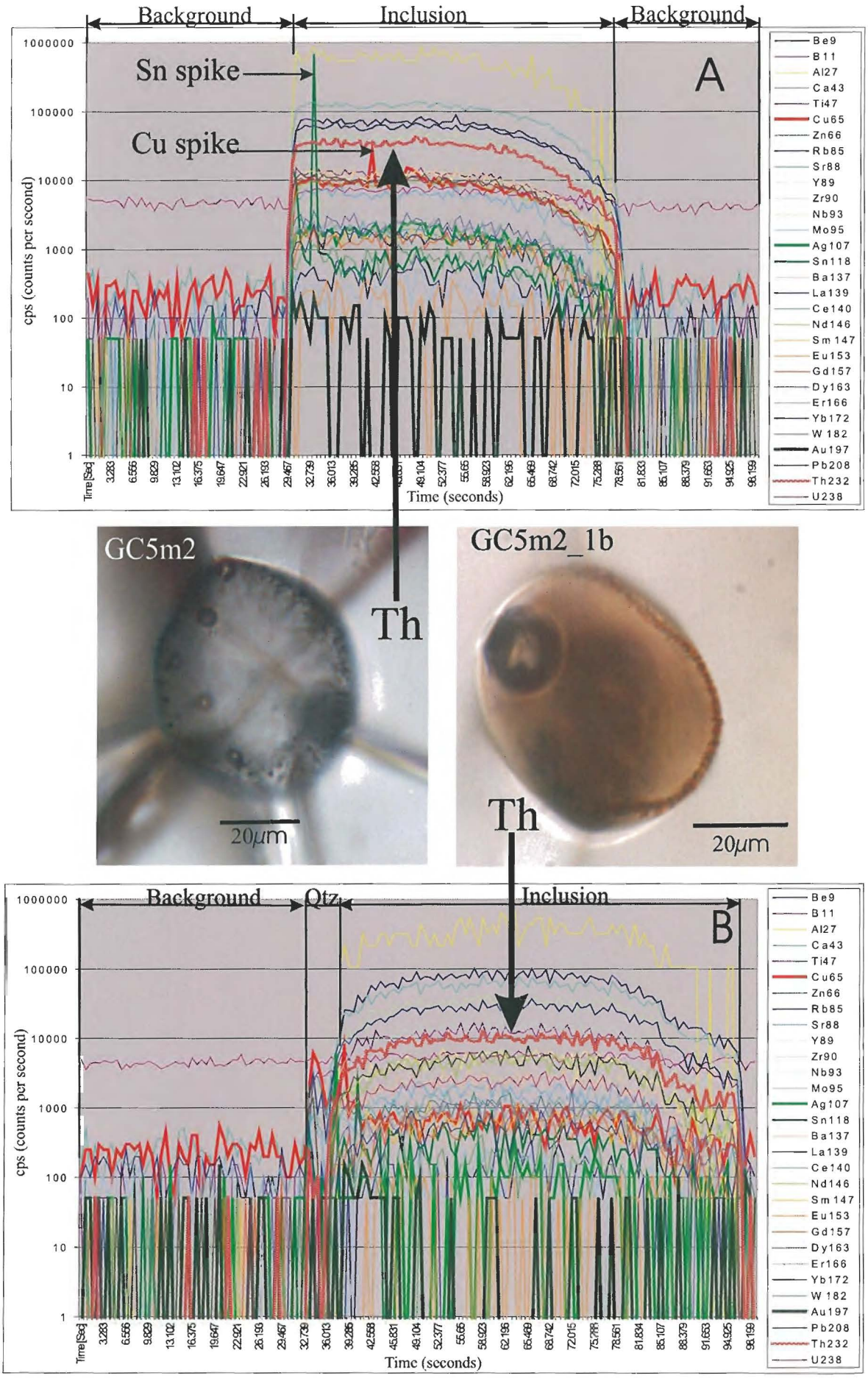

Figure 4-13 A comparison of two inclusions from the Quartz Rhyolite that have significantly different Th,U REE concentrations. Note that Th cps (arrow) for inclusion and that inclusion GC5m2 are significantly greater than those for sample GC5m2-1b. Also note that cracks around GC5m2 only occurred during polishing and exposure of the inclusion and is a common feature of most exposed inclusions, which do not have elevated trace element concentrations. Graph A shows a Cu and Sn peak due to the ablation of small crystals. For the calcuation of absolute element concentrations these spikes were excluded from the data as they do not represent glass.

element data of P_2O_5 show a strong decrease with increasing SiO_2 (Fig 4-5H), which appears to suggest that the fractionation of apatite may have been important in controlling the concentration of LREE and F in the melt; however this does not explain the depletion of elements such as Pb, Th and U with fractionation. Analysis of apatite and hornblende were carried out on samples from the Eucarro Rhyolite by Stewart (1994), and result yielded ~3 wt% and ~0.8 wt% F respectively. This supports the notion that F may have been lost during fractionation. Alternatively, some fluorine may have also been lost during degassing.

4.5.2.1. Geochemical comparison of melt inclusions with the groundmass and wholerock normalized to a primitive mantle

A spider diagram for each the Plagioclase Rhyolite, Vesicular Rhyolite and Quartz Rhyolite (Fig 4-14) shows the distribution of trace elements for melt inclusions, groundmass and whole rock all normalized to a primitive mantle (Sun and McDonough, 1989). All samples analyzed are similar in their trace element distribution trends and relative concentration of groundmass, melt inclusions and whole rock. Two similarities are observed for all samples, which include: 1) melt inclusions are lower in Ba and Sr relative to whole rock and groundmass, 2) melt inclusions are enriched in W, Th, U, Pb, Mo, F and Sn compared with the groundmass and wholerock.

4.5.3. Metals versus Cl for melt inclusions and groundmass

Metal concentrations within the groundmass and melt inclusions were plotted against uncalibrated Cl concentrations (Cl was analyzed using LA-ICPMS, without a standard and therefore does not represent true absolute concentrations, but are used here for relative concentrations) to determine if any correlation exists. Scatter plots of Pb, W, Mo, Sn, U and Th versus Cl (Figs 4-14A-F) show that melt inclusions are more enriched in metals and Cl compared to the groundmass. Furthermore melt inclusion scatter plots of Pb, W, Mo, Sn, U and Th versus Cl show strong positive linear correlations, which suggest that the distribution of the metals was controlled by the Cl content of the melt.

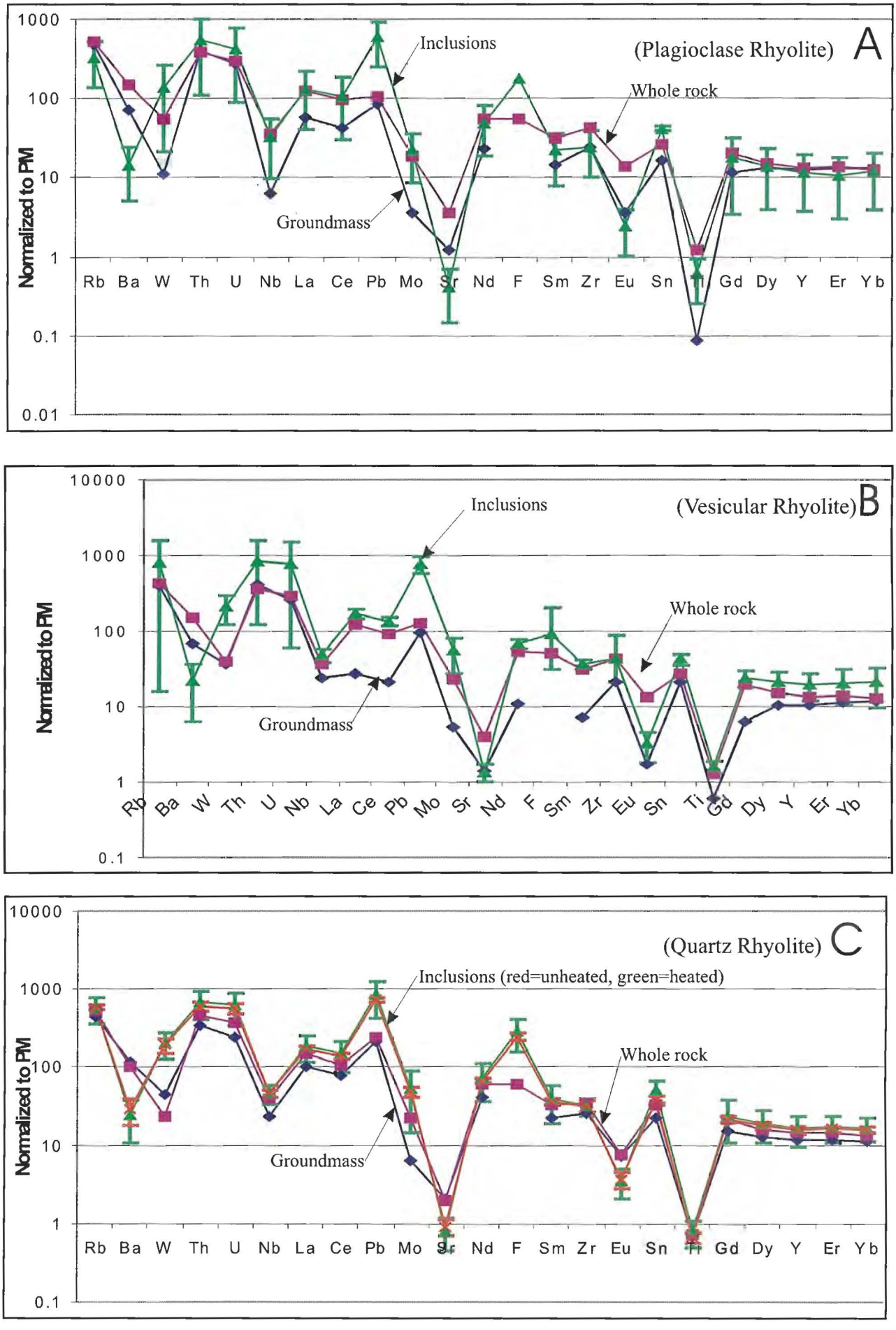

Figure 4-14 Spider diagrams of the groundmass (blue), whole rock (purple) and melt inclusions (heated green) (unheated red graph C only) for the Plagioclase Rhyolite (graph A), Vesicular Rhyolite (graph B) and the Quartz Rhyolite (graph C) normalized to a primitive mantle (Sun and Mc Donough, 1989).

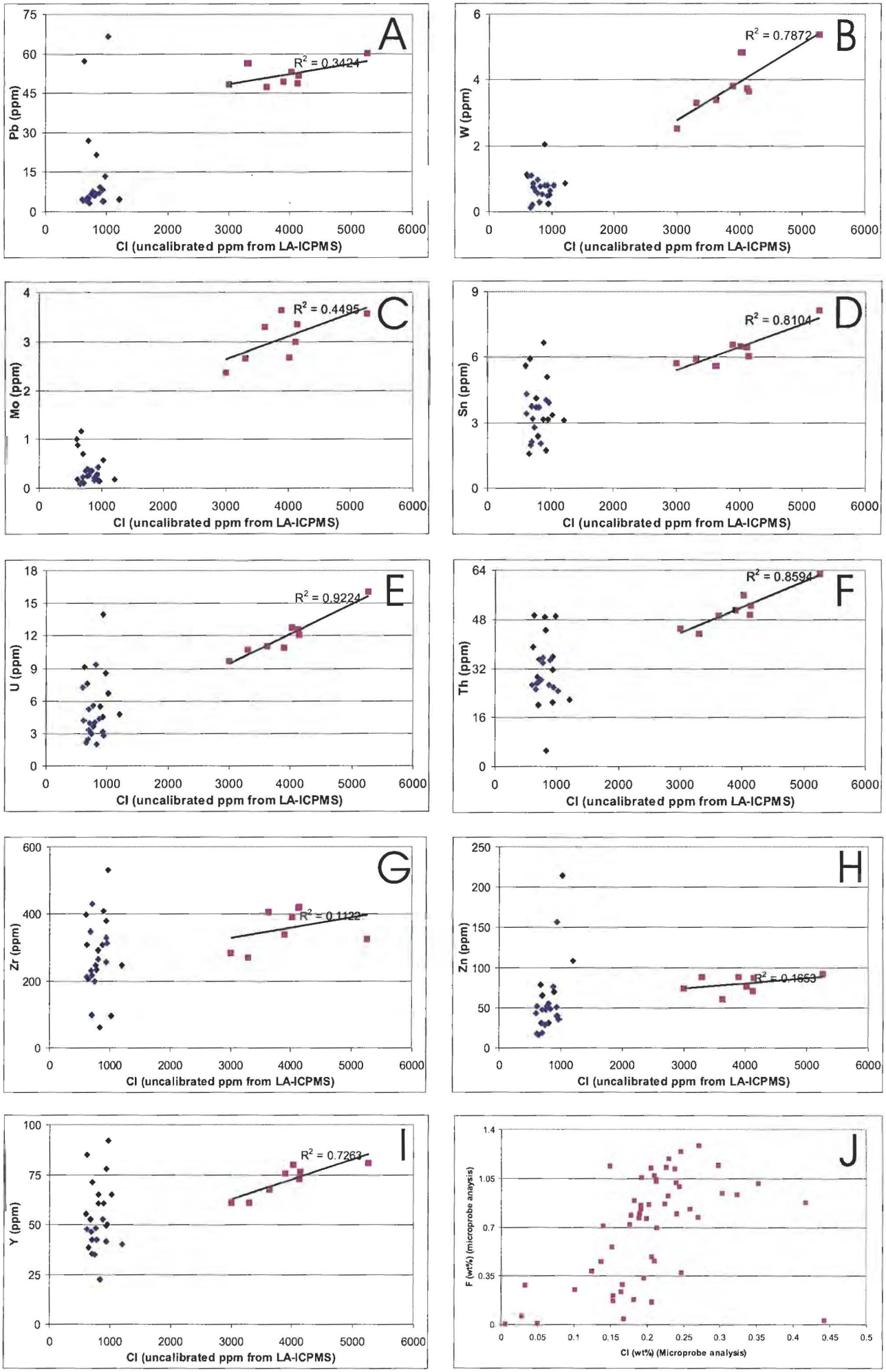

Figure 4-15 Scatter plots of groundmass (blue) and melt inclusions (purple). Note that Cl concentrations are uncalibrated and therefore do not represent absolute concentrations. They are used here to show relative concentrations. Note that figure "J" represents absolute Cl concentrations from microprobe analysis and suggests that LA-ICPMS result are most likely over estimates.

Zn, Zr and Y (Fig 4-15G-I) all show similar trends to the above metals, except that they are only marginally more enriched within melt inclusions compared to the groundmass.

Figure 4-15J shows scatter plots of F versus Cl. Plots show that there is a moderately strong positive correlation between the distribution of F and Cl. This suggests that some inclusions are more enriched in volatiles than others. There are a number of possibilities to explain why some inclusions are more enriched in volatiles and certain metals compared to others, which include; 1) some inclusions may be decrepitated and have therefore lost some of there volatiles and metals, 2) the composition of the melt at the time of trapping was not homogeneous, 3) volatiles and metals may have been lost from whole rocks during alteration.

4.6. Summary and discussion

The geochemical data of the Eucarro Rhyolite suggests that all whole rocks, groundmass and melt inclusions are positioned along fractionation trends. F, however, does not fit along fractionation trends, and is on average significantly more enriched in melt inclusions, suggesting that the whole rock has lost significant amounts of F during crystal fractionation (i.e. the crystallization of fluor-apatite and amphibole) and/or during magmatic degassing. A linear decrease in the concentration of trace elements U, Th, REE, Pb, Mo, W and Sn with fractionation is difficult to explain by crystal fractionation, and thus remobilization of these elements may have occurred within fluorine and aqueous fluids, which may have been exsolved from the melt at lower pressures. Gramenitskii and Shchekina (2005) advocated that REE always partition into the melt at temperatures above 650°C, because fluorine complexes are common in fluid at lower temperatures; thus significant losses of trace elements and F may have occurred after and during the eruption of the Eucarro Rhyolite. Furthermore Th and U are known to form complexes with F and may have also been lost after/during the eruption of the Eucarro Rhyolite. U, Th, REE, Pb, Mo, W and Sn within melt inclusions show strong positive linear correlations with Cl. This suggests that the role of Cl in the melt was important in controlling the distribution of these elements. Moreover a linear correlation also exists

between the concentration of Cl and F within melt inclusions, which suggests that F may have also been important in controlling the distribution of U, Th, REE, Pb, Mo, W and Sn.

Chapter 5
Discussion and Conclusions

5.1. Introduction

The geochemistry of magma plays an important role in the way in which magma is erupted. In particular, the volatile content of melt can determine whether an eruption will be violent or quiescent or whether lava will flow or not, thus an understanding of such volatiles is highly important.

One way of determining the nature of volatiles within an ancient volcanics province is to study melt and fluid inclusions. For the GRV, quartz, which hosts melt and volatile inclusions (*see* Chapter 3) offers insights into the nature of the volatiles. However before one can determine the nature of the volatiles, one must determine if the quartz, which hosts the inclusions is primary.

5.2. The origin of Type 1 and Type 2 quartz

Two types of quartz (Type 1 and Type 2) were identified within the Plagioclase Rhyolite and the Vesicular Rhyolite (PR/VR). Type 1 quartz was identified within the Quartz Rhyolite (QR). As noted in Chapter 3, Type 2 quartz is characterized by melt, composite, CO_2, non-silicate and aqueous fluid inclusions, and hence hosts volatile-rich inclusions. In contrast, Type 1 quartz is characterized by melt inclusions and minor aqueous fluid inclusions which occur along the same trapping plane.

In any magmatic system there is the possibility that some crystal phases may be derived from other sources (i.e. stoping of country rocks). In the case of the Eucarro Rhyolite this may be a significant problem as granite clasts have been found within the lower units of the Eucarro Rhyolite, and thus some of the quartz found within the Eucarro Rhyolite may be xenocrystic. Geochemical studies of melt inclusions from Type 1 quartz show that they have major and trace element compositions that closely resemble the host

rock. Moreover, Type 1 quartz from the Quartz Rhyolite is commonly euhedral to subhedral, contains only minor fractures, and is therefore most likely crystallized from the melt.

The origin of Type 2 quartz however is not well constrained as no glass inclusions from Type 2 quartz have been analyzed, because they were too small for LA-ICPMS analysis. However, quartz grains from granite clasts were examined and were found to contain CO_2 inclusions that closely resembled CO_2 inclusions hosted by Type 2 quartz. Furthermore, Kamenetsky *et al.* (2003) reported on the presence of non-silicate melt inclusions within quartz from granite clasts, which is consistent with inclusions observed in Type 2 quartz, and thus suggests that Type 2 quartz may have been derived from granite clasts. According to Garner and McPhie (1999) granite clasts within the upper GRV were most likely derived from the subsurface basement and coeval granitoid sources.

Alternatively Type 2 quartz may have formed within the magma chamber during magmatic degassing and magma unmixing or reactions with the wall rocks. If so, the degassing or reaction with the wall rock could be the source of CO_2 and volatile characteristics of inclusions in Type 2 quartz. Moreover, non-silicate inclusions may represent unmixing of metal-chlorides from the melt, which would have important implications for ore-forming processes.

CO_2 inclusions within quartz veins at various localities have been reported (e.g. Skirrow *et al.*, 2004), and are thought to be intimately linked with Au mineralization and the emplacement of the Hiltaba Granite (Ar^{40}/Ar^{39}: Fraser, 2004). Recently, Phillips and Evans (2004) have suggested that CO_2 may play a critical role during gold transport by buffering the fluid in a pH range at which elevated gold concentration can be maintained by complexing with reduced sulfur. Thus, an important aim for future studies should be to determine the origin of Type 2 quartz, which would be beneficial in understanding the role of CO_2 during magmatic degassing of the Hiltaba Granite.

5.3. The significance of embayed/globular quartz and subhedral/euhedral Type 1 quartz

Type 1 quartz ranges from euhedral to globular to embayed. Samples from the Quartz Rhyolite typically contain euhedral and subhedral Type 1 quartz, whereas samples from the Vesicular Rhyolite and Plagioclase Rhyolite are characterized by globular and embayed Type 1 quartz. The geochemistry of melt inclusions from all samples is similar, which suggests that Type 1 quartz crystallized from magma that was compositionally the same.

In one sample from the Vesicular Rhyolite (GC4) vermicular quartz (anhedral quartz and feldspar intergrowths) (Fig 2-10) was identified and is thought to represent rapid crystal growth due to undercooling (e.g. Swanson and Fenn, 1986). Vermicular quartz was also identified within the roof of the Hiltaba Granite, and is thought to represent quenching of the granite at the contact. Thus vermicular quartz within the Vesicular Rhyolite may represent quartz that formed along a quenched margin, which was subsequently brought to the surface during eruption.

Alternatively Chang and Meinert (2004) suggested that embayed quartz can form through: 1) resorption of quartz by the melt due to ascending and decompression; 2) resorption of quartz due to magma mixing; or 3) resorption of quartz due to decreased F activity in the melt after some F partitions into magmatic aqueous fluid. The possibility that Type 1 quartz within the Plagioclase Rhyolite and the Vesicular Rhyolite represents resorption of quartz, is consistent with magma up welling (i.e. magma ascent and decompression), and the presence of mafic xenoliths, which may represent magma mixing.

5.4. The significance of Type 1 quartz and plagioclase from the Eucarro Rhyolite

One notable feature of the Eucarro Rhyolite is that those samples that contain the greatest amount of quartz also tend to have the least feldspar (e.g. Quartz Rhyolite). Furthermore, those samples that contain the least amount of quartz are characterized by large tabular euhedral feldspar crystals and relic mafic crystals, which are though to be relic pyroxene phenocrysts (Fig 2-7). According to a number of authors (e.g. Hammer

and Rutherford, 2002; Cashman and Blundy, 2000; Couch *et al.*, 2003) the decompression and degassing of silicic melt plays a significant role in the crystallization of feldspar and other phases such as pyroxene and Fe-Ti oxides. In particular, the exsolution of water raises the liquidus of the melt and thus induces crystallization. Fluorine, which is known to form complexes with H_2O, also has a significant effect on lowering the liquidus of granitic melts (e.g. Wyllie and Tuttle, 1961) and may also induce crystallization during magmatic degassing. Thus, I suggest that the precursor magma for Eucarro Rhyolite/Vesicular Rhyolite existed in the upper region of the magma chamber where slow magmatic degassing crystallized large tabular feldspar phenocrysts, and it is possible that the precursor magma for the Quartz Rhyolite existed in a lower region of the magma chamber, where magmatic degassing was less significant.

Experiments carried out by Couch *et al.* (2003) showed that the rate of exolution of gases has important implications for the morphology of plagioclase crystals, where planar tabular crystals formed as a result of low undercooling (slow exolution of gases), and hopper, swallowtail, skeletal and dendritic varieties formed as a result high undercooling (rapid exolution of gases). Feldspar phenocrysts within the Eucarro Rhyolite are mostly tabular in shape and therefore low undercooling (slow exolution of gases) was likely dominant.

Alternatively, the large tabular feldspar phenocrysts could also have formed at lower depths in the magma chamber where cooling was slower. However, the presence of Type 2 quartz within the Plagioclase Rhyolite and Vesicular Rhyolite suggests that magmatic degassing and/or reactions with the wall rock may have been significant.

5.5. The role of fluorine within the Eucarro Rhyolite

Microprobe analysis of melt inclusions shows that there is a significant variation in the fluorine concentration within inclusions (i.e. 0.03 to 1.24 wt%)(Chapter 4). In inclusions which are depleted in F (GC4 and GC5), daughter crystals are either absent or sparse, and these inclusions tend to have the lowest shrinkage bubble volume ratios (Fig 3-11). Moreover those inclusions that contain appreciable amounts of F are also enriched in Cl, which suggests that some inclusions are more enriched in volatiles compared to

others. In some inclusions the F concentration was high enough in the melt to crystallize as daughter phases of fluorite (e.g. Fig 3-4).

An average F concentration (0.71 wt%) shows that the melt was significantly more enriched compared to the whole rock (avg 0.14 wt%), which implies that a significant amount of F was either degassed from the melt or that F was progressively depleted in melt during the fractionation of apatite and amphibole. Alternatively, some F from the whole rock may have also been lost through alteration, although the F/Sm ratio suggests that losses due to alteration were not significant (*see* Chapter 4).

One of the significant problems associated with the upper GRV is the widespread nature of the lava flows (e.g. >25,000 km^2) (Garner and McPhie, 1999; Allen *et al.*, 2003). The consensus view that these are lava flows is at odds with the high viscosity known for rhyolitic lavas. However, various authors (e.g.(Hards, 1978) Dingwell and Hess, 1998; Lange, 1994; Dingwell *et al.*, 1985; Moyen 1988) have advocated that fluorine in the melt acts as an effective depolymerizer, where fluorine substitutes for O and forms Si-F bonds, or according to Manning *et al.* (1980), F can effectively depolymerize aluminosilicates (e.g. $AlSi_3O_8^- + 6F^- \rightarrow AlF_6^{3-} + 2O^{2-} + 3SiO_2$). Dingwell *et al.* (1985) suggested that the addition of 1 wt% of F to a rhyolitic melt has the effect of reducing the viscosity by one order of magnitude at 1000°C, and due to a high melt/fluid partition coefficient, a significant amount of F can be retained in the melt at atmospheric pressures (e.g. several wt% F can be achieved at 1 bar: Mysen, 1988). In certain cases F may significantly influence eruptive style enhancing fluid flow and strongly reduce the pyroclastic component of a given eruption (Hards, 1978; Dingwell *et al.*, 1985; Mysen, 1988). Moreover the effects of fluorine are felt greatest in Si-rich volcanics (Fig 5-1) (Dingwell *et al.*, 1985).

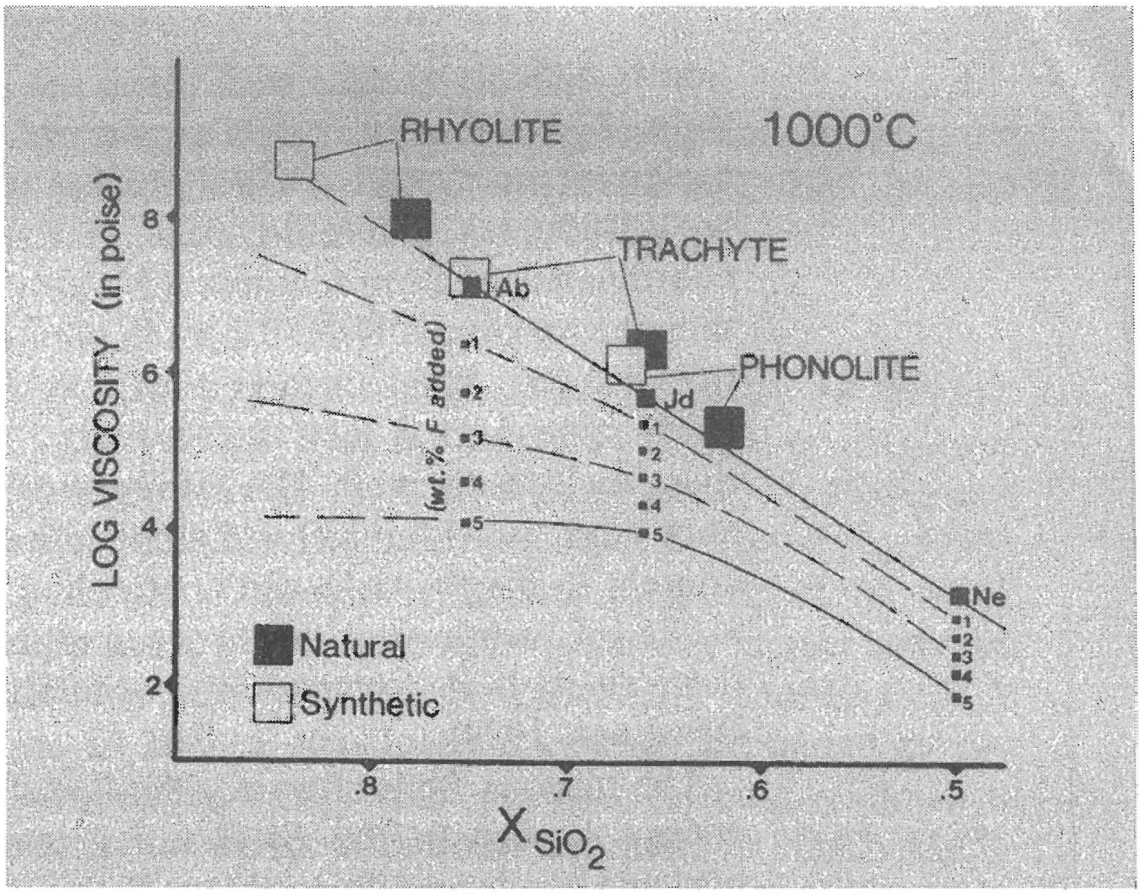

Figure 5-1. The effect of fluorine content on melt viscosity for rhyolites, trachytes and phonolites at temperatures of about 1000°C (sourced from Dingwell *et al.*, 1985).

5.5. The viscosity of the Eucarro Rhyolite

Temperature, composition and phenocryst content are three important factors which significantly affect the viscosity of lava. Temperature estimates for the upper Gawler Range Volcanics are between 900 and 1010°C based on pyroxene and feldspar geothermometry as well as apatite solubility (Creaser and White, 1991); however homogenization temperatures of melt inclusions suggest that quartz crystallized at temperatures between 800 and 850°C (pers. comm.. V.Kamenetsky, University of Tasmania). Discrepancies in temperature may reflect; 1) a difference in the timing of crystallization of quartz and pyroxene, 2) errors associated with pyroxene

geothermometry or 3) that the temperature of homogenization of melt inclusions does not represent trapping temperature.

If the pyroxene and feldspar geothermometers were not calibrated for high F concentrations, this could result in an invalid calibration, as F has a strong effect in altering the cotectic and eutectic points of phases used for geothermometry and thus may have resulted in a significant overestimation of the crystallization temperature.

Alternatively, a significant amount of undercooling can sometimes be required for shrinkage bubbles to nucleate, which may result in underestimates for the trapping temperature of melt inclusions (pers. comm. P. Davidson). For future studies heating experiments on melt inclusions within pyroxene phenocrysts should be carried out so that homogenisation temperatures of melt within pyroxene can be compared with the geothermometry estimates for pyroxene. Also, in light of higher than previously reported F concentrations in the upper GRV (e.g. Creaser, 1989), geothermometry calculations should be re-examined. An accurate measure of the temperature at the time of the eruption is extremely important for estimating the viscosity of the melt at the time of the eruption. Furthermore, Dingwell *et al.* (1985) has demonstrated that the combine effect of high temperatures and a high concentration of F and H_2O can have significant effects on lowering the viscosity of rhyolites (Fig 5-2).

The amount of water in the melt also has important implications for the viscosity of lavas and previous work by Creaser and White (1991) have estimated water contents of <1 wt% for the upper Gawler Range Volcanics. According to Lange (1994) the addition of 2 wt% water can dramatically reduce the viscosity of melts by up to ~3 log units, which is the equivalent to an increase of ~200°C for the same viscosity for rhyolitic melts. Water solubility models show that felsic magmas with 2-5 wt% water should reach saturation at crustal depths of about 1-4 km (e.g. Burnham, 1979), but lavas that contain 2 wt% of H_2O may reach saturation at very shallow levels, possibly even at the surface (Creaser and White, 1991), and thus promoted lower viscosities. Thus, low water content allied with a high F content and high eruption temperatures may be critical in promoting an effusive style eruption and lowering the viscosity of the melt. In the case of the upper GRV, geochemical studies show that these factors may have been significant in lower the

viscosity of the melt. In contrast a phenocrysts content of between 10 and 20% would have increased the viscosity of the melt.

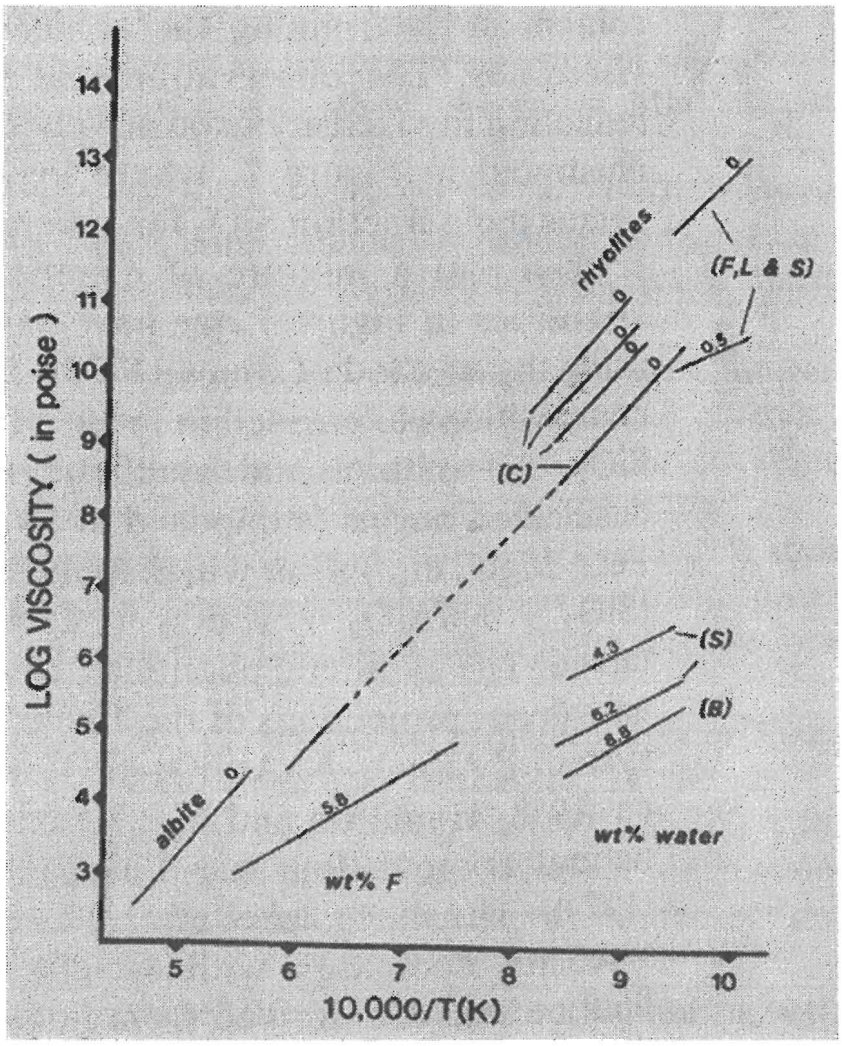

Figure 5-2 A comparison of the effects of F, H_2O and temperature on the viscosity of rhyolites (sourced from Dingwell *et al.*, 1985)

An estimation of the effective viscosity for the upper GRV was previously calculated by Stewart (1994) using the Einstein-Roscoe equation, which is appropriate for crystal bearing magmas (Pinkerton and Stevenson, 1992):

$\eta = \eta_l(1-R\Phi)^{-2.5}$,

where η_l is the viscosity of the phenocryst-free melt, R is a constant (R=1.67) and Φ is the volume fraction of phenocrysts (0.35). The effective viscosity calculated by Stewart (1994), for a magma temperature of 1000°C was 1.42 * 10^7 Pa s with a H_2O content of 1 wt%, or 1.8 * 10^6 Pa s with a H_2O content of 2wt%. Still lower viscosity would be expected with the addition of 0.75 wt% F.

5.7. A comparison of the upper GRV with other volcanics

5.7.1. Lava flows from LIP

Large and extensive rhyolitic lavas have been described from several provinces, including the North Shore Volcanic Group, Minnesota (Green and Fitz, 1993) and Snake River Plain, Idaho (Bonnichsen and Kauffman, 1987; Manley, 1992). Lavas from the Neoproterozoic North Shore Volcanic Group are described as high temperature (1000-1100°C) rhyolitic and icelandite flows that laterally extend up to 40 km and have been estimated to have volumes of 600km^3 and range in thickness from 15 to 400m and occur within units of tuffs and rheoignimbrites (Green and Fitz, 1993; Park and Ripley, 2001). According to Green and Fitz (1993) the low apparent viscosity of the lava was most likely attributed to compositional factors (F content, high Fe^{2+}) as well as high temperatures and high eruption rates.

High viscosity rhyolite flows from the 11 to 8 Ma Snake River Plain were described by Manley (1992); however, flows are smaller (9km from vent and 15 km^3) than those from the North Shore Volcanic Group (40 km from the vent 600 km^3) and were estimated to have erupted at temperatures of about 830°C. Manley (1992) suggested that the lavas flowed very slowly over a period of 10 to 18 years at a rate of 0.59 to 2.5 km/yr, and were able to retain heat due to insulation from a carapace that contained vesicles. Lava flows are interpreted to have erupted in an effusive manner from a fissure

which is about 50 km across strike (Manley, 1992). A fissure model has also been suggested for the GRV by Giles (1980) and Allen *et al.* (2003).

It is difficult to physically compare the upper units of the GRV with volcanics from other LIP. The thick homogenous widespread (>12,000km^2) felsic lava-like units of the upper GRV are to my knowledge not observed anywhere else. However, large flow units reported from the North Shore Volcanics (Green and Fitz, 1993) demonstrates that felsic lava can flow over considerable distances, particularly when they contain significant amounts of F. It may be that the upper GRV erupted from a number of vents and flowed out laterally, and therefore represents an integrated network of lava flows.

5.7.2. Geochemical comparison of melt inclusions from arc and anorogenic rhyolites

Quartz-hosted melt inclusions from the 0.76 m.y. Bishop Tuff Rhyolite (BTR) (arc-related volcanics), California were analyzed using microprobe (major elements) and an ion microprobe (trace element) by Anderson *et al.* (2000). The BTR was formed during a plinian style eruption and is characterized by ignimbrites (no lava flows are reported). Melt inclusions from the BTR and Eucarro Rhyolite (ER) have similar major elements compositions, apart from F (BTR ~0.02 wt% versus ER 0.78 wt%) and H_2O (BTR ~5 wt% versus ER <1 wt%). Furthermore, trace elements such as U (BTR ~7ppm versus ER ~12ppm), Th (BTR ~18ppm versus ER ~50ppm), La (BTR ~17ppm versus ER ~130ppm) are all significantly more enriched within the Eucarro Rhyolite. Thus the geochemistry of the GRV appears significantly different to that of arc-related volcanics. Furthermore the volatile concentration shows that the GRV is F-rich, but H_2O-poor compared to the Bishop Tuff Rhyolite, which suggests that the former is more likely to have erupted in an effusive manner compared to the latter.

Chabiron *et al.*, (2001) performed a melt inclusion study on thick (50-100m) anorogenic rhyolites tuffs and minor lavas from the Streltsovka caldera (Transbaikalia, Russia). Microprobe analysis of melt inclusions revealed that they are significantly enriched in F (i.e. 1.4 to 2.7 wt%) and have comparable trace element concentrations to the Eucarro Rhyolite. In contrast, whole rock analysis show higher concentrations of H_2O (2.4 wt%) than the Gawler Range Volcanics (1 wt% H_2O) and are characterized by high

temperatures (1000±20°C) (determined by the homogenization temperature of quartz-hosted melt inclusions). Furthermore Chabiron *et al.* (2001) reported that the volcanics and the underlying granites are deeply altered by hydrothermal fluids, which suggests that the eruption style of the volcanics from the Streltsovka caldera may have been largely affected by hydrothermal fluids during eruption. In other parts of the Transbaiklia large widespread rhyolites have been reported (e.g. Kiselev and Saltykovskiy, 1967), however due to the lack of translated literature it is difficult to determine if these are lava flows or ignimbrites.

5.8. Conclusions

Two main groups of quartz (Type 1 and Type 2) were identified within the Eucarro Rhyolite. Type 1 quartz includes abundant large (30-120μm) silicate melt inclusions and only minor aqueous fluid inclusions. Analysis of silicate melt inclusions reveals that their major element composition is similar to the host rock (apart from F), although, a comparison of inclusions with the groundmass shows that melt inclusions are significantly less fractionated than the groundmass. One significant difference between the major element concentration of whole rock and melt inclusions is that the latter is characterized by high concentrations of F (up to 1.25 wt%). F, known as an effective depolymeriser, may have significantly reduced the viscosity of the magma. Moreover the combined effects of a dry melt (~1 wt%) and a high F composition would have promoted an effusive style eruption, as high concentrations (several wt%) of F can be retained within the melt at 1 bar of pressure (Mysen, 1988).

Melt inclusions from Type 1 quartz are also enriched trace elements (apart from Ba, Sr and Eu), compared to the groundmass and whole rock (Fig 4-14), with W, Sn, U, Th and Pb (Figs 4-14 and 4-15) showing the greatest amount of enrichment. A strong correlation between Cl and W, Sn, U, Th and Pb within melt inclusions shows that the distribution of metals in the melt is largely controlled by the volatile content. Thus, the relative depletion of metals within the groundmass may be explained by magmatic degassing. Alternatively, alteration of the groundmass may have also contributed a

relative depletion of the groundmass, however F/Sm ratios suggests that the remobilization of mobile elements was not significant during alteration.

Evidence for magmatic degassing and magma unmixing is observed in Type 2 quartz, which includes non-silicate melt inclusions, CO_2 inclusions, aqueous fluid inclusions, composite inclusions and a low abundance of silicate glass inclusions. The origin of Type 2 quartz however is not well constrained and it is unknown if it is primary or xenocrystic. Raman Spectroscopy analysis suggests that non-silicate inclusions consists of Cl-rich compounds and possibly Sn-chloride (pers. comm. Terry Mernagh, Geoscience Australia). If Type 2 quartz is primary then it suggests that significant amounts of CO_2 and non-silicate melt were degassed within the magma chamber and thus may have resulted in mineralization.

References

Allen, S.R., Simpson, C. J., McPhie, J. and Daly, S. J., 2003. Stratigraphy, distribution and geochemistry of widespread felsic volcanic units in the Mesoproterozoic Gawler Range Volcanics, South Australia. Australian Journal of Earth Sciences, 50(no.1): 97-112.

Anderson, A.T., Davis, A.M. and Lu, F.Q., 2000. Evolution of Bishop Tuff rhyolitic magma based on melt and magnetite inclusions and zoned phenocrysts. Journal of Petrology, 41(3): 449-473.

Blissett, A.H., 1975. Rock units in the Gawler Range Volcanics, South Australia. Geological Survey of South Australia, Quarterly Geological Notes, 55: 2-14.

Blissett, A.H., Creaser, R.A., Daly, S.J., Flint, R.B. and Parker, A.J., 1993. Gawler Range Volcanics. In: J.F. Dextral, Preiss, W.V. and Parker, A.J. (Editor), The Geology of South Australia. Vol.1, The Precambrian. Geological Survey of South Australia, Bulletin 54, pp. 33-50.

Bonnischen, B., Kauffman, D.F., 1987. Physical features of rhyolite lava flows in the Snake River Plain volcanic province, southwestern Idaho. Geological Society of America Special Paper, 212: 119-145.

Cashman, K. and Blundy, J., 2000. Degassing and crystallization of ascending andesite and dacite. Philosophical Transactions of the Royal Society of London Series a-Mathematical Physical and Engineering Sciences, 358(1770): 1487-1513.

Chabiron, A. et al., 2001. Geochemistry of the rhyolitic magmas from the Streltsovka caldera (Transbaikalia, Russia): a melt inclusion study. Chemical Geology, 175(3-4): 273-290.

Chang, Z.S. and Meinert, L.D., 2004. The magmatic-hydrothermal transition - evidence from quartz phenocryst textures and endoskarn abundance in Cu-Zn skarns at the Empire Mine, Idaho, USA. Chemical Geology, 210(1-4): 149-171.

Couch, S., Sparks, R.S.J. and Carroll, M.R., 2003. The kinetics of degassing-induced crystallization at Soufriere Hills volcano, Montserrat. Journal of Petrology, 44(8): 1477-1502.

Creaser, C.A., and White, A.J.R., 1991. Yardea Dacite - Large-volume, high-temperature silicic volcanism from the Middle Proterozoic of South Australia. Geology, 19: 48-51.

Daly, S.J., Fanning, C.M. and Fairclough, M.C., 1998. Tectonic evolution and implications for exploration potential of the western Gawler Craton. AGSO Journal of Australia Geology and Geophysics, 17: 145-168.

Deer, W.A., Howie, R.A. and Zussman, J., 1992. An Introduction to the Rock-Forming Minerals. 2nd Edition. Longman.

Dingwell, D.B. and Hess, K.U., 1998. Melt viscosities in the system Na-Fe-Si-O-F-Cl: Contrasting effects of F and Cl in alkaline melts. American Mineralogist, 83(9-10): 1016-1021.

Dingwell, D.B., Scarfe, C.M., and Cronin, D., 1985. The effect of fluorine on viscosities in the system Na_2O-Al_2O_3-SiO_2: implications for phonolites, trachytes and rhyolites. American Mineralogist, 70: 80-87.

Ekren, E.B., McIntyre, D.H., Bennett, E.H., 1984. High-temperature, large-volume, lava-like ashflow tuffs without calderas in southwestern Idaho. US Geological Survey Professional Paper, 1272: 1-70.

Ellam, R.M., Hawkesworth, C.J., Ormerod, D.S. and Rogers, N.W., 1988. Rb/Sr and U/Pb Fractionation in Subduction Related Processes - Implications for Mantle Evolution. Chemical Geology, 70(1-2): 49-49.

Fanning, C.M., Flint, R.B., Parker, A.J., Ludwig, K.R. and Blissett, A.H., 1988. Refined Proterozoic Evolution of the Gawler Craton, South Australia, through U-Pb Zircon Geochronology. Precambrian Research, 40-1: 363-386.

Ferris, G.M., 2001. The geology and geochemistry of granitoids in the CHILDARA region, western Gawler Craton, South Australia: implications for the Proterozoic tectonic history of the western Gawler Craton and the development of lode-style gold mineralisation at Tunkillia. M.Sc. Thesis, University of Tasmania (unpublished).

Ferris, G.M., Schwarz, M.P. and Heithersay, P., 2002. The Geological Framework, Distributions and Controls of Fe-oxide Cu-Au Mineralisation in the Gawler Craton, South Australia: Part 1: Geological and Tectonic Framework; *in* Porter, T.M. (Ed.), *Hydrothermal Iron Oxide Copper-Gold & Related Deposits: A Global Perspective*. PGC Publishing, Adelaide, *Volume 2*: 9-31.

Flint, R.B., 1993. Chapter 5: Mesoproterozoic. The geology of South Australia. Vol 1. The Precambrian. South Australian Geological Survey Bulletin, 54, 107-170 pp.

Garner, A., and McPhie, J., 1999. Partially melted lithic megablocks in the Yardea Dacite, Gawler Range Volcanics, Australia; implications for eruptions and emplacement mechanisms. Bulletin of Volcanology, 61: 396-410.

Giles, C.W., 1988. Petrogenesis of the Proterozoic Gawler Range Volcanics, South Australia. Precambrian Research, 40/41: 407-427.

Gramenitskii, E.N. and Shchekina, T.I., 2005. Behavior of rare earth elements and yttrium during the final differentiation stages of fluorine-bearing magmas. Geochemistry International, 43(1): 39-52.

Green, J.C. and Fitz, T.J., 1993. Extensive Felsic Lavas and Rheoignimbrites in the Keweenawan Midcontinent Rift Plateau Volcanics, Minnesota - Petrographic and Field Recognition. Journal of Volcanology and Geothermal Research, 54(3-4): 177-196.

Hammer, J.E. and Rutherford, M.J., 2002. An experimental study of the kinetics of decompression-induced crystallization in silicic melt. Journal of Geophysical Research-Solid Earth, 107(B1).

Hards, N., 1978. Distribution of elements between fluid phase and silicate melt granites and nepheline syenites. NERC Progress in Experimental Petrology, IV: 88-90.

Henry, C.D. and Wolff, J.A., 1992. Distinguishing Strongly Rheomorphic Tuffs from Extensive Silicic Lavas. Bulletin of Volcanology, 54(3): 171-186.

Hildreth, W. and Moorbath, S., 1988. Crustal Contributions to Arc Magmatism in the Andes of Central Chile. Contributions to Mineralogy and Petrology, 98(4): 455-489.

Kamenetsky, V.S., DeVivo, B., Naumov, V.B., Kamenetsky, M.B., Mernagh, T.P., van Achterbergh, E., Ryan, C.G., and Davidson, P.,, 2003. Magmatic inclusions in the search for natural silicate-salt melt immiscibility: methodology and examples.

Melt inclusions: methods, applications and problems. Developments in Volcanology: 5. Melt inclusions in volcanic systems: methods, applications and problems. Elsevier, Amsterdam, 65-82 pp.

Kamenetsky, V.S., Morrow, N. and McPhie, J., 2000. Origin of high-Si dacite from rhyolitic melt: evidence from melt inclusions in mingled lavas of the 1.6 Ga Gawler Range Volcanics, South Australia. Mineralogy and Petrology, 69(3-4): 183-195.

Kamenetsky, V.S., Wolfe, R.C., Eggins, S.M., Mernagh, T.P. and Bastrakov, E., 1999. Volatile exsolution at the Dinkidi Cu-Au porphyry deposit, Philippines: A melt-inclusion record of the initial ore-forming process. Geology, 27(8): 691-694.

Kempton, P.D., Fitton, J.G., Hawkesworth, C.J. and Ormerod, D.S., 1991. Isotopic and Trace-Element Constraints on the Composition and Evolution of the Lithosphere beneath the Southwestern United-States. Journal of Geophysical Research-Solid Earth and Planets, 96(B8): 13713-13735.

Kiselev, A.I., Saltykovskiy, A. Y., 1967. The pattern of mesozoic volcanism in the volcanic belt of western Transbaikalia. Mosk. Obshchest. Ispyt. Prir., Byull., Otd. Geol, 42(6): 76-84.

Krauskopf, K.B., and Bird, D.K., 1995. Introduction to Geochemistry. McGraw-Hill.

Lange, R., 1994. The effect of H_2O, CO_2 and F on the density and viscosity of silicate melts. In Mineralogical Society of American Reviews in Mineralogy, 30: 331-369.

Manley, C.R., 1992. Extended Cooling and Viscous-Flow of Large, Hot Rhyolite Lavas - Implications of Numerical Modeling Results. Journal of Volcanology and Geothermal Research, 53(1-4): 27-46.

Manley, C.R., 1995. How Voluminous Rhyolite Lavas Mimic Rheomorphic Ignimbrites - Eruptive Style, Emplacement Conditions, and Formation of Tuff-Like Textures. Geology, 23(4): 349-352.

Manley, C.R., 1996. Physical volcanology of a voluminous rhyolite lava flow: The Badlands lava, Owyhee plateau, southwestern Idaho. Journal of Volcanology and Geothermal Research, 71(2-4): 129-153.

Milner, S.C., Duncan, A.R. and Ewart, A., 1992. Quartz Latite Rheoignimbrite Flows of the Etendeka Formation, North-Western Namibia. Bulletin of Volcanology, 54(3): 200-219.

Morrow, N., 1998. Mingled felsic lavas in the Gawler Range Volcanics. B.Sc (Honours) (unpublished) Thesis, The University of Tasmania.

Morrow, N., and McPhie, J., 2000. Mingled silicic lavas in the Mesoproterozoic Gawler Range Volcanics, South Australia. Journal of Volcanology and Geothermal Research, 96: 1-13.

Mysen, B.O., 1988. Structure and Properties of Silicate Melts. Developments in Geochemistry, 4. Elsevier, 247-253 pp.

Pandalai, H.S. et al., 2003. Dissolution channels in quartz and the role of pressure changes in gold and sulfide deposition in the Archean, greenstone-hosted, Hutti gold deposit, Karnataka, India. Mineralium Deposita, 38(5): 597-624.

Park, Y.R. and Ripley, E.M., 2001. Mechanisms and patterns of O and H isotopic exchange during hydrothermal alteration of the North Shore Volcanic Group and related hypabyssal sills, Midcontinent Rift System, Minnesota. Chemical Geology, 172(3-4): 331-345.

Parker, A.J., 1993. Palaeoproterozoic. In: J.F. Drexel, Priess, W.V. and Parker, A.J., (Editor), The Geology of South Australia. Vol 1, The Precambrian. South Australia Geological Survey Bulletin 54, pp. 50-104.

Phillips, G.N. and Evans, K.A., 2004. Role of CO2 in the formation of gold deposits. Nature, 429(6994): 860-863.

Pinkerton, H. and Stevenson, R.J., 1992. Methods of Determining the Rheological Properties of Magmas at Sub-Liquidus Temperatures. Journal of Volcanology and Geothermal Research, 53(1-4): 47-66.

Renne, P.R., Glen, J.M., Milner, S.C. and Duncan, A.R., 1996. Age of Etendeka flood volcanism and associated intrusions in southwestern Africa. Geology, 24(7): 659-662.

Roache, M.W., Allen, S.R. McPhie, J., 2000. Surface and subsurface facies architecture of a small hydroexplosive, rhyolite centre in the Mesoproterozoic Gawler Range Volcanics, South Australia. Journal of Volcanology and Geothermal Research, 104: 237-259.

Roedder, E., 1984. Fluid inclusions. Reviews in Mineralogy, 12. Book Crafters, Michigan.

Schmitt, A.K., Trumbull, R.B., Dulski, P. and Emmermann, R., 2002. Zr-Nb-REE mineralization in peralkaline granites from the Amis Complex, Brandberg (Namibia): Evidence for magmatic pre-enrichment from melt inclusions. Economic Geology and the Bulletin of the Society of Economic Geologists, 97(2): 399-413.

Skirrow, R.G., Fraser, G., Schmidt-Mumm, A., Budd, A., 2004. New constraints unifying Au mineralised systems in the central Gawler Craton: alteration, mineralisation, and fluids. In: PIRSA (Editor), Gawler Craton State of Play, pp. 24.

Stewart, K.P., 1994. High temperature felsic volcanism and the role of mantle magmas in Proterozoic crustal growth: the Gawler Range Volcanic Province. PhD Thesis, University of Adelaide, 1-213 pp.

Sun, S.S., and McDonough, W.F.,, 1989. Chemical and isotopic systematics of oceanic basalts: implications for mantle composition and processes. *In*: saunders, A.D., and Norry, M.J., (eds.) *Magmatism in ocean basins*. Geological Society of London Special Publication, 42: 313-345.

Swanson, S.E. and Fenn, P.M., 1986. Quartz Crystallization in Igneous Rocks. American Mineralogist, 71(3-4): 331-342.

Webster, J.D., 1990. Partitioning of F between H2o and Co2 Fluids and Topaz Rhyolite Melt - Implications for Mineralizing Magmatic-Hydrothermal Fluids in F-Rich Granitic Systems. Contributions to Mineralogy and Petrology, 104(4): 424-438.

Wedepohl, K.H., 1978. Nobium. Hand Book of Geochemistry.

Wyllie, K.M., and Tuttle, O.F., 1961. Experimental investigation of silicate systems containing two volatile components; Part II. American Journal of Science, 256: 128.

Appendix 1

AMG coordinates for samples collected for melt inclusion studies from Nicole Morrow's (1998) collection. (Samples are stored at the School of Earth Sciences, University of Tasmania).

Rock Unit	Sample No.	Easting	Northing
Plagioclase Rhyolite	GC17	562111	6389117
Vesicular Rhyolite	GC4	558200	6389650
Vesicular Rhyolite	GC14	559633	6389544
Vesicular Rhyolite	GC15	560640	6389538
Quartz Rhyolite	GC5	569612	6390900
Quartz Rhyolite	GC8	549880	6389780
Quartz Rhyolite	GC11	560520	6389320
Quartz Rhyolite	GC16	562175	6389190

Appendix 2

Results from Laser Raman Spectroscopy of silicate and non-silicate inclusions

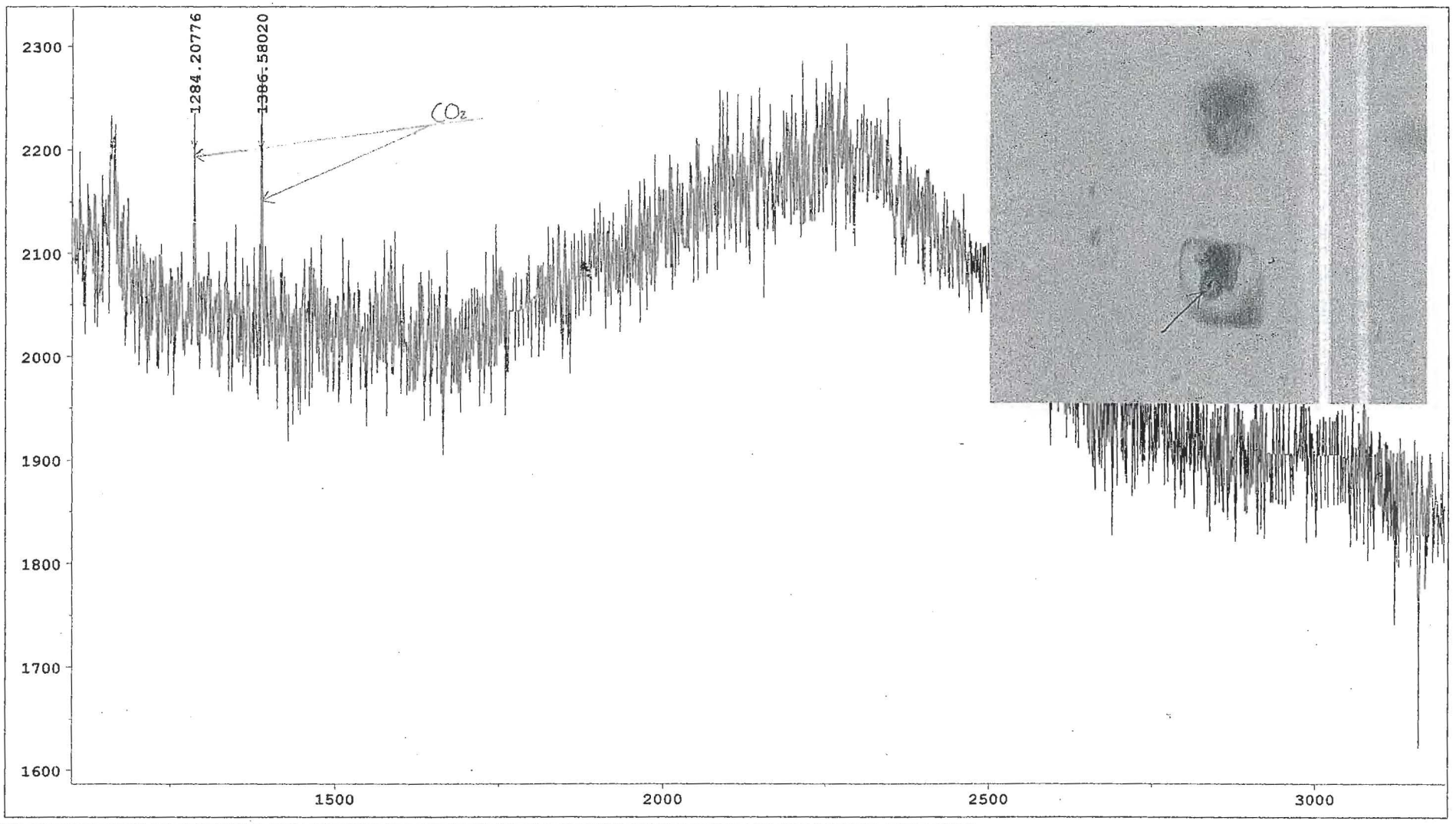

Sample	: GC4EX1	Excit_line	: 514.532	Filtr	: ----
Operator	: Mernagh	Spectro	: 1893.22	Accum	: 1
Date	: 8-12-104	Grating	: 1800	Objectiv	: x100
Power	: 50	Slit	: 100	File	: 5 Sample GC4 Ex1
Time	: 30	Hole	: 400	Remark	: vapour bubble CO_2

Glass inclusion with crystals

Australian Government
Geoscience Australia

CO_2 CO_2

Inclusion 3

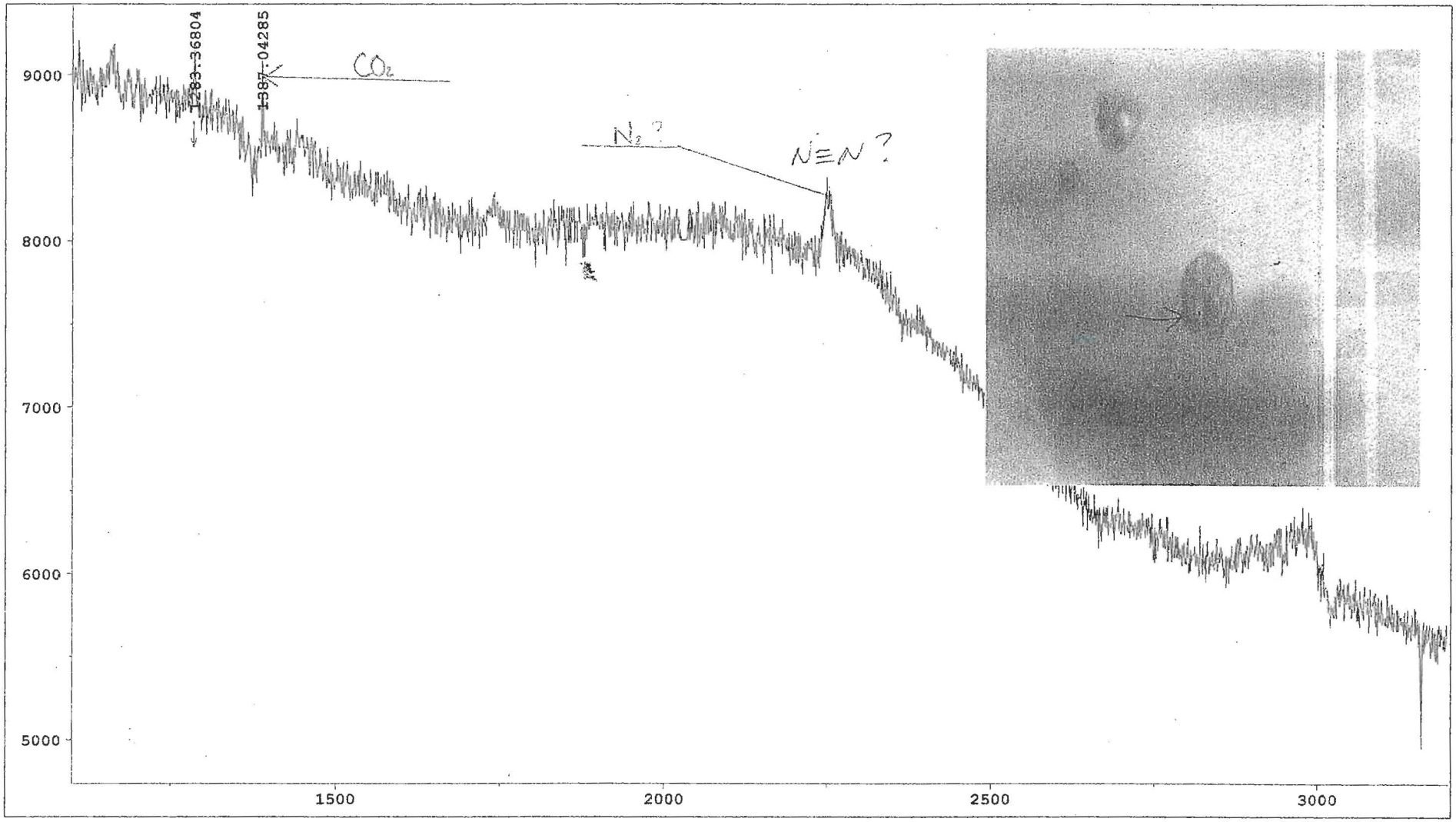

Sample	: GC4EX1	Excit_line	: 514.532	Filtr	: ----
Operator	: Mernagh	Spectro	: 1893.22	Accum	: 1
Date	: 8-12-104	Grating	: 1800	Objectiv	: x100
Power	: 50	Slit	: 100	File	: 8 GC4 EX1
Time	: 30	Hole	: 400	Remark	: vapour bubble

Non-silicate melt inclusion

Australian Government
Geoscience Australia

Inclusion 2

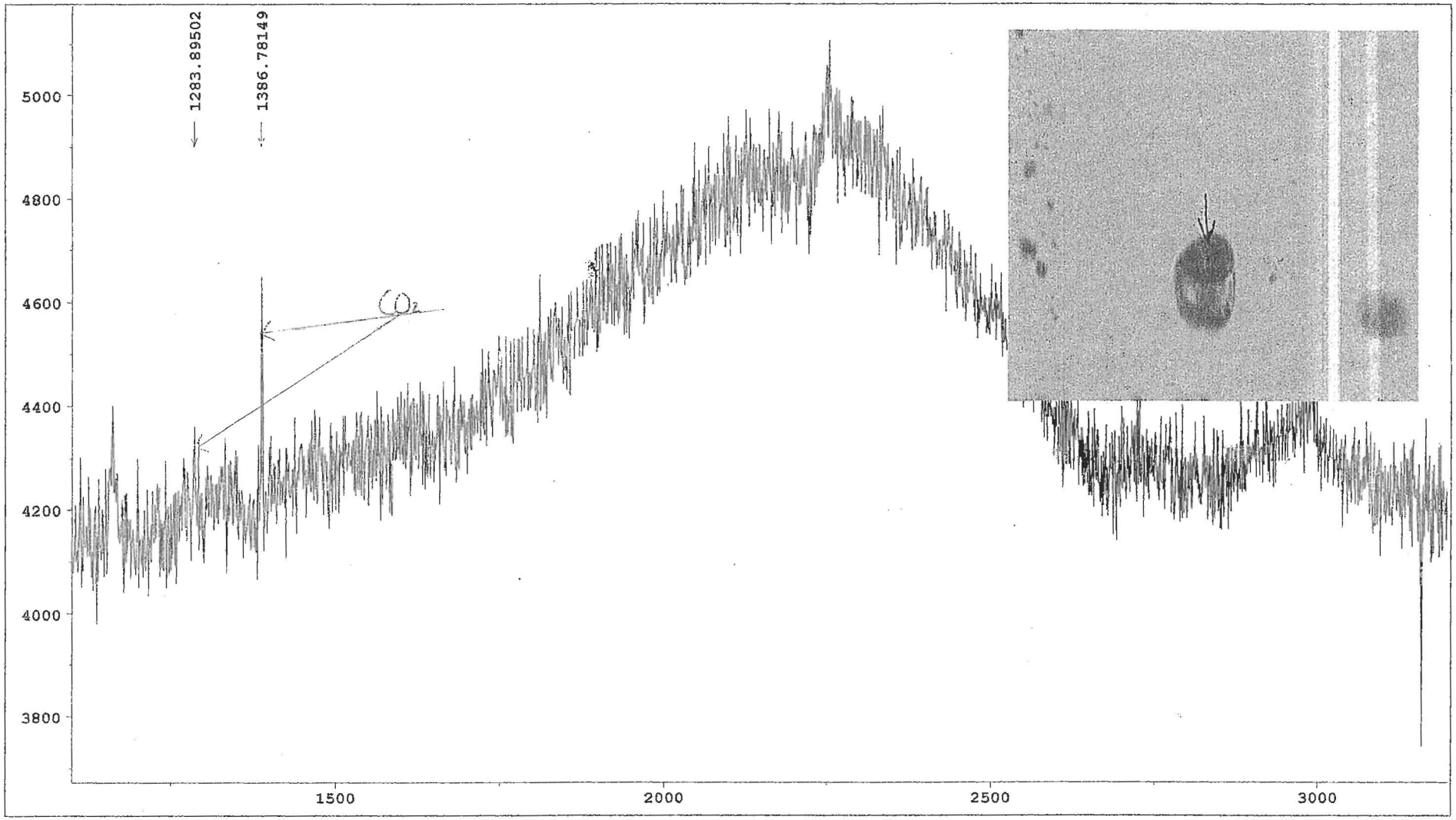

Sample	: GC4EX1	Excit_line	: 514.532	Filtr	: ----
Operator	: Mernagh	Spectro	: 1893.22	Accum	: 1
Date	: 8-12-104	Grating	: 1800	Objectiv	: x100
Power	: 50	Slit	: 100	File	: 6 Sample GC4EX1
Time	: 60	Hole	: 400	Remark	: vapour bubble CO_2 Non-silicate melt inclusion

Australian Government
Geoscience Australia

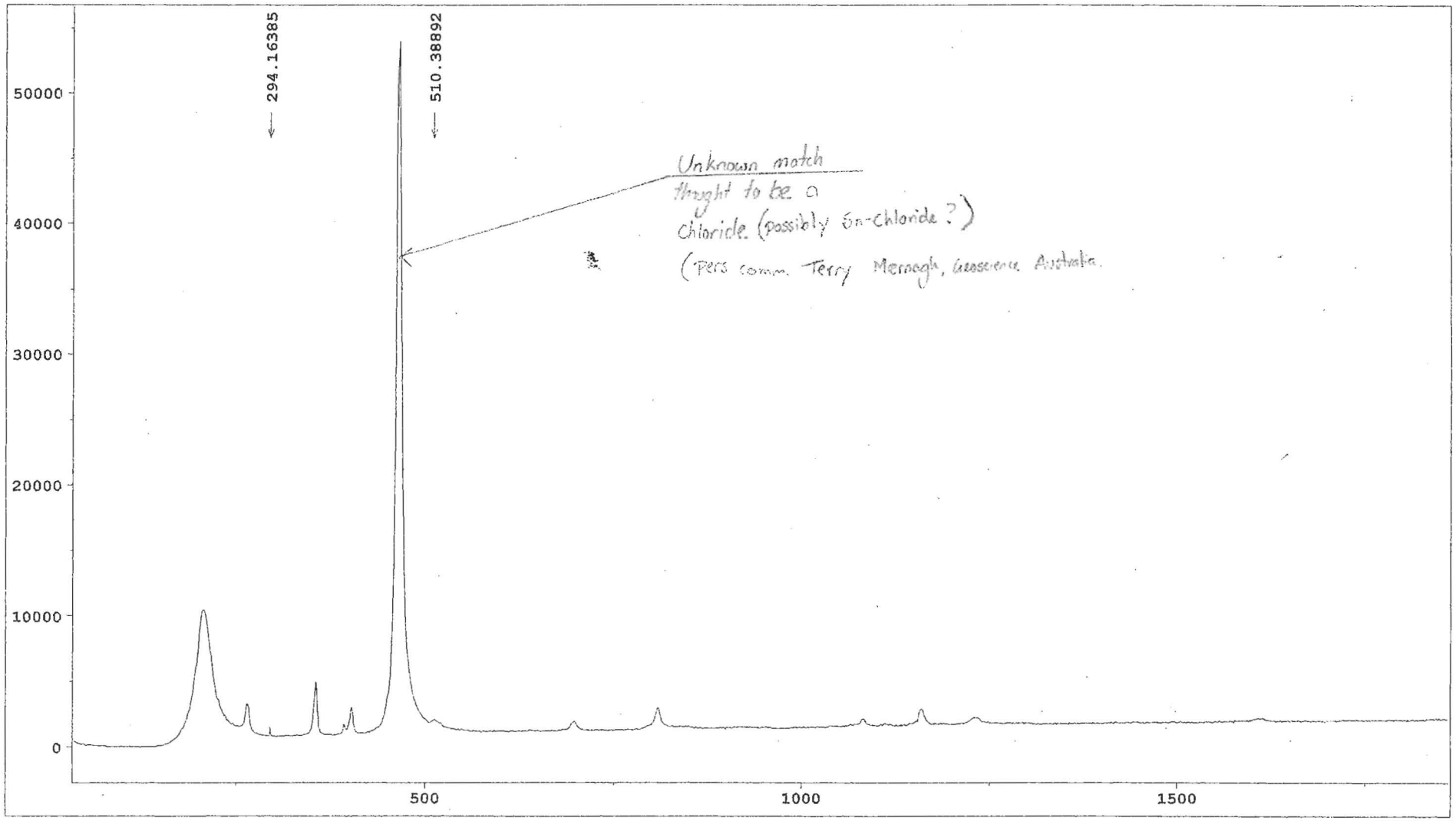

Sample	: BM1-2/2	Excit_line	: 514.532	Filtr	: ----
Operator	: Mernagh	Spectro	: 999.87	Accum	: 1
Date	: 15-02-105	Grating	: 1800	Objectiv	: x100
Power	: 50	Slit	: 100	File	: BM1__4 GC4Ex2
Time	: 30	Hole	: 400	Remark	: solid phase

Non-Silicate melt inclusion

Australian Government
Geoscience Australia

Appendix 3

Microprobe analysis of green mineral from sample GC14bm1 (see Figure 3-4)

	Na2O	MgO	SiO2	Al2O3	Cl	K2O	CaO	TiO2	MnO	FeO	Total
GC14 B1_1	1.2511	0.649	34.7127	10.4607	3.4922	2.1835	9.448	0.2226	0.44	28.7209	91.611

A best fit for the microprobe analysis suggests that the mineral is:

Potassic-chlorohastingsite

General Potassic-chlorohastingsite Information

Chemical Formula: (K,Na)Ca2(Fe++,Mg)4Fe+++[Si6Al2O22](Cl,OH)2

Composition: Molecular Weight = 994.80 gm

Potassium	2.36 %	K	2.84 %	K_2O
Sodium	0.92 %	Na	1.25 %	Na_2O
Calcium	8.06 %	Ca	11.27 %	CaO
Magnesium	2.44 %	Mg	4.05 %	MgO
Aluminum	5.42 %	Al	10.25 %	Al_2O_3
Iron	22.46 %	Fe	21.67 %	FeO / 8.03 % Fe_2O_3
Silicon	16.94 %	Si	36.24 %	SiO_2
Hydrogen	0.06 %	H	0.54 %	H_2O
Chlorine	4.99 %	Cl	4.99 %	Cl
_	- %	Cl	-1.13 %	$-O=Cl_2$
Oxygen	36.35 %	O		
	100.00 %		100.00 %	= TOTAL OXIDE

Empirical Formula: $K_{0.6}Na_{0.4}Ca_2Fe^{2+}{}_3MgFe^{3+}(Si_6Al_2O_{22})Cl_{1.4}(OH)_{0.6}$

IMA Status: Approved IMA 1998 (Dana # Added)

Locality: Dasshkesan Co-Fe deposit, Azerbaidzhan. Link to MinDat.org Location Data.

Name Origin: Named after its composition and for Hastings Co., Ontario, Canada..

Synonym: Chlorohastingsite-K
Dashkesanite

(Sourced from Mineral Data (http://www.webmineral.com))

Appendix 4

Sample preparation for whole rock major and trace element analysis (from Morrow, 1998).

Samples were collected from the least weathered rock, each weighing about 1.5 kg. The samples were broken into small fragments with a hydraulic splitter and any weathered rines or unusually altered portions were removed. The Vesicular Rhyolite and Plagioclase Rhyolite were carefully examined to avoid any contamination from basaltic magmatic inclusions within the rocks, and minimize contamination from quartz- and fluorite-filled amygdales. Approximately 500g of each sample were crushed into <10 mm chips in a hydraulic jaw crusher, and then split to ensure a representative sample.

Split samples, of around 60g weight, were ground in a Fe-Cr ring mill for geochemical analyses. Further sample preparation was carried out by Mineral Resources, Tasmania, where major and trace element concentrations were determined by XRF using a Phillips 1400 x-ray spectrometer. For each sample, 400 mg of ignited sample, 5.2g of flux (12:22 type) and 3-4 drops of 25% LiBr solution were mixed, and underwent 2*6 minute heating cycles to produce a fused disc for major element analysis. Mineral samples for trace element analysis are pressed composite pellets of ~10g – 15g of sample homogenized with ~0.36 g Palaroid (3.6 % weight to weight ratio), and mixed with 2 to 3 ml of Acetone. The mixture was redried and hand crushed in an agate mortar, then encased in a Borax sheath and pressed to 10 tonnes to give an overall depth of 15 mm by 30 mm.

Appendix 5

Major (microprobe) and trace element (LA-ICPMS) data for analysis of the groundmass

Major element analysis of the Eucarro Rhyolite groundmass by microprobe (after Kamenetsky *et al*., 2003)
Note that all values are in weight percent.

Label	Si2O	TiO2	Al2O3	Fe2O3	MnO	MgO	CaO	Na2O	K2O	Cr2O3	total
GC8 A1	76.84	0.00	11.98	0.79	0.00	0.02	0.20	3.42	5.42	0.00	98.66
GC8 A2	78.34	0.03	11.27	0.71	0.05	0.00	0.19	3.15	5.12	0.01	98.87
GC8 A3	79.82	0.01	10.66	0.73	0.05	0.02	0.14	2.83	4.34	0.05	98.64
GC8 A4	77.82	0.04	12.00	0.69	0.03	0.03	0.16	3.14	5.39	0.01	99.31
GC8 B1	77.97	0.03	11.78	0.68	0.02	0.03	0.16	3.58	4.87	0.00	99.12
GC8 B2	85.97	0.04	6.79	0.98	0.05	0.05	0.43	1.32	3.83	0.00	99.46
GC8 B3	78.42	0.06	10.42	0.91	0.03	0.02	0.79	1.44	6.73	0.04	98.87
GC8 B4	81.60	0.06	10.00	0.61	0.04	0.00	0.35	3.36	3.44	0.00	99.46
GC8 C1	80.70	0.07	9.62	0.77	0.10	0.02	0.13	1.43	6.11	0.00	98.95
GC8 C2	76.24	0.02	12.20	1.32	0.00	0.02	0.16	3.50	5.21	0.00	98.67
GC8 C3	80.96	0.18	9.41	0.47	0.12	0.01	0.29	2.66	4.13	0.00	98.24
GC8 D1	81.73	0.02	9.50	0.63	0.00	0.01	0.20	2.77	3.82	0.00	98.69
GC8 D2	77.09	0.01	11.17	0.69	0.04	0.02	0.67	2.26	6.11	0.02	98.08
GC8 D3	79.82	0.01	10.80	0.73	0.05	0.01	0.16	3.20	4.46	0.04	99.26
Average	79.52	0.04	10.54	0.77	0.04	0.02	0.29	2.72	4.93	0.01	98.88
Stdev	2.48189	0.04508	1.390803	0.195098	0.034453	0.011204	0.200697	0.770232	0.943388	0.017077	0.404525

Label	Si2O	TiO2	Al2O3	Fe2O3	MnO	MgO	CaO	Na2O	K2O	Cr2O3	total
GC4 A1	77.15	0.07	11.80	1.30	0.02	0.02	0.15	3.04	5.70	0.02	99.27
GC4 A2	76.58	0.01	11.64	0.97	0.04	0.01	0.21	1.36	7.91	0.01	98.74
GC4 A3	73.45	0.04	13.40	0.92	0.04	0.03	0.09	2.26	8.06	0.00	98.29
GC4 A4	74.44	0.06	12.75	0.71	0.00	0.01	0.02	1.22	9.09	0.04	98.33
GC4 A5	79.07	0.06	10.20	0.73	0.02	0.02	0.05	1.11	7.19	0.01	98.46
GC4 B1	78.43	0.02	10.81	0.55	0.00	0.03	0.06	2.16	6.27	0.02	98.34
GC4 B3	82.09	0.01	9.12	0.66	0.04	0.03	0.05	1.84	5.01	0.05	98.89
GC4 B4	82.06	0.04	8.62	0.67	0.02	0.05	0.07	0.84	6.11	0.04	98.51
GC4 C1	84.53	0.08	7.39	0.41	0.02	0.00	0.04	1.10	4.55	0.00	98.13
GC4 C2	80.59	0.01	9.46	0.64	0.04	0.06	0.06	2.08	4.87	0.02	97.82
GC4 C3	77.49	0.03	11.13	0.67	0.00	0.02	0.06	0.76	8.08	0.02	98.25
GC4 C4	76.47	0.08	11.77	1.14	0.01	0.03	0.13	1.89	7.09	0.00	98.63
GC4 C5	80.32	0.02	9.85	0.54	0.01	0.03	0.08	1.19	6.56	0.00	98.60
GC4 D1	76.45	0.04	11.83	0.88	0.04	0.06	0.15	2.31	6.83	0.00	98.59
GC4 D2	77.01	0.03	11.59	0.79	0.00	0.01	0.06	2.44	6.55	0.00	98.49
GC4 D3	82.10	0.07	8.94	0.91	0.00	0.00	0.12	2.75	3.35	0.00	98.25
GC4 D4	72.54	0.05	14.08	1.06	0.04	0.04	0.12	2.66	8.10	0.05	98.73
GC4 D5	80.95	0.05	10.04	0.50	0.01	0.02	0.37	2.74	4.27	0.03	98.97
Average	78.43	0.04	10.80	0.78	0.02	0.03	0.10	1.88	6.42	0.02	98.52
Stdev	3.284227	0.025496	1.74982	0.236431	0.015464	0.016615	0.081576	0.724867	1.560794	0.017636	0.337681

Label	Si2O	TiO2	Al2O3	Fe2O3	MnO	MgO	CaO	Na2O	K2O	Cr2O3	total
GC17a A3	76.24	0.01	12.05	0.96	0.00	0.06	0.06	3.20	5.64	0.00	98.24
GC17a A4	79.36	0.10	10.52	0.96	0.06	0.03	0.07	1.92	6.06	0.03	99.11
GC17a A5	75.80	0.06	12.18	1.39	0.04	0.06	0.14	3.42	5.30	0.00	98.39
GC17a A6	75.97	0.06	11.96	0.76	0.05	0.05	0.05	2.09	7.10	0.00	98.08
GC17a C1	70.46	0.02	15.15	0.90	0.02	0.03	0.07	3.35	8.22	0.00	98.22
GC17a C2	82.22	0.02	8.30	0.76	0.00	0.02	0.01	1.22	5.43	0.00	97.98
GC17a C5	66.70	0.01	15.94	1.08	0.00	0.02	1.58	4.08	7.69	0.00	97.11
GC17a C6	90.09	0.05	4.68	0.57	0.04	0.05	0.03	1.03	2.28	0.00	98.81
GC17a C7	76.95	0.05	11.47	0.82	0.00	0.04	0.04	1.41	7.64	0.00	98.41
GC17a C8	70.95	0.13	14.26	1.05	0.01	0.03	0.00	1.59	9.93	0.01	97.97
GC17a B1	71.21	0.02	14.36	1.85	0.05	0.08	0.08	3.46	7.01	0.00	98.13
GC17a B2	77.11	0.03	10.77	0.98	0.01	0.01	0.23	1.09	7.50	0.04	97.79
GC17a B3	81.04	0.03	9.03	1.13	0.00	0.03	0.03	1.67	5.46	0.00	98.43
GC17a B4	74.65	0.04	13.27	1.45	0.04	0.03	0.14	4.05	5.28	0.00	98.95
GC17a B5	68.89	0.03	16.61	1.15	0.04	0.03	0.21	5.33	6.61	0.00	98.91
GC17a B6	74.37	0.06	13.02	1.63	0.00	0.08	0.10	2.94	6.67	0.00	98.86
GC17a B7	78.54	0.05	10.95	0.66	0.04	0.03	0.10	2.38	6.24	0.01	98.99
GC17a B8	81.08	0.04	10.08	0.89	0.03	0.07	0.07	3.21	3.77	0.00	99.24
GC17a B9	76.65	0.03	11.77	0.81	0.00	0.01	0.06	1.94	7.30	0.06	98.61
GC17a B10	81.39	0.07	9.31	1.41	0.04	0.04	0.08	2.58	4.23	0.01	99.17
Average	76.48	0.04	11.78	1.06	0.02	0.04	0.16	2.60	6.27	0.01	98.47
Stdev	5.399169	0.028881	2.821497	0.335017	0.021118	0.021155	0.340177	1.164424	1.704852	0.015853	0.546777

Major element analysis of the Eucarro Rhyolite groundmass by microprobe (after Kamenetsky *et al*., 2003)
Note that all values are in weight percent.

Label	Si2O	TiO2	Al2O3	Fe2O3	MnO	MgO	CaO	Na2O	K2O	Cr2O3	total
GC11 A1	79.92	0.00	10.15	0.77	0.00	0.09	0.06	2.18	5.12	0.02	98.31
GC11 A2	78.60	0.01	10.84	0.90	0.01	0.04	0.03	1.68	6.50	0.03	98.63
GC11 A3	79.00	0.01	10.85	0.62	0.04	0.03	0.03	2.31	6.15	0.01	99.04
GC11 A4	83.51	0.01	8.39	0.72	0.09	0.02	0.07	2.09	4.29	0.00	99.19
GC11 A5	84.83	0.00	7.94	0.65	0.00	0.08	0.03	1.56	4.01	0.02	99.13
GC11 A6	77.47	0.00	11.69	0.48	0.00	0.02	0.07	2.94	5.58	0.00	98.25
GC11 A7	75.54	0.00	11.96	0.87	0.04	0.10	0.07	1.66	6.99	0.02	97.23
GC11 A8	81.93	0.28	8.75	0.76	0.00	0.08	0.06	1.32	4.93	0.01	98.12
GC11 A9	80.86	0.01	8.04	0.40	0.00	0.02	2.87	1.68	4.15	0.02	98.06
GC11 A10	78.69	0.04	10.42	2.07	0.07	0.19	0.04	2.57	4.29	0.00	98.36
GC11 B1	86.92	0.02	6.31	0.34	0.06	0.02	0.03	1.34	3.44	0.00	98.48
GC11 B2	84.48	0.00	7.94	0.25	0.00	0.02	0.03	1.98	3.67	0.00	98.36
GC11 B3	82.97	0.01	8.38	0.39	0.00	0.03	0.03	1.87	4.28	0.03	98.00
GC11 B4	82.30	0.02	9.20	0.52	0.05	0.03	0.05	2.86	3.45	0.00	98.48
GC11 B5	86.92	0.00	6.79	0.39	0.00	0.01	0.04	1.44	3.47	0.01	99.08
GC11 B6	85.39	0.04	7.45	0.44	0.04	0.01	0.06	1.78	3.68	0.00	98.89
GC11 B7	81.49	0.02	9.47	0.34	0.02	0.01	0.04	2.59	4.47	0.03	98.47
GC11 B9	85.90	0.02	6.95	0.82	0.00	0.04	0.02	1.29	3.78	0.00	98.82
GC11 B10	76.40	0.02	11.26	1.01	0.05	0.14	0.36	2.88	5.15	0.00	97.27
GC11 C1	76.94	0.03	11.68	0.96	0.07	0.10	0.06	2.09	6.19	0.00	98.13
GC11 C2	78.73	0.00	11.08	0.56	0.00	0.04	0.02	1.81	6.51	0.01	98.75
GC11 C3	77.88	0.01	11.82	0.44	0.00	0.01	0.07	2.63	5.80	0.00	98.67
GC11 C6	77.56	0.02	11.52	0.56	0.01	0.03	0.05	1.99	7.31	0.02	99.07
GC11 C7	81.94	0.03	8.94	0.54	0.00	0.03	0.03	1.65	4.84	0.00	98.00
GC11 C10	81.94	0.03	9.50	0.97	0.02	0.03	0.04	2.50	4.18	0.00	99.20
GC11 D1	76.85	0.01	11.37	0.86	0.00	0.10	0.05	1.48	7.89	0.05	98.65
GC11 D2	78.29	0.01	11.00	0.67	0.07	0.06	0.07	2.22	6.02	0.00	98.42
GC11 D3	73.99	0.00	11.54	0.90	0.01	0.14	1.86	1.41	7.57	0.04	97.46
GC11 D4	81.35	0.05	9.71	0.57	0.00	0.04	0.06	2.38	4.37	0.04	98.57
GC11 D5	82.89	0.03	8.63	0.50	0.00	0.01	0.06	1.94	4.37	0.00	98.44
GC11 D6	79.56	0.00	10.75	0.56	0.00	0.02	0.06	2.90	4.79	0.01	98.66
GC11 D7	82.73	0.03	8.99	0.59	0.05	0.03	0.06	2.21	4.13	0.02	98.84
GC11 D8	81.14	0.00	9.12	0.95	0.03	0.21	0.02	1.20	5.45	0.00	98.12
GC11 D9	80.78	0.03	9.62	0.73	0.02	0.14	0.05	1.81	5.12	0.03	98.34
GC11 D10	81.27	0.03	8.83	1.55	0.04	0.22	0.07	1.91	4.25	0.03	98.21
GC11 D11	77.26	0.00	11.48	0.70	0.01	0.08	0.02	2.02	6.30	0.00	97.87
Average	80.67	0.02	9.68	0.70	0.02	0.06	0.18	2.01	5.07	0.01	98.43
Stdev	3.253623	0.04556	1.604231	0.345163	0.026134	0.058028	0.552471	0.497356	1.240136	0.013943	0.497507

Label	Si2O	TiO2	Al2O3	Fe2O3	MnO	MgO	CaO	Na2O	K2O	Cr2O3	total
GC14 A1	77.21	0.02	12.55	0.70	0.04	0.06	0.19	4.07	4.48	0.01	99.34
GC14 A2	85.38	0.01	7.91	0.55	0.01	0.03	0.11	2.81	2.50	0.00	99.29
GC14 A3	85.24	1.51	6.55	0.64	0.01	0.08	0.10	0.70	4.33	0.03	99.19
GC14 A6	85.49	0.02	7.70	0.76	0.01	0.10	0.05	1.37	4.31	0.02	99.84
GC14 A8	78.86	0.04	10.78	0.85	0.06	0.04	0.05	1.35	7.08	0.00	99.12
GC14 A9	82.68	0.03	9.14	0.62	0.00	0.05	0.03	1.99	4.80	0.01	99.35
GC14 B3	77.78	0.24	11.18	0.90	0.00	0.04	0.08	1.97	6.41	0.00	98.59
GC14 B4	78.65	0.10	11.27	1.12	0.04	0.07	0.11	4.07	3.31	0.01	98.74
GC14 B5	77.46	0.00	11.42	0.63	0.03	0.04	0.04	1.53	7.41	0.00	98.57
GC14 B6	80.51	0.00	9.89	0.93	0.06	0.11	0.05	0.87	6.28	0.01	98.72
GC14 B7	84.72	0.05	7.98	0.62	0.01	0.05	0.05	2.08	3.49	0.00	99.05
GC14 B8	80.95	0.04	9.46	1.13	0.04	0.06	0.08	2.11	4.66	0.00	98.53
GC14 B9	78.71	0.13	11.75	1.09	0.02	0.05	0.13	5.00	2.35	0.01	99.23
GC14 B10	75.95	0.00	12.27	0.91	0.01	0.07	0.08	1.91	7.49	0.00	98.69
GC14 C1	72.82	0.03	14.78	0.88	0.00	0.04	0.19	5.99	3.22	0.04	97.98
GC14 C2	82.20	0.01	8.46	0.79	0.02	0.07	0.05	0.59	6.04	0.00	98.23
GC14 C3	75.13	0.02	13.63	0.89	0.07	0.05	0.13	4.98	3.96	0.01	98.85
GC14 C4	79.53	0.34	10.37	0.76	0.06	0.08	0.05	2.21	5.22	0.00	98.63
GC14 C5	75.08	0.07	12.93	1.07	0.01	0.06	0.09	3.64	5.51	0.00	98.47
GC14 C6	89.26	0.04	5.02	0.54	0.03	0.04	0.03	0.30	3.36	0.01	98.64
GC14 C7	81.90	0.04	9.53	0.81	0.01	0.07	0.07	2.30	4.62	0.01	99.37
GC14 C8	71.91	0.02	14.93	0.83	0.01	0.05	0.12	3.36	7.22	0.00	98.45
GC14 C10	83.61	0.00	8.24	0.70	0.05	0.08	0.00	0.70	5.74	0.02	99.15
GC14 D1	87.38	0.06	6.59	0.51	0.07	0.03	0.07	1.79	3.07	0.00	99.57
GC14 D2	81.06	0.21	9.97	0.70	0.00	0.03	0.10	3.19	3.81	0.03	99.11
GC14 D3	77.47	0.25	11.55	0.91	0.00	0.05	0.09	2.07	6.89	0.00	99.28
GC14 D4	83.97	0.08	8.46	0.57	0.03	0.02	0.07	2.28	3.79	0.00	99.29
GC14 D5	76.07	0.02	12.97	0.70	0.01	0.04	0.13	3.49	5.35	0.00	98.80
GC14 D6	83.64	0.01	8.31	0.76	0.04	0.04	0.05	1.71	4.52	0.00	99.09
GC14 D7	78.61	0.03	11.59	0.72	0.00	0.05	0.11	4.19	3.54	0.00	98.84
GC14 D9	72.64	0.03	14.50	1.34	0.00	0.12	0.20	5.55	3.54	0.00	97.93
GC14 D10	79.83	0.06	10.29	0.66	0.00	0.00	0.07	2.31	5.86	0.02	99.10
Average	80.05	0.11	10.37	0.80	0.02	0.06	0.09	2.58	4.82	0.01	98.91
Stdev	4.372308	0.268184	2.495267	0.19556	0.022449	0.026103	0.046338	1.491058	1.482281	0.010914	0.441687

Figure 3-2 Polished quartz grain from sample GC16 (Quartz Rhyolite) that shows a fracture intersecting a decrepitated melt inclusion. Note that inclusions like this one, which are dark and appear to be altered, were excluded from this study.

Figure 3-3 Polished quartz grain from sample GC4 (Vesicular Rhyolite), which shows the co-existence of non-silicate melt inclusions (NS) and granular-textured melt inclusions (GTMI). Note that the co-existence of NS and GTMI demonstrates that silicate melt and non-silicate melt were trapped at the same time during the growth of quartz.

Figure 3-4 Glass inclusion with crystals (GIC) from sample GC11B1 (Quartz Rhyolite). Note that this inclusion was exposed for microprobe analysis. Two spots were analyzed in order to determine the major element composition of the glass (lower circle) and the approximate composition of the bladed crystal (upper circle). Note that the results from the analysis are presented on Table 3-3 (adjacent), which shows that the bladed crystal (note that some glass was probed together with the crystal) is significantly more enriched in Ca, Fe and F when compared to the glass. Table 3-3 also shows that the ratio between Ca:2F from the analysis quite similar to that of fluorite. Hence the bladed crystals are likely daughter crystals of fluorite, which crystallized from a fluorine-rich melt.

Table 3-3 A comparison of major group elements from microprobe analysis on glass and a bladed crystal within a GIC from sample GC11B1 (Quartz Rhyolite). See above (Figure 3-4).

Figure 3-5 GIC from sample GC14 (Vesicular Rhyolite). Microprobe analysis of the blue-green crystal (arrow) suggests that it most likely potassic-chlorohastingsite amphibole. (*see* Appendix 3).

Figure 3-6 Glass inclusions (GI) from sample GC5 (Quartz Rhyolite) that are aligned along a single crystal growth plane. Note that the darker inclusion at the bottom left hand side of the diagram is an aqueous fluid inclusion (arrow). This demonstrates that aqueous fluids and silicate melt co-existed at the time of quartz crystallization.

Figure 3-7 Polished quartz grain from sample GC14 (Vesicular Rhyolite), which shows GI and vapour + non-silicate melt inclusions aligned along a single crystal growth plane. This demonstrates that vapour-rich non-silicate melt and silicate melt co-existed as separate phases in the melt at the time of quartz crystallization.

Figure 3-8 Negative crystal shape vapour-rich inclusions (likely CO_2) from sample GC4 (Vesicular Rhyolite).